An Ionic Liquid as Polar Phase in Low-Temperature-Stable Microemulsions

Dissertation zur Erlangung des Doktorgrades der Naturwissenschaften
(Dr. rer. nat.)
der Fakultät IV der Universität Regensburg

vorgelegt von

Agnes Harrar
geb. Kolodziejski

aus
Regensburg

2011

Promotionsgesuch eingereicht am:	13.01.2011
Tag des Kolloquiums:	25.02.2011
Die Arbeit wurde angeleitet von:	Prof. Dr. Werner Kunz
Prüfungsausschuss:	Prof. Dr. Dr. h. c. Josef Barthel (Vorsitzender)
	Prof. Dr. Werner Kunz
	Prof. Dr. Richard Buchner
	Prof. Dr. Henri Brunner

Meinem Mann Klaus,
meinen Eltern und meiner Schwester

Preface

The work presented in this PhD thesis was carried out at the Institute of Physical and Theoretical Chemistry, University of Regensburg, Germany, under the supervision of Prof. Dr. W. Kunz in the period from 10/2007 to 12/2010. This work would not have been possible without the help and support of many people whom I am deeply grateful.

First of all I would like to express my sincere gratitude to my supervisor Prof. Dr. W. Kunz for giving me the opportunity to work on this topic.

Further, I would like to thank Dr. Didier Touraud for helpful ideas at the beginning of my thesis. Additionally, I would like to thank PD Dr. Rainer Müller, Prof. Dr. A. Pfitzner, Prof. Dr. H. Gores, and Prof. Dr. R. Buchner for supporting my work by providing their equipment.

Special thanks go to Dr. Pierre Bauduin and Dr. Olivier Diat for giving me the possibility to measure SAXS at the Institut de Chimie Séparative de Marcoule (ICSM), CEA, Marcoule, France and specially for helping me with the equipment and data evaluation. In this regard I would like to thank Prof. Dr. Thomas Zemb for very fruitful discussion concerning the evaluation and discussion of scattering data of colloidal systems.

I am also very grateful to Prof. C. Santini and Dr. Paul Campbell (Institut de Chimie de Lyon, Lyon University) for the fruitful collaboration and for performing the experiments on Ru-nanoparticles in the low-temperature-stable microemulsions.

Big thanks go to my lab colleagues Dr. Oliver Zech and Josef Eiblmeier for constructing a friendly working atmosphere. Additionally, I would like to thank Dr. Oliver Zech for the good collaboration in the field of ionic liquids and microemulsions and for his calculations on the DOC model.

I am also very grateful to all colleagues from the lab for scientific collaborations. Among those special thanks should go to Dr. Johannes Hunger, Dr. Alexander Stoppa, Dr. Christian Schreiner, Eva Maurer, Angelika Klaus, Robert Hartl, Doris Rengstl, and Andreas Eiberweiser. Further, thanks go to the secretaries, Wolfgang Simon, Roland Neueder, and Georg Berger.

Further, I am grateful to many people for critical reading parts of my manuscript, their ideas and suggestions: Klaus Harrar, Ludwig Pilsl, Eva Maurer, Angelika Klaus, Dr. Matthias Stich, Dr. Stefanie Gärtner, Dr. Oliver Zech, and Andreas Eiberweiser.

In addition, I would like to thank all my friends for their understanding and encouragement during my thesis.

Thanks go also to one of my best friends Stefanie Gärtner for her friendship and her constitutive encouragements.

My special thanks go to my husband Klaus Harrar for his extraordinary scientific and private support and his appreciation especially in hard times. Further thanks got to my parents and my sister for their constant encouragements in the last three years.

Agnes Harrar

Constants and Symbols

Constants

Elementary charge	e_0	= $1.6022 \cdot 10^{-19}$ C
Avogadro's constant	N_A	= $6.0221 \cdot 10^{23}$ mol^{-1}
Boltzmann's constant	k_B	= $1.3807 \cdot 10^{-23}$ J/K

Symbols

T	Temperature [°C]	λ	Wavelength [nm]
κ	Conductivity [S/m]	q	Scattering vector [$Å^{-1}$]
ρ_m	Density [g/m^3]	$I(q)$	Scattering intensity [cm^{-1}]
w	Weight fraction	Σ	Specific surface [cm^2/cm^3]
ϕ	Volume fraction	Q	Invariant [cm^{-4}]
c	Molarity [mol/dm^3]	d	Domain size [Å]
ρ	Scattering length density [cm^{-1}]	ξ	Correlation length [Å]
σ	Surface tension [mN/m]	G	Gordon Parameter [J/m^3]
η	Dynamic viscosity [mPas = cP]	v	Kinematic viscosity [mm^2/s]

Introduction

There is a still growing interest in ionic liquids (ILs) in general and room temperature ionic liquids (RTILs) in particular resulting from their fascinating and outstanding properties and wide range of potential applications. ILs are defined as salts with a melting point below the boiling point of water. The research field of ILs often deals with aprotic ILs: imidazolium, pyridinium or pyrolidinium based substances.[1-3] Beside this class of ILs, attention has also been paid to protic[4-5] ionic liquids. ILs often are considered as green solvents. This classification was made according to their low vapour pressures, hindering both the evaporation and enrichment of these solvents in the atmosphere. However, ILs often exhibit high toxicities that cannot be neglected. During the last years research activities have been focused on the development of less toxic ILs.[6-9] Moreover, ILs are also termed "designer" solvents as the appropriate combination of anion and cation delivers ILs with specific properties. Hence, ILs are often considered as future solvents for catalysis,[1, 3, 10-11] chemical reactions,[12-13] extractions,[14] and electrochemical purposes.[15] The amount of publications concerning the synthesis, properties, and applications of ionic liquids is rapidly growing to date. In this context, one promising aspect of the variety of possible applications of ionic liquids is their use in the formulation of non-aqueous microemulsions.

Lately, ILs stimulated research in classical colloid and surface chemistry. The formation of amphiphilic association structures in the inside and by means of ionic liquids, such as micelles, vesicles, microemulsions and liquid crystalline phases has been reviewed three times between 2007[16] and 2008,[17-18] reflecting the growing interest and progress in this field.

Microemulsions are thermodynamically stable, isotropic, transparent mixtures of at least one hydrophilic, one hydrophobic and one amphiphilic component. Apart from classical microemulsions consisting of water, oil, and surfactant (and cosurfactant, where appropriate), it has been demonstrated that the polar phase is not necessarily water and the non-polar phase not compulsorily oil. The idea of non-aqueous microemulsions is not new.[19-20] For example, water can be replaced by glycerol,[21] glycol or formamide.[22] Efforts have further been made to replace water by a mixture of molten salts (nitrate mixtures of ethylenediamine/ammonia/potassium) in a system composed of sodium dodecyl sulfate (SDS), 1-pentanol, and decane.[23]

These pioneer studies stimulated research on the formulation of non-aqueous microemulsions containing ionic liquids. The first microemulsion, where water has been replaced by an RTIL has been reported by *Gao et al.*[24] They replaced water by the aprotic IL 1-butyl-3-methylimidazolium tetrafluoroborate ([bmim][BF_4]), while cylcohexane has been used as apolar phase and Triton X-100 as surfactant. Microemulsions based on protic ILs have been reported by *Atkin & Warr*: non-ionic alkyl oligoethyleneoxide surfactants (C_iE_j), alkanes and ethylammonium nitrate (EAN) as polar phase.[25]

Beside the studies of other groups, IL based amphiphilic systems also have been investigated by the group of *Kunz*. This research has its origin in the investigation of surfactant like ionic liquids (SLILs). Among those are imidazolium based ILs with long alkyl chains that exhibit surfactant properties but still have melting points below 100 °C. The aggregation of these surfactants was studied in water and ILs, like the protic IL EAN and the aprotic IL [bmim][BF_4].[26] Among other results not discussed in detail here, these systems exhibited high temperature-stability. The micellar aggregates turned out to be present not only at room temperature but also at elevated temperatures up to 150 °C.

In the next step these SLILs and ILs were applied in microemulsion systems. Mixtures of 1-hexadecyl-3-methylimidazolium chloride ([C_{16}mim][Cl])+decanol/RTIL/dodecane with EAN and [bmim][BF_4] as polar phase, respectively, first have been investigated and compared to each other at ambient temperature.[27] A significant difference concerning phase behaviour and microemulsions structure has been found. The area of the one phase region was considerably larger in the case of EAN than for microemulsions with [bmim][BF_4]. Since all ingredients exhibit excellent thermal stability combined with high boiling points and decomposition temperatures, respectively, the thermal stability of the [C_{16}mim][Cl]+decanol/ EAN/dodecane microemulsions has been investigated in detail. It could be demonstrated that these microemulsions were stable within a temperature range between (30 – 150) °C. Therefore, these systems represent the first high temperature stable microemulsions with ILs, exhibiting a thermal stability that cannot be achieved with their aqueous counterparts.[28-29] Moreover, it could be demonstrated that biodiesel can act as oil phase in high temperature microemulsions highlighting a way towards the formulation of biocompatible microemulsions.[30] These model systems can be extended to other ILs, with [bmim][BF_4] instead of EAN as polar phase, where also a remarkable thermal stability could be observed.[31] Surprisingly, not many studies benefit from the temperature-stability that can be achieved by the application of ILs in microemulsions. Beside our own research, *Gao et al.* studied temperature dependent changes on microstructure in IL-based microemulsions.[32] They described the effect of temperature on

[bmim][BF_4]-in-cyclohexane and [bmim][BF_4]-in-toluene reverse microemulsions. They concluded the existence of an IL/o structure up to 60 °C. The studies of *Warr et al*. on the system EAN/C_iE_j/alkanes[25] and propylammonium nitrate (PAN)/C_iE_j/alkanes[33] comprised structural studies at varying temperature. However, these studies describe a temperature dependent investigation in a temperature range that does not extend the possible range that can be achieved with water, (0 - 100) °C. ILs exhibit wide liquid ranges and the exchange of water in "traditional" microemulsions by ILs in principle allows the formulation of high or low-temperature-stable microemulsions. Consequently, after successful formulation of high temperature stable microemulsions, the aim of this work was to go a step further: to temperatures far below 0 °C.

The present work focuses on the formulation of low-temperature-stable microemulsions. For this purpose ingredients with low crystallization temperatures are required. Therefore, the IL 1-ethyl-3-methylimidazolium ethylsulfate ([emim][$etSO_4$]), which exhibits a glass transition temperature of -80 °C was chosen as polar phase. Furthermore, limonene with a melting point of -96 °C is used as apolar phase. In this work the effect of different surfactants has been studied on possible formation of low-temperature-stable microemulsions. Three systems that presented the most promising candidates for applications have been investigated in more detail and will be presented in the "results and discussion" section. These include microemulsions with Triton X-100, Triton X-114, and tetraethyleneglycol monodecylether ($C_{10}E_4$) as amphiphile, respectively. The systems have been investigated at ambient temperatures as well as at temperatures down to -10 °C.

I. Fundamentals

1. Ionic Liquids

Ionic liquids (ILs) in general attract soaring scientific interest during the past years which is reflected by the increasing number of publications in this field. A typical literature search on the topic “ionic liquid” in Scifinder results in 200 hits in the year 2000, 1800 hits in 2005 and already 3400 hits in 2010 (until November 2010).

ILs may be either considered as new class of solvents or as substances that have a long and useful history just depending on their definition.[34] Indeed, “molten salts”, high-melting substances also have been called ionic liquids and were known and applied a long time before ILs became popular. However, applications thereof often were very specialized, mainly for electrochemical purposes. Nowadays, ILs can be clearly distinguished from “molten salts” that are often highly viscous, high-melting, and corrosive. As other synonyms appear in literature that can meet the working definition of ILs like “room temperature molten salt”, “ambient temperature molten salt”, “low temperature molten salt”, “ionic fluid”, and “liquid organic salt”, an explicit definition will be given in the following paragraph.[34]

Publications dealing with ILs appear in a very fast rate. Hence, only a short overview about the properties and applications of ILs can be treated in the framework of this work.

1.1 Definition and Classification

As mentioned before, ILs require a clear definition: ILs have melting points below 100 °C and are compounds consisting exclusively of an anion and a cation. The first IL reported meeting this definition was ethanolammonium nitrate, with a melting point between (52 - 55) °C, discovered by *Gabriel* in 1888.[35]

A subclass of ILs is formed by room temperature ionic liquids (RTILs), being already liquid at temperatures below or at ambient temperature. *Walden* reported water-free ethylammonium nitrate (EAN) with a melting point of 14 °C in 1914,[36] being the first true RTIL published in literature. Nowadays, a broad variety of RTILs is known. Due to their sensibility towards hydrolysis some are more suitable for applications and others like chloroaluminates ($[AlCl_4]^-$)

are less applicable.[34] Finally, the discovery of hydrolytic stable ILs increased the interest in this class of solvents.[37]

In general, ILs can be subdivided into two big classes: protic and aprotic ILs. "Protic" describes ILs that are synthesised from a traditional Brønsted base and Brønsted acid reaction. Therefore, all other ILs are named aprotic. The first ILs discovered, ethanolammonium nitrate and EAN belong to the class of protic ionic liquids (PILs). The latter is probably the best studied IL in literature, mainly due to its water-like properties. Among those, especially the ability to form a three-dimensional hydrogen-bond network is of particular interest.[38-39] Recently, a comprehensive overview about types and characteristics of PILs has been given by *Greaves & Drummond*.[5] As the acid base reaction will rarely proceed completely in practice, the neutral acid or base species will still be present in the IL system. Therefore, a classification to define the amount of neutral species allowed in a substance that is named ionic liquid is necessary. *MacFarlane et al*. suggested setting a limit of 1 % of neutral species for a compound that is a pure ionic liquid.[40] Hence, substances containing a higher amount of neutral species have to be classified as mixtures of ionic liquids and neutral species.

Aprotic ILs consist of bulky organic cations with a low degree of symmetry, for example imidazolium, pyrrolidinium, or pyridinium. Some cations and anions commonly used for the formation of ILs are given in Figure I-1.

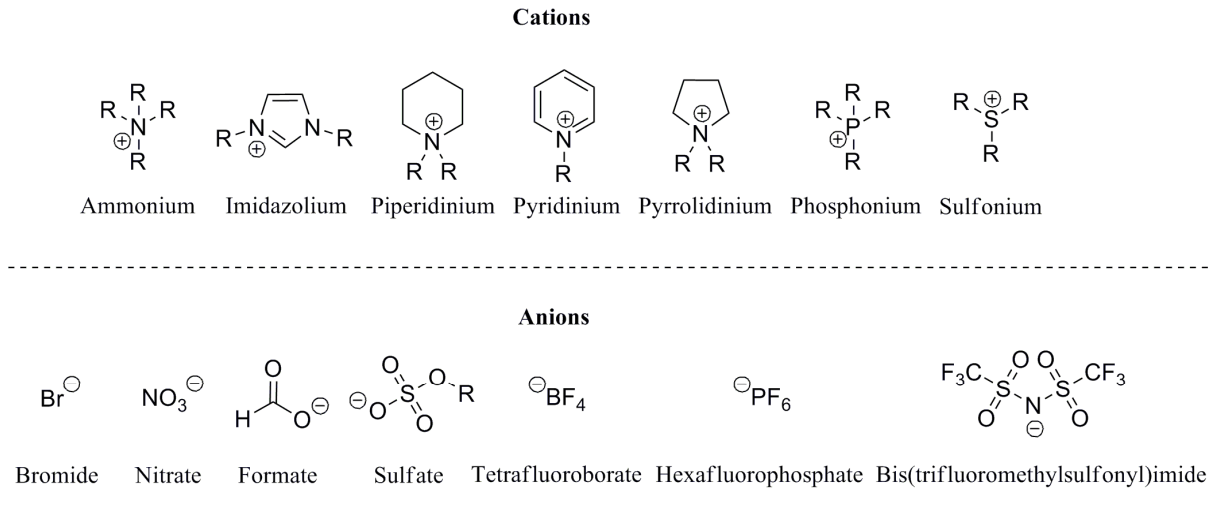

Figure I-1. Some examples for common anions and cations used in ILs.

Quite often, ILs are also denoted as "designer solvents" or "task-specific ionic liquids" according to the fact that by the future properties of the compound can be tuned varying the molecular structure of the ions.[1] One can visualize this "task-specifity" by regarding the

hydrophobicity of some ILs. Anions like hexafluorophosphate ($[PF_6]^-$) or bis(trifluoromethylsulfonyl)imide ($[(CF_3SO_2)_2N]^-$) lead to hydrophobic ILs. In contrast, diethylsulfate, halides, or acetates tend to build hydrophilic ILs while tetrafluoroborate ($[BF_4]^-$) builds ILs that can be located in between hydrophilic and hydrophobic ones. The "task-specifity" can be enlarged to properties like polarity, viscosity, melting point, solvent ability, and thermal or electrochemical stability, just to name only some of them.

1.2 Properties

Literally speaking, the difference between ILs and "molten salts" seems to be just a matter of degree. "Molten salts" have high melting points compared to ILs. In practice, ILs developed during the last decades have many advantages compared to traditional "molten salts" like for instance lower working temperatures and a minor sensitivity to corrosion. Therefore, they can be handled mostly like ordinary solvents.[34] Consequently, ILs have found applications as solvents for reactions, extraction media, and working fluids in mechanical implementations, where the usage of "molten salts" would have been impossible.

Nevertheless, most ILs still have some characteristics hindering their normal handling. An important aspect of ILs is that they are often hygroscopic and sometimes prone to hydrolysis. Even the ILs considered to be hydrophobic will assimilate a certain amount of water until saturation is obtained. Consequently, synthesis, purification, characterization, and storage should be performed under inert atmosphere. Additionally, the water content should always be measured when working with ILs because even small amounts can influence the physicochemical properties presented in the following chapter.

1.2.1 Liquidus Range-Lower and Upper Limit

The essential feature of ILs rendering them interesting for research and application is their very wide liquidus range. This is the interval between the melting point or glass transition temperature and the boiling point or decomposition point of a liquid.[34] The liquidus range of water is 100 °C (0 – 100 °C) and 135 °C (-95 – 40 °C) for dichloromethane (DCM). In contrast, ILs can have liquidus ranges up to several hundreds of degrees, like 1-ethyl-3-methylimidazolium ethylsulfate ([emim][$etSO_4$]) that has a liquidus range of 436 ° C (-80 - 356 °C). Several ILs with corresponding liquidus ranges are given and compared to some common solvents in Table I-1.

Table I-1. Some physicochemical values for common solvents and ionic liquids. T_m: melting point, T_g: glass transition temperature, T_b: boiling point, T_d: decomposition temperature, ΔT_{liquid}: resulting liquidus range.

solvent	T_m or T_g [°C]	T_b or T_d [°C]	ΔT_{liquid} [°C]
DCM	-95[41]	40[41]	145
Toluol	-95[41]	111[41]	206
EAN	14[31]	252[31]	266
[emim][$etSO_4$]	-80	356	436
[bmim][PF_6]	-80[31]	437[31]	517

The melting point of an IL depends on the chemical structure of the cation and anion. Several factors influence the crystal packing and therefore the melting points of ILs. For example the size, charge, charge distribution, and symmetry of the ions are of importance.[34, 42] The dominant force in ILs is the *Coulomb* attraction between ions given by Equation I-1

$$E_c = \frac{MZ^+Z^-}{4\pi\varepsilon_0 r} \qquad \textbf{(I-1)}$$

where Z^+ and Z^- are the ion charges and r is the inter-ion separation.[34] The overall lattice energy, as treated by *Born-Landé*[43] or *Kapustinskii*[44], mainly depends on this term multiplied by an additional factor. Thus, a reduction of the *Coulomb* interaction results in a reduction of the modulus of the crystal lattice energy. The crystal lattice energy is defined as the energy that is released when the solid is formed (negative value). A low modulus of the lattice energy is in consistence with low melting points. This should therefore be preferred when the charges of the ions are +1 and -1, respectively and when the size of the ions is large leading to a large ion-separation length, r. Moreover, large ions lead to a delocalization of charge and further reduce the melting points.[34] *M* in the coulombic energy equation represents the *Madelung* constant and reflects the packing efficiency of the ions and affects the overall lattice energy as well.

The effect of size can be easily demonstrated for simple sodium salts. By increasing the thermochemical radius from Cl^- (1.7 Å) to $[BF_4]^-$ (2.2 Å) to $[PF_6]^-$ (2.4 Å) and finally to $[AlCl_4]^-$ (2.8 Å) the melting point decreases from 801 to 185 °C. The values can be extrapolated and lead to a necessary radius of (3.4 – 4) Å to obtain a molten salt at room

temperature.[34] A similar effect can be observed for the cations' size. For example by moving down the period in the same group in the periodic table, the melting points of the corresponding salts tend to lower temperatures for cesium to lithium analoga. Ionic liquids usually contain large, bulky organic cations in contrast to small inorganic ones. This results in a significant reduction of the melting point.[45] The *Coulombic* attraction is then of comparable order of magnitude to the intermolecular interactions in molecular liquids.

Melting points of organic salts also are related to the symmetry of the ions. An increasing symmetry leads to a more efficient ion-ion packing in the crystal lattice and therefore to increased melting points.

The length of the alkyl chain in alkyl-methyl-imidazolium salts plays an important role in the melting points of this class of ILs. The increase of alkyl chain length up to n = 8-10 (n: number of C-Atoms in an alkyl chain) decreases the melting point. Beyond n = 10 the melting point increases again according to *van-der-Waals* interactions that superpose the first effect of destabilisation of *Coulomb* packing.[34] Further, the size of the anion influences the melting point of 1-alkyl-3-methylimidazolium salts drastically. An example based on the 1-ethyl-3-methylimidazolium cation is given in Table I-2.

Table I-2. Melting points of the 1-ethyl-3-methylimidazolium cation combined with various anions, reproduced from Ref. 43.

Anion	T_m [°C]
Cl^-	87
Br^-	81
I^-	79-81
$[BF_4]^-$	15
$[AlCl_4]^-$	7
$[PF_6]^-$	62
$[AsF_6]^-$	53
$[CF_3SO_3]^-$	-9
$[CF_3CO_2]^-$	-14

Additionally, increasing anion sizes and delocalized charge distribution yield lower melting points. However, combinations like 1-ethyl-3-methylimidazolium tetraphenylborate can lead to increased melting points compared to anions of the same size. This is due to attractive aromatic π-π stacking that favours the packing in a crystal lattice.[34]

ILs generally exhibit little measurable vapour pressure and therefore are often not distillable. Thus, in many cases the upper limit is a decomposition temperature rather than a boiling point. The only possible way to distil an IL is via the uncharged starting materials for protic ionic liquids. The starting materials that react to the protic IL are formed during distillation and will vaporize and react again in the collecting flask to reconstruct the ionic liquid. This procedure requires extreme conditions, by means of high temperatures and high vacuum. Additionally, it is limited to PILs with weak Lewis bases, otherwise the starting materials will decompose during distillation.[46-48]

The previously described attributes of ILs also entail challenging purification procedures. Care has to be taken in the choice of starting materials. First, they have to be purified and reactions have to be performed in the appropriate molar ratios. Once the IL is synthesized the

possible purification methods are rare: distillation for some protic ILs if the conditions are available or recrystallization for some ILs exhibiting melting points in a feasible temperature range. As most RTILs do not feature a melting point, but a glass transition far below 0 °C instead, purification is made almost impossible. The only solution is to use high purity starting materials in the exact molar ratios. The advantages of ILs can simultaneously lead to several obstacles in purification. Hence, one should always be aware of the possible impurities when working with ILs.

1.2.2 Viscosity and Conductivity

In this section transport properties, such as viscosity and conductivity are introduced and discussed. They represent key parameters to evaluate the performance and potential of fluids.

The viscosity of a fluid arises from the internal friction of a fluid. With respect to viscosity, there are two broad classes of fluids, *Newtonian* and non-*Newtonian*. *Newtonian* fluids have a constant viscosity when strain is applied. Non-*Newtonian* fluids will either thicken or thin with applied strain. Ionic Liquids are treated as *Newtonian* fluids and up to now no other evidence has been published. Most ILs exhibit a much higher viscosity compared to water (0.890 cP) or ethylene glycol (16.1 cP) at ambient temperature.[41] The dynamic viscosities for ionic liquids are in the range between 10 cP and 500 cP.[34] Impurities influence the viscosities of ILs drastically, especially a high water content. This complicates the evaluation of data if no information about water content or purity of the IL is provided.

Nevertheless, some conclusions in viscosity dependence of the anion and cation can be drawn. The viscosity increases in the order: bis(trifluoromethylsulfonyl)amide, tetrafluoroborate, trifluoromethyl acetate, trifluoromethyl sulfonate, pentafluoroethyl sulfonate, heptafluoropropyl acetate, methyl acetate, methyl sulfonate, nonafluorobutyl sulfonate for ionic liquids composed of the same cation. For ionic liquids with the same anion the trend is that larger alkyl substituents lead to more viscous fluids. The addition of co-solvents to ionic liquids influences the viscosity drastically as well. For example an addition of 5 wt% acetonitrile leads to a reduction of the absolute viscosity of [emim]Cl-$AlCl_3$ to 50 % of its initial value.[34]

The conductivity of a solvent results from the available charge carriers and their respective mobility. As ILs exclusively consist of ions, a high conductivity seems reasonable. Unfortunately, ILs possess mediocre but not excellent conductivities (~ 1 S/m). These values lie in the range of good non-aqueous solvents/electrolyte systems but are significantly lower than those for concentrated aqueous electrolytes. The reduced conductivity can be attributed

to the presence of ion pairing or ion aggregation. Ionic liquid conductivities seem to be weakly related to the size and type of the cation. Increasing the cation size tends to lead to lower conductivities. This can be explained by a decreasing mobility of the ions with increasing size. For anions there is no clear relationship between size and conductivity.[34]

Both: viscosities and conductivities of ionic liquids are highly temperature dependent, especially when approaching the glass transition temperature (if existent). The influence of temperature can be best described using the correlation according to *Vogel-Fulcher-Tammann* (VFT), equation I-2 and I-3.[49]

$$\ln \eta = \ln A + \frac{B}{T - T_0} \qquad \textbf{(I-2)}$$

$$\ln \kappa = \ln A - \frac{B}{T - T_0} \qquad \textbf{(I-3)}$$

A and B represent constants and T_0 is the ideal glass transition temperature lying in most of the cases about 50 °C below the glass transition temperature of the ionic liquid.

Conductivity and viscosity can also be brought in relation according to *Walden*'s rule (equation I-4),[50]

$$\Lambda \eta = const. \qquad \textbf{(I-4)}$$

where Λ represents the molar conductivity ($\Lambda = \kappa M / \rho$, M is the molecular weight and ρ the mass density). The corresponding classification diagram referred to as *Walden* plot (log Λ versus log(1/η)), is shown exemplarily in Figure I-2. The *Walden* plot has first been used for ILs from *Angell et al.* in 2003[51-53] and *MacFarlane et al.* in 2007[54]. If the liquid can be well represented as an ensemble of independent ions the data will fit closely with the 1:1 ideal line. The ideality corresponds to the absence of ion-ion interactions, the slope should be unity. The position of this ideal line was established using aqueous KCl solutions at high dilution.[53] According to Figure I-2 ILs can be classified in dependence on their deviation from the ideal line in following subgroups: super-ionic liquids, good ionic liquids, poor ionic liquids, and non-ionic liquids.[53]

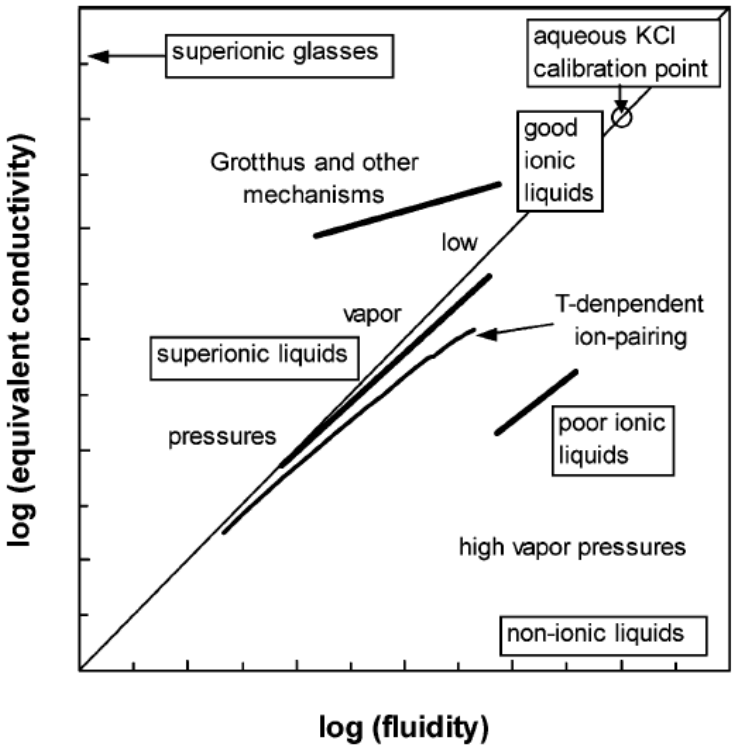

Figure I-2. Classification diagram for ionic liquids, based on the classical Walden rule, and deviations therefrom. Reproduced from *Yoshizawa et al. J. Am.Chem. Soc*., 2003,[53] with permission, copyright American Chemical Society.

1.2.3 Polarity & Solubility Properties

Different solvents have different effects on chemical reactions. This influence has led to the necessity of a solvent classification. Most modern discussions on solvent effects rely on the concept of solvent polarity. Solvent polarities can be studied using different techniques like microwave dielectric spectroscopy, chromatographic measurements, absorption spectra, fluorescence spectra, refractive indices, electron paramagnetic resonance (EPR) spectroscopy, and the study of chemical reactions. Among those measurements of dielectric constants are widely available for common solvents but not for ionic liquids, because the measurement requires non-conducting media. However, a very efficient method is the indirect way of measuring absorption spectra of solvatochromic dyes like Nile Red or *Reichardt*'s dye.[55-56] An empirical polarity scale called the $E_T(30)$ or E scale has been defined for the standard betaine dye 30 (*Reichardt*'s dye). Many ionic liquids could be already classified using this method.

Despite the great interest in ILs, the polarities for only a small number of those substances have been investigated using more than one technique, and only for a small part of those a sufficient classification is present in literature. Most classifications are based on the idea that

if the response of a particular probe molecule is the same as that of a known solvent, the polarity then is considered to be the same. In general, ionic liquids do not seem to be more polar than other molecular solvents. Most of them can be located in the region of short- or middle-chain alcohols.[34]

Different combinations of anion and cation lead to different polarities. The choice of an anion like $[PF_6]^-$ leads for example to an hydrophobic IL that is immiscible with water. In contrast, an anion like $[etSO_4]^-$ leads to an IL that is miscible with water and therefore considered to be more polar.

The solubility of organic and inorganic compounds in ILs is of main interest, especially in the context of reaction media and separation processes. The solubility strongly depends on the combination of cation and anion. According to the high number of possible combinations the potential of ILs is obvious. It is always possible to find task-specific ILs dissolving the desired compound. Nevertheless, systematic studies on this topic are rare.

1.3 Applications

According to this enormous number of possible IL-compositions, their potential in industry and research is indisputable.

ILs build a variable class of solvents that can be found in several chemical processes, for example as reaction media,[12-13] in biocatalysis,[10] in catalysis,[1, 11] and in separation processes.[14] Further, ILs are known in organic, inorganic and polymer synthesis. The range of applications is wide, not only in synthesis but as well in more industrial relevant topics like their utilization as electrolyte solutions for batteries[57] or in solar cells.[58-59]

Table I-3 summarizes some industrial applications of ILs reported in literature, reflecting the wide capability of these compounds.

Table I-3. Reported industrial applications of ionic liquids, reproduced from Ref. 43.

Company	Process	IL acting as
BASF	acid scavenging	auxiliary
	extractive distillation	extractant
	chlorination	solvent
IFP	olefin dimerization	solvent
Degussa	hydrosilylation	solvent
	compatibilizer	performance additive
Arkema	fluorination	solvent
Chevron Philips	olefin oligomerization	catalyst
Scionix	electroplating (Cr)	electrolyte
Eli Lilly	cleavage of ether	catalyst/reagent
Air Products	storage of gases	liquid support
Iolitec/Wandres	cleaning fluid	performance additive
Linde	gas compression	liquid piston

The first industrial-scale ionic liquid-based process was established by BASF in 2002. The so-called BASIL™ process (BASIL= **B**iphasic **A**cid **S**cavenging utilizing **I**onic **L**iquids) is used to produce alkoxyphenylphosphines that are important raw products for the production of photoinitiators. The process is carried out in a multi-ton scale and is far more efficient than the previous process where tertiary amines have been used instead.[34]

2. Microemulsions

2.1 Definition

Microemulsions are thermodynamically stable, isotropic, transparent mixtures of at least one hydrophilic, one hydrophobic, and one amphiphilic component. The first microemulsion structures, at that time referred to as “oleophatic hydro-micelle”, were discovered in 1943 by *Hoar & Schulman.*[60] The term microemulsion was introduced afterwards by *Schulman et al.* in 1959 describing optically isotropic transparent solutions consisting of water, oil, surfactant, and alcohol.[61] A more recent definition was given by *Danielsson & Lindman*: “A microemulsion is a system of water, oil, and an amphiphile, which is a single optically isotropic and thermodynamically stable liquid solution”.[62] Herein, “water” corresponds to a polar phase that is classically an aqueous solution which can contain electrolytes and other additives. The word “amphiphile” from amphi (both sides) and philos (liking) was coined by *Winsor*[63] to describe substances with an affinity towards both non-polar and polar phases. In this context, surfactants are the most important amphiphiles, since their amphiphilic character is strong enough to drive them to the interface where the polar part of the molecule is located in the polar phase and vice versa. The term “oil” refers to an organic phase that is immiscible or at least immiscible to a certain extend with the polar phase. Consequently, non-polar substances such as hydrocarbons, partially or totally halogenated hydrocarbons, cyclic or aromatic hydrocarbons, but also triglyceride natural oils can be applied as apolar phase.[64]

2.2 Classification

Conventional microemulsions consist of at least three components, namely oil, water, and an amphiphile. Herein, they are called conventional as neither oil nor water has to build compulsorily the polar or apolar phase. Consequently, one or both components can be replaced by other hydrophilic or hydrophobic substances such as ILs. However, this chapter introduces the general aspects of conventional microemulsions. A separate abstract about IL based microemulsions is given at the end of section 2.

It is generally known that water and oil do not mix. Energy input by means of stirring maintains very unstable dispersions that separate immediately when stirring is interrupted. For the formation of stable emulsions the interfacial tension between water and oil has to be reduced. This can be realized by adding an amphiphile (hydrotrope or surfactant) to the dispersion. Generally speaking, high amounts of hydrotropes are required to dissolve two

immiscible phases and, in contrast to surfactant system, this method results in unstructured emulsions. The utilization of surfactants leads to ordered systems that can be thermodynamically unstable dispersions, macroemulsions with big droplet sizes (0.2 - 10) µm, or thermodynamically stable microemulsions with small droplet sizes (3 - 20) nm.[65] The unstable macroemulsions remain stable for a certain period of time as the separation is kinetically inhibited. They are formed by single chain ionic surfactants without the addition of cosurfactants. In contrast, when using non-ionic surfactants or ionic double chain surfactants such as sodium bis(2-ethylhexyl)sulfosuccinate (AOT) no cosurfactant is needed for the formation of stable microemulsions.[66] This results from the ability of these amphiphiles to reduce the interfacial tension between oil and water to a very low value, which is a major requirement in order to form stable microemulsions. Many other surfactants like single-chain ionic surfactants do not exhibit this characteristic and hence cosurfactants, *i.e.* *n*-alcohols or *n*-amines are indispensable to obtain the required low interfacial tension for the formation of stable microemulsions.[67-68] A great variety of structures of single phase microemulsions is known in literature ranging from water-in-oil (w/o) over bicontinuous to oil-in-water (o/w) structures. In the case of a w/o microemulsion, oil is the continuous phase with water droplets stabilized by surfactant molecules and vice versa for o/w structures. The microstructure strongly depends on the volume fraction of oil, water, and amphiphile as well as on the nature of the interfacial film. O/w microemulsion structures preferentially form when the oil volume fraction is low and vice versa for w/o microemulsions. Bicontinuous structures, which are networks of oil and water nanodomains separated and stabilized by a surfactant interfacial film with a net curvature close to zero can be found at almost equal amounts of water and oil. The possible microstructures of a droplet microemulsion phase are illustrated in Figure I-3.

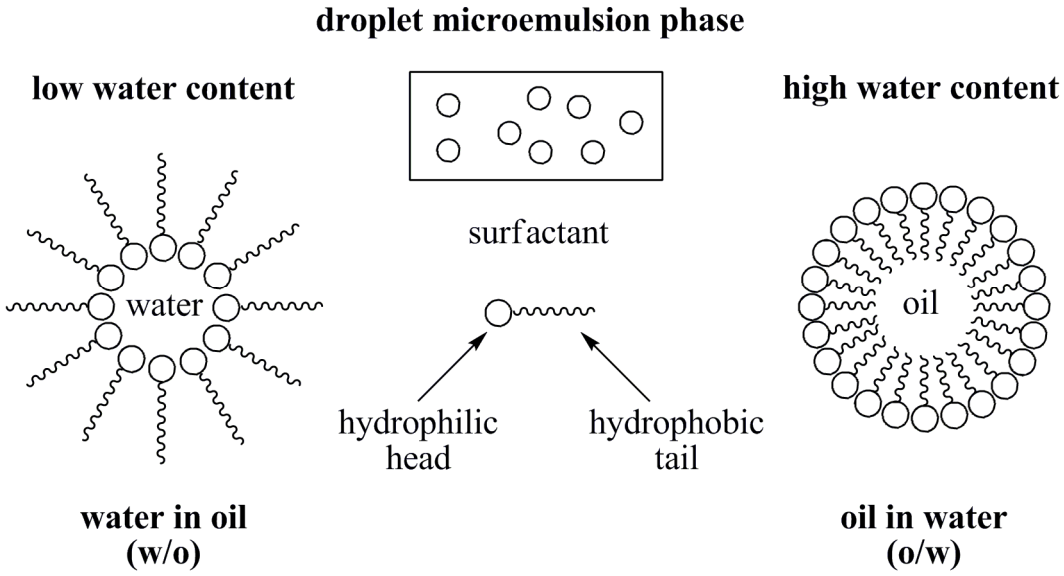

Figure I-3. Droplet microemulsion phase: left: w/o microemulsion. right: o/w microemulsion. middle: surfactant structure. In the case of non-ionic surfactants and AOT: no cosurfactant; in the case of ionic surfactants: an additional cosurfactant has to be inserted into the interface.

Figure I-4 shows a possible bicontinuous microstructure.[69] O/w structures often are abbreviated as L_1-phases, w/o as L_2-phases, and bicontinuous structures often are termed L_3-phases or sponge phases.

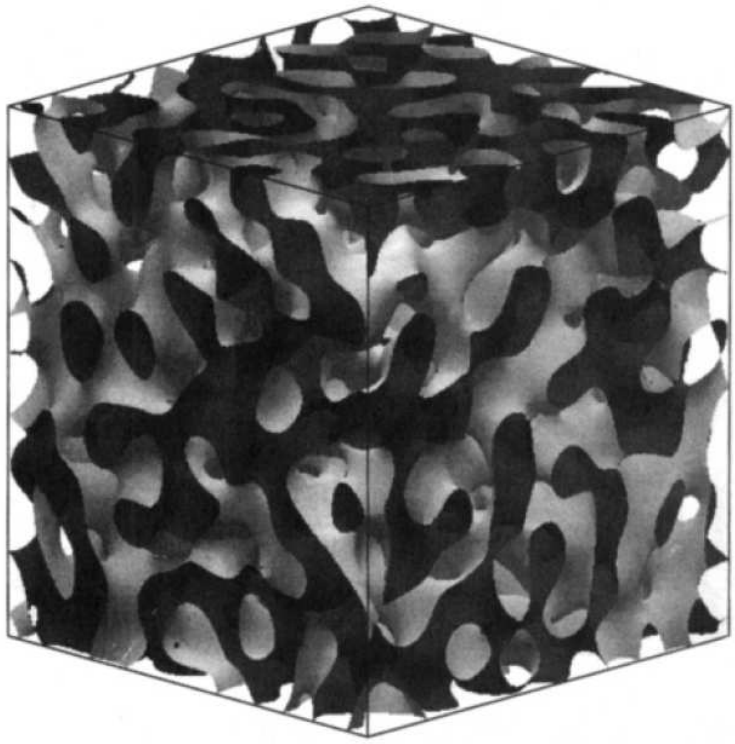

Figure I-4. 3-Dimensional illustration of a bicontinuous phase (sponge phase). Reproduced from *Pieruschka & Marcelija, Langmuir*, 1994,[69] with permission, copyright American Chemical Society.

Another important phase classification that can be found in literature frequently has been introduced by *Winsor*,[70] who discovered four general types of phase equilibria. A *Winsor* type IV phase corresponds to a classical single phase microemulsions. This is consistent with *Hoar´s & Schulman´s* definition[60]. The possible microstructures have been discussed in the previous paragraphs. A *Winsor* type I system denotes two phases in equilibrium, an o/w structure and an almost pure upper oil phase. In contrast, in a *Winsor* type II system an aqueous phase containing surfactant is in equilibrium with a w/o microemulsion in the upper phase. Finally, *Winsor* type III structures equals a three-phase system consisting of a surfactant poor water phase, a bicontinuous middle phase, and an almost pure upper oil phase.

The *Winsor* phases I, II, and III are illustrated in Figure I-5. *Winsor* IV is not illustrated as it corresponds to a single phase microemulsion that can be L_1, L_2 or L_3.

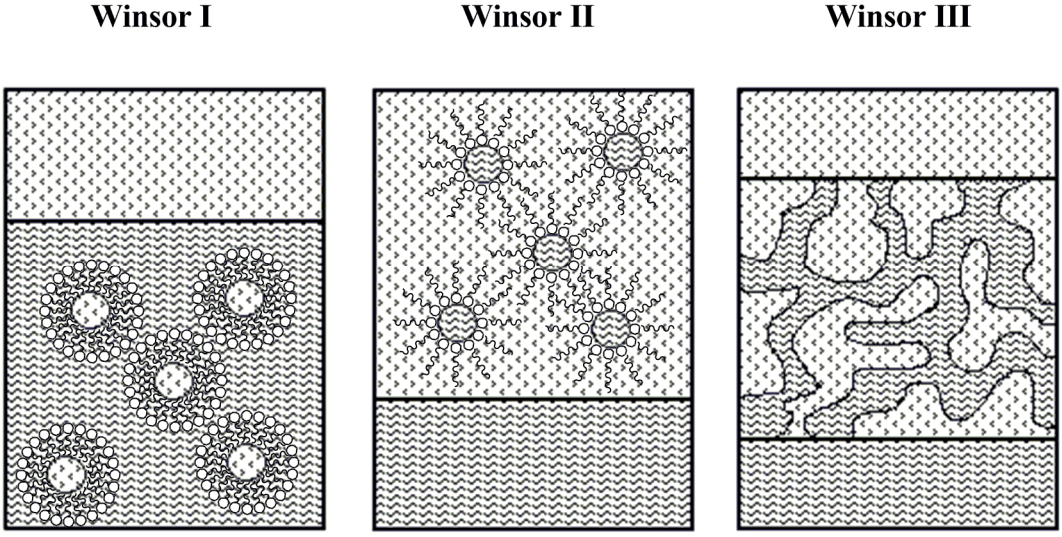

Figure I-5. Illustration of a *Winsor* I, a *Winsor* II and a *Winsor* III phase. *Winsor* I: o/w microemulsion in equilibrium with an excess oil phase (upper phase). *Winsor* II: w/o microemulsion in equilibrium with excess water phase (lower phase). *Winsor* III: bicontinuous microstructure in equilibrium with excess water and excess oil phase.

Depending on surfactant, composition, and present temperature in the microemulsion system, a *Winsor* type I-IV phase is formed preferentially. The effect of some parameters can be monitored by recording phase diagrams, which is the topic of the following chapter.

2.3 Phase Diagrams

Studying the microstructure of microemulsions generally has its origin in the establishment of a phase diagram.

Two important variables have to be defined in order to classify a microemulsion: the ratio between oil and water α (equation I-5) as well as the amount of added surfactant γ (equation I-6).

$$\alpha = \frac{m_o}{m_w + m_o} \qquad \textbf{(I-5)}$$

$$\gamma = \frac{m_s}{m_s + m_o + m_w} \qquad \textbf{(I-6)}$$

The masses of surfactant, oil, and water are denoted as m_s, m_o, and m_w, respectively.

The first phase diagram that has to be discussed when dealing with microemulsions is the so-called "*Gibbs*-triangle". It represents the composition of a ternary system in 2-dimensional space. Triangular phase diagrams at constant temperature *T* and constant pressure *p* are frequently used and provide important information about a given system. In Figure I-6 a typical phase diagram for non-ionic surfactants is depicted. The emphasis will lie on non-ionic surfactants because the work presented in the following exclusively deals with this class of surfactants. The three axes correspond to weight fraction water, oil, and surfactant, respectively. In the case of ionic surfactants the weight fraction surfactant has to be replaced by the weight fraction of surfactant plus cosurfactant. The position of phases according to *Winsor* is marked in Figure I-6 as well.

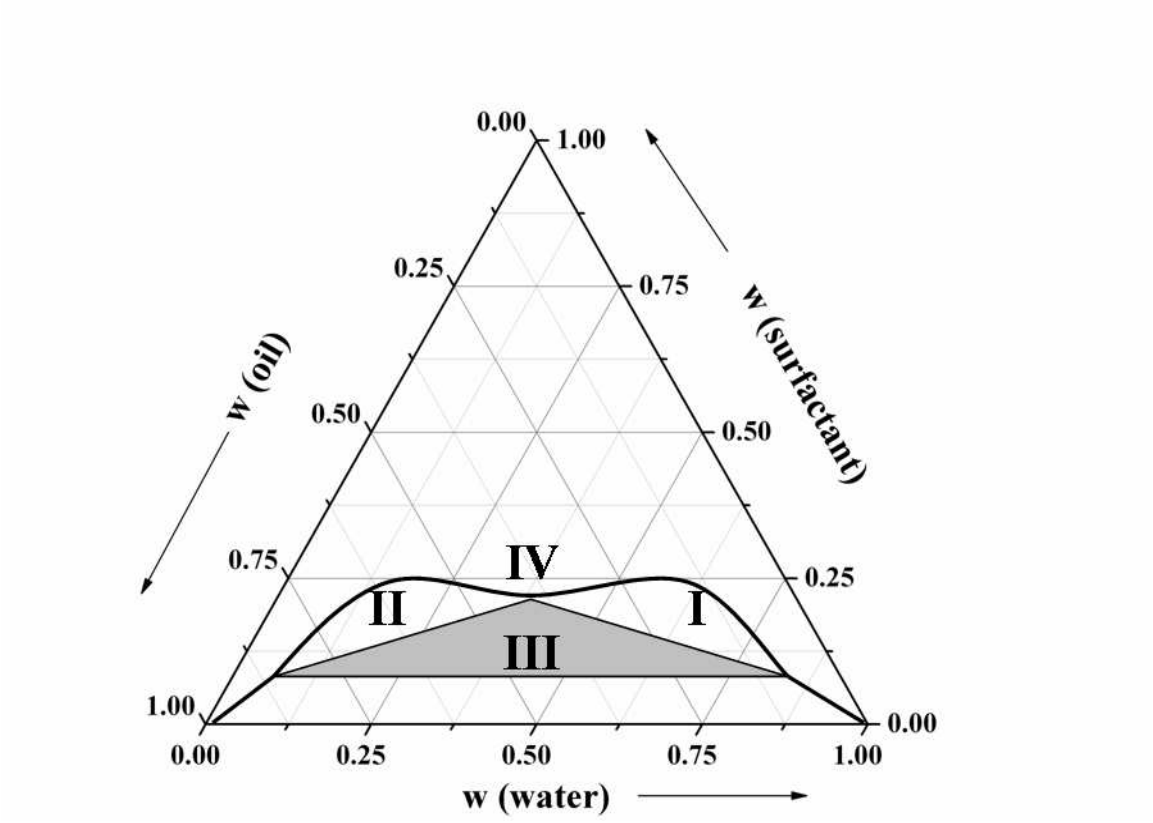

Figure I-6. Schematic illustration of a ternary phase diagram including the phase classification according to Winsor (I-IV).

This shape of a ternary phase diagram can only be observed when the diagram is recorded at a temperature close to the phase inversion temperature (PIT). The PIT denotes the temperature, at which the mean curvature of the surfactant film is zero and the film is therefore perfectly balanced between water and oil phase. A three phase body can then be formed according to *Winsor* III. The mean curvature of an amphiphilic film is given by

$$H = \frac{1}{2}(c_1 + c_2) \qquad \textbf{(I-7)}$$

where $c_1 = 1/R_1$ and $c_2 = 1/R_2$ are principal curvatures at a certain point on the film.[71]

The temperature effect on the ternary phase diagrams of non-ionic surfactant microemulsions is illustrated in Figure I-7, focusing on the changes in the multi phase region. Below the PIT the mean curvature is positive and the surfactant film is tilted towards oil, resulting in a reduction and finally a disappearance of the three phase body and an enlargement of the *Winsor* I phase. In contrast, high temperatures lead to a negative curvature and to an enlargement of the *Winsor* II phase.

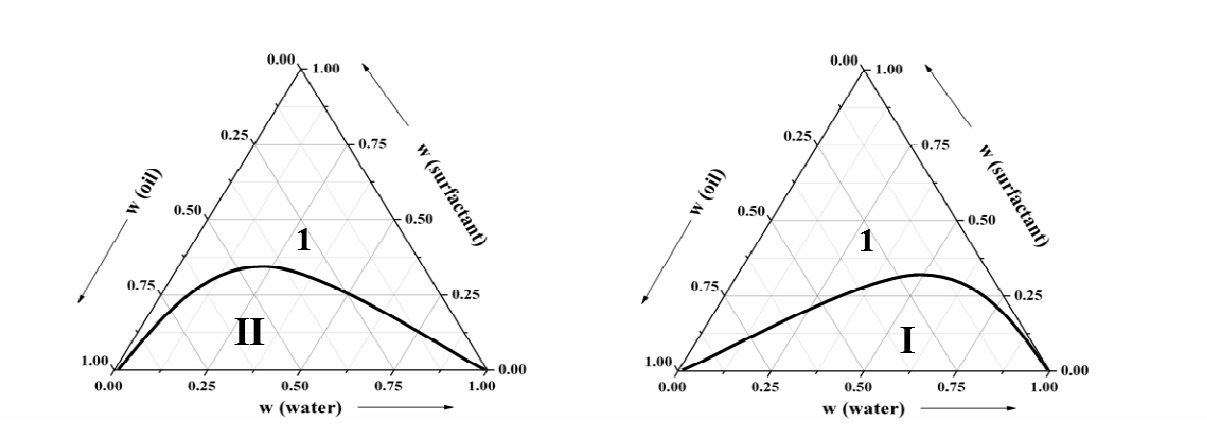

Figure I-7. Left phase diagram: above PIT, mean curvature is negative, *Winsor* type II phase is formed, *Winsor* III disappeared. Right phase diagram: below PIT, mean curvature positive, *Winsor* I is formed, *Winsor* III disappeared. 1: single phase region.

Mapping several ternary phase diagrams at different temperatures for studying the effect of temperature is time consuming and arduous. Therefore, the effect of temperature is usually studied by recording a two dimensional phase diagram, by means of temperature versus surfactant concentration. This corresponds to "slices" in the phase prism at equal amounts of water and oil, *i.e.* $\alpha = 0.5$. The ratio of water to oil is kept constant while the surfactant concentration is varied. The shape of the diagram reminds the shape of a "fish". Therefore, the diagram earned its name "fish"-cut. Figure I-8 represents a schematic illustration of a "fish"-cut with resulting phases according to the *Winsor* I-IV classification. *Kahlweit et al.* extensively studied the effect of temperature on oil-water-surfactant systems. [72-77] These studies mostly focused on ethoxylated alcohol surfactants, a common abbreviation is C_iE_j, where i denotes the number of carbon in the hydrophobic tail of the surfactant and j the repeating number of oxyethylene groups in the hydrophilic part of the surfactant (C_iE_j: $CH_3(CH_2)_{i-1}$-$O(CH_2CH_2O)_j$-H). Furthermore, unbranched aliphatic alkanes are often used as oil phases. The choice of these systems in order to study the phase behaviour of microemulsions results from the simplification in varying the hydrophilicity/hydrophobicity of the surfactant by changing the ratio of i and j and in varying the hydrophobicity of the alkane by varying the chain length of the alkanes. Thus, systematic studies of these systems can be realized readily in a straight forward procedure.

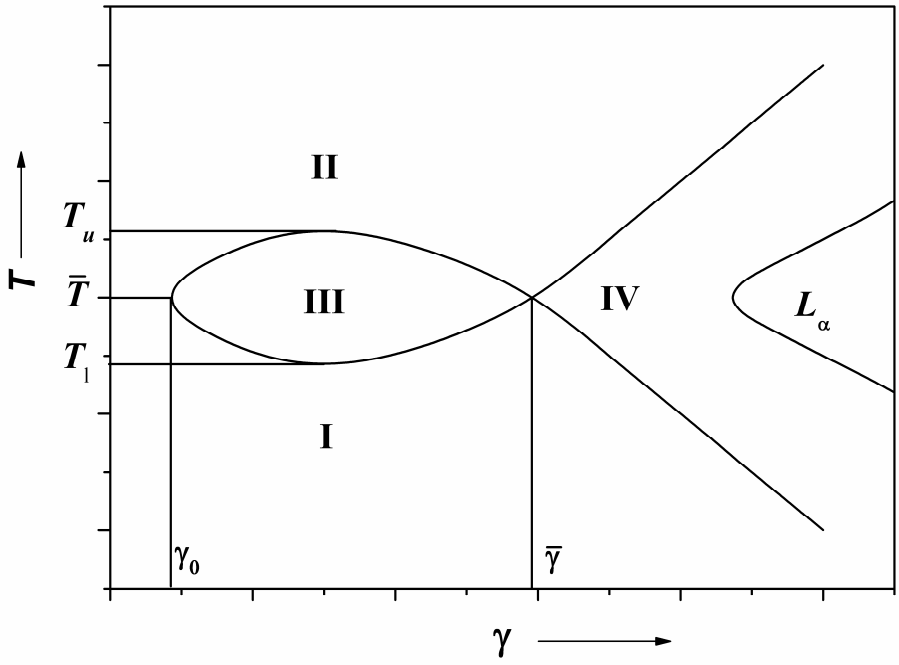

Figure I-8. Schematic illustration of a "fish" diagram including the phase classification according to Winsor and characteristic values that can be extracted from the diagram.

The appearance of the three phase body in the "fish" results from miscibility gaps in the three binary systems: water-surfactant, water-oil, and oil-surfactant.[76, 78] At low temperatures the surfactant is dissolved in the water phase, while it diffuses into the oil phase at high temperatures. At intermediate temperatures the surfactant shows high solubility in both water and oil, producing a surfactant rich middle phase with excess oil and water phase according to *Winsor* III.

The shape and position of the three phase body defines characteristic values of microemulsions. The minimum amount of surfactant needed to form three phases in equilibrium is γ_0. The lowest temperature required to obtain this three phase body is T_l and the temperature above which this three phase body disappears is T_u.[78] The maximum temperature interval over which a three phase body occurs is defined as $\Delta T = T_u - T_l$. The minimum surfactant concentration where a single phase microemulsion is formed is $\bar{\gamma}$ and the corresponding temperature $\bar{T}$. $\bar{\gamma}$ defines the surfactant efficiency that is the minimum surfactant concentration required to combine the immiscible oil and water phase to a microemulsion. $\bar{T}$ corresponds to the PIT. At high surfactant concentration the appearance of a lamellar phase L_α is possible. Lamellar phases are not strictly microemulsions, but related

structures. A lamellar phase is a liquid crystalline phase composed of sticks of bilayers separated by solvent.[79]

The following symbols also can be found in literature, which all correspond to an already described *Winsor* phase: 1 for a single phase region according to *Winsor* IV, 3 for a *Winsor* type III phase, $\bar{2}$ corresponds to a *Winsor* II phase and the symbol $\underline{2}$ is a frequently-used symbol for *Winsor* I phases.

Nevertheless, temperature is not the only variable that can induce phase changes in ternary systems. Some qualitative effects of increasing parameters on the phase behaviour of ethoxylated alcohols, non-polar oil, and water mixtures are summarized in Table I-4.[80]

Table I-4. Qualitative effects of increasing variables upon phase behaviour of C*i*E*j* surfactants, oil and water mixtures, reproduced from Ref. 75.

Increasing parameter	$\underline{2}$	3	$\bar{2}$
Temperature (T)		→	
Pressure (p)		←	
Salt concentration (lyotropic)		→	
Oil hydrophobicity		←	
Surfactant lipophilicity (i)		→	
Surfactant hydrophobicity (j)		←	

The phase change that can be induced for non-ionic surfactants also can be effectuated for ionic surfactant based microemulsions. However, temperature is not the critical variable but electrolyte concentration. By increasing the salinity in the water phase, a phase change from *Winsor* I over *Winsor* III to *Winsor* II can be observed.[67]

2.4 Applications

The unique properties of microemulsions render them interesting for commercial products and technical applications. In particular, the ability to dissolve large amounts of oil or water, the low interfacial tension, the low viscosity and large interfacial area favour their use as solvents for a large number of processes. They have been applied in a variety of technological

processes, formulation of consumer and commercial cleaning products, delivery systems, polymerization and chemical reaction media. Oxidation, hypochlorination, nitration, and enzymatic reactions are only a few examples of chemical reactions performed in microemulsions. In general, all reactions where a polar reagent reacts with an oily substrate are imaginable.[81]

O/w microemulsions for example are widespread substances in cleaners, cosmetics, and personal care products. They also are used as solvents for pharmaceuticals. Therein, the main aim is to dissolve pharmaceutical products which are poorly soluble or insoluble in water in o/w droplet microemulsions.[82]

Another promising aspect of microemulsions is the enhanced oil recovery. It is well known that after an oil well is abandoned, a large proportion of the original oil still remains in the ground. When microemulsions are used up to 30 % of oil can be extracted by the primary recovery and further 20 % by the second recovery.[82]

2.5 Ionic Liquids in Microemulsions

Apart from classical microemulsions consisting of water, oil, and surfactant (and cosurfactant, where appropriate), it has been demonstrated that the polar phase not necessarily has to be water and the non-polar phase not compulsorily oil. The idea of non-aqueous microemulsions is not new,[19-20] as for example water can be replaced by glycerol,[21] glycol or formamide.[22] Further, efforts have been made to replace water by a mixture of molten salts (nitrate mixtures of ethylenediamine / ammonia / potassium) in a system composed of sodium dodecyl sulfate (SDS), 1-pentanol, and decane.[23]

These pioneering studies stimulated research on the formulation of non-aqueous microemulsions containing ionic liquids. Before going into detail with ternary and quaternary systems, self-assembled[16] structures in binary IL/surfactant mixtures remain to be mentioned. As a matter of principle, solvents promoting the ability of amphiphiles to form micelles should exhibit a high dielectric constant, a high solvating power, and should be highly structured.[83] Micelle formation of alkyltrimethylammonium bromides, alkylpyridinium bromides, and octylphenol ethoxylate (TX-100) in EAN was first reported almost 30 years ago.[39, 84] In addition to micellar structures in binary IL/EAN mixtures, liquid crystals of lipids in EAN have been found.[85] There has been a renewed strong research interest in this field mainly in the past few years. ILs as solvents to promote self-assembly have been reviewed recently.[17] Although a detailed discussion of the phase behaviour of binary IL/surfactant

mixtures is beyond the scope of this work, some general conclusions have to be mentioned. The critical micelle concentration (cmc) is significantly higher in ILs than in water. For example *Evans et al.* found that the cmc of conventional surfactant in EAN is between 5 and 10 times higher compared to water.[84] The self-assembly is not restricted to protic ILs. It has been documented for several aprotic ILs as well.[86-88] In addition to the extensive amount of research conducted into binary IL/surfactant mixtures, progress has been made in the formulation and characterization of non-aqueous microemulsions.

Studies concerning the use of aprotic ILs in microemulsions are almost entirely related to imidazolium based substances. Herein, the most extensively studied microemulsions comprise the RTIL 1-butyl-3-methylimidazolium tetrafluoroborate ([bmim][BF_4]) as water substitute, the non-ionic surfactant TX-100, and any kind of oil as apolar phase. The first microemulsion, where water was replaced by a RTIL has been reported by *Gao et al.*[24] They utilized [bmim][BF_4] as polar phase, while cylcohexane was implemented as apolar phase and TX-100 as surfactant.

Concerning PILs in microemulsions, *Atkin & Warr* reported microemulsions composed of non-ionic alkyl oligoethyleneoxide surfactants (C_iE_j), alkanes and EAN as polar phase.[25] They presented “fish”-cuts obtained for an equal ratio of water to oil for surfactants with increasing amphiphilicity (C_8E_2, $C_{12}E_3$, $C_{14}E_4$). With dodecane as oil, the phase diagrams are very similar to the corresponding aqueous systems.[77] A tricritical point,[72-73] where the formation of a three phase body occurs, can be found for the EAN/C_iE_j/dodecane systems at amphiphilicities between C_8E_2 and $C_{12}E_3$. Compared to water[72] and formamide[89] the tricritical point is shifted to higher amphiphilicities *i.e.* longer alkyl chain lengths for EAN. Additionally, *Atkin & Warr* studied the microemulsion’s phase behaviour as a function of the oil alkyl length (octane, decane, dodecane, tetradecane, and hexadecane) and polar headgroup size.

Beside the implementation of protic ILs in microemulsions with non-ionic surfactants, pseudo-ternary systems with ionic surfactants have been reported as well. *Zech et al.* compared microemulsions composed of [C_{16}mim][Cl]+decanol/RTIL/dodecane with EAN and [bmim][BF_4] as polar phase, respectively, at ambient temperature.[27] A significant difference with respect to phase behaviour and microemulsions structure has been found. The area of the one phase region was considerably larger in the case of EAN than for microemulsions with [bmim][BF_4]. For the microemulsions with EAN a typical percolation behaviour for the EAN/o region with increasing EAN content has been found. Dynamic light

scattering (DLS) measurements indicated a swelling of particle size with increasing EAN content, which was further confirmed by small angle X-ray scattering (SAXS) measurements. At low EAN content a droplet EAN/o structure was supposed followed by the formation of larger connected EAN/o aggregates. In the case of [bmim][BF_4] a bicontinuous structure is more likely to exist. Since all ingredients show an excellent thermal stability combined with high boiling points and decomposition temperatures, respectively, we have recently investigated the thermal stability of the [C_{16}mim][Cl]+decanol/EAN/dodecane microemulsions. It could be demonstrated that these microemulsions were stable within a temperature range between (30 - 150) °C. Therefore, these microemulsions represent the first high temperature microemulsions with ILs, exhibiting a thermal stability that cannot be achieved with their aqueous counterparts.[28-29]

Cheng et al. provided a major contribution towards the formulation of non-aqueous microemulsions with two types of ionic liquids.[90] For the first time they reported ionic liquid in ionic liquid (IL/IL) structures. For this purpose, the hydrophobic ionic liquid [bmim][PF_6] and the hydrophilic protic ionic liquid propylammonium formate (PAF) were used as apolar and polar phase, respectively. Moreover, these microemulsions contained the anionic surfactant sodium bis(2-ethylhexyl)sulfosuccinate (AOT). One important precondition for the formation of stable microemulsions is that the polar and the apolar phase do not mix. By the tricky combination of PAF and [bmim][PF_6], whose solubility in PAF was less than 0.1 wt% under ambient temperature,[90] this condition can be fulfilled. However, the single phase region in the ternary phase diagram was exceptionally small.

Applications in the field of non-aqueous microemulsions containing ionic liquids are still scarce up to date. Nevertheless, the few studies available in the open literature demonstrate the great potential of these microemulsions in a diversity of different fields. Nanoparticles have been synthesized by *Zhao et al.* who used benzene/TX-100/[bmim][BF_4] microemulsions as template for the synthesis of silica nanoparticles under both basic and acidic conditions.[91] *Moniruzzaman et al.* reported a strategy for drug delivery by non-aqueous microemulsions with ILs.[92] A large number of drugs are sparingly soluble in both water and most organic solvents. Since the solubility of several drugs is remarkably higher in ILs, IL microemulsions can provide an effective carrier for transdermal drug delivery. *Gayet et al.* studied the efficiency of *Matsuda-Heck* coupling in reverse microemulsions by replacing the ionic liquid [bnpyr][NTf_2] by a chiral structural analogue, 1-phenylethylpyridinium bis(trifluoromethanesulfonyl)imide ([pyr*][NTf_2]) in the system.[93] The reaction was regioselective regardless of the nature of the media, while the yields were increased upon

raising the amount of IL. However, no enantioselectivity could be detected although “chiral” microemulsions with [R-(+)-pyr*][NTf_2] and [S-(-)-pyr*][NTf_2] were applied. IL microemulsions have also been used for the fabrication of polymer electrolyte membranes.[94] These non-aqueous proton conducting membranes have been prepared via the polymerization of microemulsions comprising PILs, surfactant and a polymerizable oil, which was a mixture of styrene and acetonitrile. Although the resulting vinyl polymers were insoluble in the IL, the emerged nanodomains were found to be uniform, transparent, and flexible. The conductivity of these membranes was up to 0.1 S/m due to connected PIL nanochannels preserved in the membrane. Further, these proton conducting membranes offered good mechanical properties as well as thermal and chemical stability. On the other side, a progressive release of the PIL that may affect the long-term stability of these new promising materials can be observed.

All these preliminary studies demonstrate the high potential of these microemulsions for industry and research.

3. Characterization of Microemulsions

A huge variety of possible characterization methods for microemulsions has been developed so far, starting from conductivity over microscopy to spectroscopic methods. This chapter focuses on methods that have been applied to characterize low-temperature-stable microemulsions, the main topic of this thesis.

3.1 Electrical Conductivity and Viscosity

Investigations of transport properties of microemulsions, such as electrical conductivity and viscosity provide important information about their internal dynamics: flexible microemulsions have a monotonic behaviour of conductivity that can be described by a single power law, while rigid ones present a maximum in conductivity due to local microstructure comparable to the situation in liquid crystals. Moreover, isolated non-coalescing water droplets are easily identified by means of very low conductivity values. Similar observations hold also for non-aqueous microemulsions with ionic liquids as polar phase.[95-96]

The conductance of w/o or equivalent IL/o microstructures at low water or ionic liquid volume fractions can be interpreted in terms of the charge fluctuation model of *Eicke et al.*[97] This model assumes spherical droplets with radius *r* that move independently from each other. In a thermal equilibrium these droplets are uncharged on average, as the number of positively charged cations is equal to the number of negatively charged counter ions. However, due to spontaneous fluctuations, charged droplets will form that carry an excess charge *z*, yielding an increased conductivity compared to the pure apolar solvent.

The theory finally leads to an equation that allows relating the specific conductivity κ and the volume fraction of the droplets ϕ (equation I-8):

$$\kappa = \frac{\varepsilon\varepsilon_0 k_B T}{2\pi\eta}\frac{\phi}{r^3} \qquad \textbf{(I-8)}$$

where the volume fraction is defined as $\phi = 4\pi r^3/3$ (k_B: Boltzmann constant, T: temperature, r: radius, ε: relative permittivity, ε_0: electric permittivity of free space, η: dynamic viscosity). Extensions of the charge fluctuation model have been proposed by *Kallay et al.*,[98-99] *Hall*,[100] and by *Halle & Björling*.[101] All these models describe the conductivity behaviour at low water content.

The first study concerning the interpretation of the drastic conductivity increase with droplet volume fraction was reported by *Lagües et al.*[102-103] Increasing the water content of a microemulsion (or in case of non-aqueous microemulsions the IL-content) the conductivity rises continuously up to a certain point, the percolation threshold.[104] Beyond this point the conductivity increases over several orders of magnitude. One explanation for this enormous increase in conductivity above the percolation threshold can be the formation of associated clusters that come sufficiently close to each other, so that an undisturbed transport of charge carriers over the whole sample can take place. In other words: an infinite path appears through the system and various physical properties like conductivity vary steeply around the percolation threshold.[102] At high water content the conductivity can either form a maximum that would be a sign for rigid microemulsions: over a bicontinuous phase finally o/w droplets are formed and further diluted by the addition of water and cause a decrease in conductivity. The second possibility is the formation of a plateau without further decrease in conductivity that would be a sign for flexible microemulsions. In this context the words rigid and flexible deal with the nature of the interfacial film, where flexible means the film is disordered and easily deformable, while rigid designates the reverse behaviour of the film.

Figure I-9 gives a schematic example of a conductivity curve of a microemulsion in dependence of the water content.

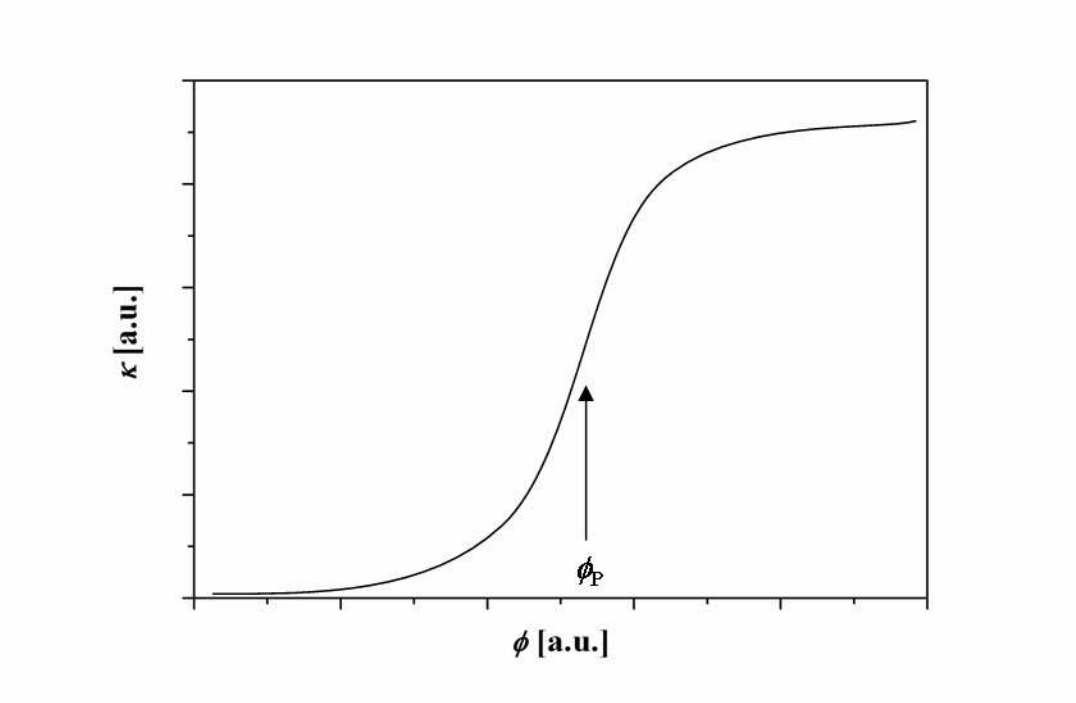

Figure I-9. Ideal conductivity behaviour of a "traditional" flexible microemulsion in dependence of volume fraction of polar phase. ϕ_P denotes the percolation threshold volume fraction.

Electric percolation phenomena can be explained by the formation of channels exchanging matter between the dispersed droplets and the continuous phase. Percolation can be induced by increasing volume fraction of the dispersed phase ϕ as well as by temperature *T*. When log(κ) is plotted versus ϕ or *T*, a sigmoid shape of the corresponding curve is observed.[105] The percolation threshold can then be calculated by fitting a fourth order polynomial to the curves and by setting the second derivate equal to zero, thus determining the inflection point of the curve.[106] Two models exist to explain the percolation phenomenon, static or dynamic. Dynamic percolation[102-103, 107] describes droplets that are in motion and the increase in conductivity is related to rapid fusion-fission processes among the dispersed droplets. Static percolation describes the idea of an isolating solution with solid conductors and is based on the appearance of a bicontinuous structure.[105] The increase in conductivity for w/o microemulsions can be explained by the existence of a water path through the system.

According to the most widely used dynamic percolation model, two pseudo phases can be assumed: one in which charge is transported by the diffusion of microemulsion globules and the other phase in which charge carriers itself diffuse in the reverse micellar cluster.[105] According to this theory two separate asymptotic power laws can be used to describe the conductivity behaviour above and below the percolation threshold ϕ_P along the oil dilution line.

$$\ln \kappa = \ln \kappa_1 + \mu \ln\left(\left|\phi - \phi_P\right|\right) \qquad \text{(above percolation threshold)} \qquad \textbf{(I-9)}$$

$$\ln \kappa = \ln \kappa_2 - s \ln\left(\left|\phi - \phi_P\right|\right) \qquad \text{(below percolation threshold)} \qquad \textbf{(I-10)}$$

The two characteristic parameters μ (equation I-9) and *s* (equation I-10) can be determined by the two slopes of the plot ln*k*($|\phi$-$\phi_P|$). Computer simulations determined parameters of $\mu = 1.94$ and $s = 1.2$ for dynamic percolation and $\mu = 2$ and $s = 0.6$-0.7 for static percolation.[107-108]

It is also possible to observe an “antipercolation” phenomenon in microemulsions. Conductance will decrease when droplet volume fraction or temperature is increased. *Ajith et al.*[109] observed such behaviour in dependence on temperature for water based systems at low temperature. At high temperatures finally percolation was induced. The decrease of conductivity at low temperatures was explained by the absence of interconnections between the droplets and the existence of a barrier for ions, preventing them traveling from one droplet to the other.

The viscosity of microemulsions can have characteristic features. It has been shown by *Cates & Candau*[110] that locally cylindrical and random flexible films are low viscous, while lamellar and other rarer structures such as "molten" cubic phases are forming extremely viscous microemulsions. Unfortunately, no accurate theory on the viscosity behaviour of microemulsions exists to date. Similar to conductivity measurements, equations for percolation have been suggested but a quantitative verification is only possible if the viscosity η of the polar compound is sufficiently different from η of the oil.[111] *Boned et al.*[21] replaced water in traditional microemulsions by glycerol and therefore fulfilled the precondition of highly different viscosities for polar and apolar phase. Hence, extraction of the critical parameters μ and s was possible.

3.2 Small Angle Scattering

Small angle scattering (SAS) techniques are a widely used tool for the characterisation of colloidal particles. Information about size, shape, and structure of the particles can be obtained. Therefore, the sample is irradiated with an incident wavelength λ that has to be in the same size range as the studied system.[112] Consequently, neutron in small angle neutron scattering (SANS) and X-rays in small angle X-ray scattering (SAXS) are the most widely used techniques applied to colloidal systems.

A typical setup of a scattering experiment is illustrated in Figure I-10. Radiation is focused on a scattering medium, for example colloidal particles in solution. A fraction of the radiation will be scattered, while the rest will pass unaffected through the sample. A detector is typically set up in line with the radiation source and the sample. The beams, incident or scattered ones are typically shaped by slits, apertures, or optics such as lenses.

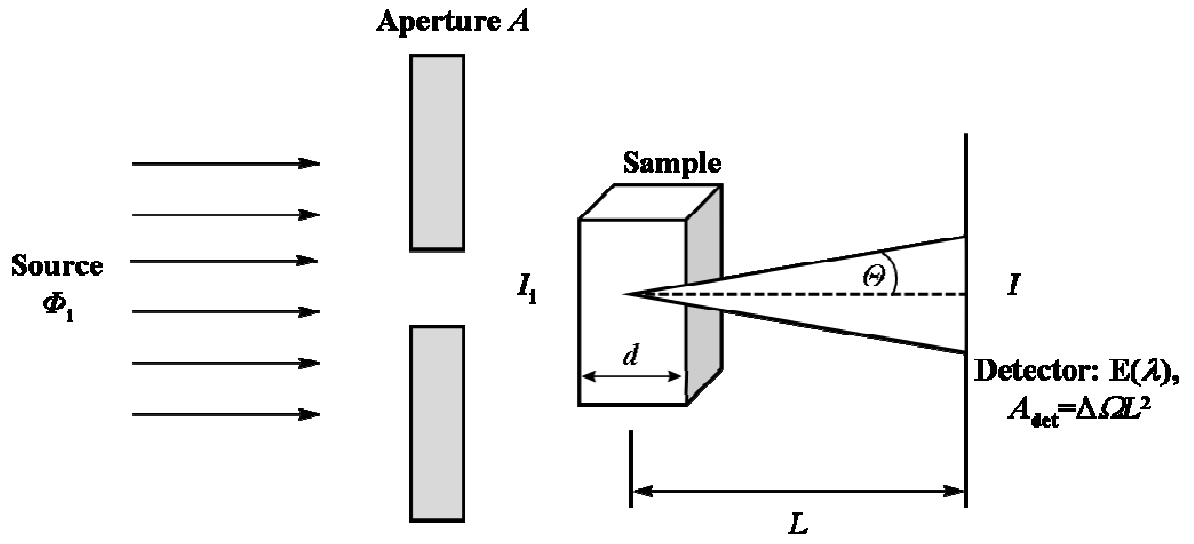

Figure I-10. General setup of a scattering experiment. Radiation source with incident flux Φ_i, sample aperture with area A, incident intensity I_i, sample with thickness d, detector with efficiency $E(\lambda)<1$ and surface area $A_{det} = \Delta\Omega L^2$ at distance L from sample position and at a scattering angle θ.

The scattering in a medium occurs from fluctuations in the sample that are associated to variations in the density of the scattering material. These are electrons in the case of X-ray scattering and nuclei in the case of neutron scattering. As this work deals with the application of static scattering methods to colloidal systems, the following paragraphs will exclusively emphasize this kind of scattering. Static scattering means that the dependence of scattering angle θ of the average scattering intensity I is measured, whereas the energy changes are neglected. In dilute systems this can lead to structural information by means of shape and size of the particles. In concentrated systems information can be collected about correlations like the average spatial arrangement of the particles.[112]

X-rays (λ = 0.5-2.3 Å) are scattered by electrons. Consequently, all observations result from a difference in the electron density. The scattering at a single electron is given by its scattering length $b_0 = 2.8 \cdot 10^{-15}$ m and the scattering of z electrons can hence be estimated to $b = zb_0$. In contrast, the scattering of neutrons is caused by different nuclei in the sample. The scattering length for nuclei can have significant differences as can be visualized on different isotopes, hydrogen ($b_H = -3.74\ 10^{-13}$ cm)[113] and deuterium ($b_D = 6.67\ 10^{-13}$ cm)[113]. According to this crucial discrepancy the scattering properties can be tuned by a partial or total deuteration. This advantage is not provided by the scattering of X-rays. The scattering lengths for the different nuclei can be found in literature.[113] From the scattering length, the more practical value of scattering length density ρ can be obtained (equation I-11). This is a real measure for the efficiency of a scattering probe and can be calculated for each compound according to:

$$\rho = \frac{\sum_{i=1}^{n} b_i}{V_m} = \frac{\rho_m N_A}{M} \sum_{i=1}^{n} b_i \qquad \textbf{(I-11)}$$

where M is the molar mass, V_M is the molar volume and N_A is *Avogadro*'s constant. Finally, the contrast of the whole scattered sample can be obtained by the difference of the scattering length of the particle, ρ_P, and the scattering length of the solvent, ρ_S, according to equation I-12.

$$\Delta\rho = \left|\rho_P - \rho_S\right| \qquad \textbf{(I-12)}$$

If an experimental setup as described before in Figure I-10 is considered, one can assume a radiation beam with a specific wavelength λ_i and Energy E_i that is focused on a sample with the thickness d. The incident radiation can be absorbed, scattered, or passed through the sample without interaction. The latter builds the principal point of the emerged beam. The important value transmission T is defined as ratio of the outgoing to the incoming intensity of the radiation beam at an angle $\theta = 0$ (equation I-13).

$$T = \frac{I(\theta = 0)}{I_i} = \exp[-\mu d] \qquad \textbf{(I-13)}$$

where μ is a linear attenuation factor. In general, only a small fraction of the incident radiation beam is scattered by the sample at an angle $\theta > 0$. Apart from scattering, an energy transfer between radiation and sample can occur. A typical scattering experiment is therefore just the observation of the scattering intensity I in dependence of the scattering angle θ and the energy E of the scattered beam in a distance L to the sample. The scattering curve ($I = f(\theta, E)$) then includes the complete information about the structure and the dynamics of the sample.

The scattering vector q should be mentioned here as it represents an important parameter for scattering. q can be related to the scattering angle θ according to equation I-14. The introduction of this parameter enables the comparison between measurements at different wavelengths, detector distances, and scattering angles. Finally, the scattering intensity can be discussed as a variation of the "momentum transfer" q.

$$q = \left|k_f - k_i\right| = \frac{4\pi n}{\lambda} \sin\frac{\theta}{2} \qquad \textbf{(I-14)}$$

The scattering vector is also defined as difference between incident wave vector k_i and scattered vector k_f. This relation is illustrated in Figure I-11.

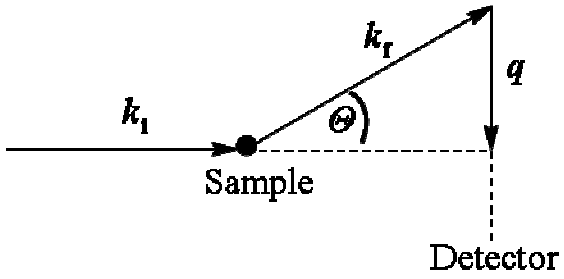

Figure I-11. Definition of scattering vector q. k_i: incident wave vector, k_f: scattered wave vector, θ: scattering angle.

As mentioned at the beginning of this chapter, static scattering experiments build the core of this work and hence the focus will lie on experiments where the energy transfer can be neglected ($E \cong 0$ and $\lambda \cong \lambda_i$). A small angle in the experimental setup is defined as $\theta \leq 10°$.[112]

The incident intensity per second can be written as:

$$I_i(s^{-1}) = \Phi_i(\lambda) A E(\lambda) \qquad \textbf{(I-15)}$$

where A is the area of the used aperture, defining the size of the beam. The incident radiation has a flux $\Phi_i(\lambda)$. At a defined scattering angle θ and at a distance L (cm) the scattered intensity I is observed within a solid angle $\Delta\Omega$ on the detector with the efficiency $E(\lambda)$ <1 and the detector area $A_{det} = \Delta\Omega L^2$. The beam interacts with the sample at the position x ($0 \leq x \leq d$) with a probability of $\mathrm{d}\sigma/\mathrm{d}\Omega$ per unit solid angle. For the sake of simplicity the assumption is made that only one scattering process occurs. Before the beam can interact with the sample, the incident intensity is attenuated by a factor $\exp[-\mu x]$ with μ being a sample and radiation specific linear attenuation coefficient. After the scattering process the scattered intensity as well is attenuated by the sample with the factor $\exp[-\mu(d-x)]/\cos\theta$. The intensity that can finally be measured at a scattering angle θ is obtained after integration over the sample along x (equation I-16).[112]

$$I(\theta) = \int_0^d \phi_x E \Delta\Omega \exp[-\mu x] A \rho \frac{\exp[-\mu(d-x)]}{\cos\theta} \frac{\mathrm{d}\sigma}{\mathrm{d}\Omega} \mathrm{d}x \qquad \textbf{(I-16)}$$

As the angles θ for neutrons and X-rays are sufficiently small the assumptions that $\cos\theta \approx 0$ holds and one obtains $I(\theta)$ from equation I-17.

$$I(\theta) = \Phi_i E \Delta\Omega A d \exp[-\mu d] \rho \frac{\mathrm{d}\sigma}{\mathrm{d}\Omega} = \Phi_i E \Delta\Omega A d \exp[-\mu d] \frac{\mathrm{d}\Sigma}{\mathrm{d}\Omega} = \Phi_i E \Delta\Omega A d T \frac{\mathrm{d}\Sigma}{\mathrm{d}\Omega} \qquad \textbf{(I-17)}$$

Equation I-17 is basically composed of two separate terms, one term being the instrumental constant C(λ).

$$C(\lambda) = \Phi_i E \Delta\Omega A = I_i \Delta\Omega \qquad \textbf{(I-18)}$$

This term depends on the configuration of the experimental setup itself, wavelength, type of detector, collimation distances, and the size of the sample aperture. The second term, $\mathrm{d}T\mathrm{d}\Sigma / d\Omega$ on the contrary is specific to the sample only.[112]

$\mathrm{d}\Sigma/\mathrm{d}\Omega$ is the sample's differential scattering cross section per unit sample volume and can be derived from the differential scattering cross section of the sample per unit solid angle, $\mathrm{d}\sigma/\mathrm{d}\Omega$. As the experiment comprises comparing the incident intensity I_i with the scattered intensity I measured at an angle θ and a distance L on the detector with an area A_det, the ratio of both intensities is called the differential scattering cross section per unit solid angle (equation I-19).[112]

$$\frac{IL^2}{I_i} = \frac{\mathrm{d}\sigma}{\mathrm{d}\Omega}(cm^2) \qquad \textbf{(I-19)}$$

Normalization to unit sample volume V (cm^3) yields finally the differential scattering cross section per unit sample volume (equation I-20).

$$\frac{\mathrm{d}\Sigma}{\mathrm{d}\Omega}(cm^{-1}) = \left(\frac{1}{V}\right)\frac{\mathrm{d}\sigma}{\mathrm{d}\Omega} \qquad \textbf{(I-20)}$$

$\mathrm{d}\Sigma/\mathrm{d}\Omega$ represents the probability of a wave of the incident beam being scattered out from the unit sample volume into the solid angle $\Delta\Omega$.[112]

The scattering intensity is also proportional to the form factor ($P(q)$) for an ideal diluted solution, where the particles are independent from each other. When the concentration increases, interactions between the particles increase as well and the position of one particle is no longer independent from the position of the others. The interaction between the particles is described by the structure factor, $S(q)$. The scattering intensity therefore can be described as well as:

$$I(q) = nP(q)S(q) \qquad \textbf{(I-21)}$$

where n is the number density, $n = N/V$.

Small angle scattering experiments comprise several steps, including measurements of the sample intensity, background, standard cells, and transmission measurements. SAS has been applied widely to colloidal systems, among those also to microemulsions. As microemulsions

do not represent dilute systems at all the scattering is usually broad and intensity is dependent on both form and structure factor. Additionally, the broad peak is usually followed by a q^{-4} decay at high q-values. These observations hold well for traditional aqueous[114-116] as well as for IL-based[25, 28, 33, 117] microemulsions.

There are three general methodologies used to determine a microstructure:

- Direct evaluation of some features of the microstructure, such as specific area and invariant.
- Fitting the scattering data by a parametric expression.
- Using dilution lines and comparing experimental data to theoretical models.

Direct determination from the scattering curve

The two most important parameters are specific area Σ (cm^2/cm^3) and volume fraction ϕ. In the common case of a sample composed of two homogenous media 1 and 2, characterized by the two scattering length densities ρ_1 and ρ_2 (cm^{-1}), the volume fraction has to be determined by the composition in the sample, independent to the scattering experiment. In the case of microemulsions one medium corresponds to the polar phase and the other one to the apolar phase. The specific area can be determined by *Porod*'s law.[118] For a sharp interface the scattering intensity $I(q)$ decreases with q^{-4} at large q-values (equation I-22).[112]

$$\lim_{q\to\infty}(Iq^4) = 2\pi^2\Delta\rho^2\Sigma \qquad \textbf{(I-22)}$$

where $\Delta\rho = \left|\rho_{polar} - \rho_{apolar}\right|$ is the contrast between the scattering densities of the two media, the polar and the apolar one. The *Porod* regime in general is just observed after the subtraction of the background. From the plot $I(q)q^4$ versus q^4 as $I(q)q^4 = B + Aq^4$ the background A can be determined.

At least mathematically one can go far enough in q so that a piece of surface is isolated and not correlated to any other part of the surface. At a rough surface no *Porod* limit can be deduced.[119] In contrast, if the surface allows a determination of the Prod limit another important value can be calculated, the experimental invariant Q_{exp}.[112] The experimental invariant is calculated according to equation I-23, where the integral goes from zero to infinity. As the experiment is limited to an experimental q-range, a term has to be added that takes this contribution into account.

$$Q_{\exp} = \int_0^{\infty} I(q)q^2 \mathrm{d}q = \int_0^{q_{\exp}} I(q)q^2 \mathrm{d}q + \frac{[I(q)q^4]}{q_{\exp}} \qquad \textbf{(I-23)}$$

The invariant owns its name the fact that the value is independent from the structure of the sample and thus depends on the composition.[112] The value of the experimental invariant should be equal to the value of the theoretical invariant Q_{theo} that can be calculated independently of the experiment according to equation I-24.

$$Q_{theo} = 2\pi^2 \Delta\rho^2 \phi_{pol}(1-\phi_{pol}) \qquad \textbf{(I-24)}$$

A mismatch of the two invariants, the experimental and theoretical one, is either an experimental error or an evidence of an expected or unexpected high solubility of the surfactant in one of the phases present.[112]

Fitting of the present scattering curve

The introduction of two length scales to describe microemulsions is of main interest. This can be realised by fitting the scattering data to a parametric expression of the intensity which merges at high q to the *Porod* limit. This has been proposed by *Teubner & Strey* in 1987[115] (equation I-25) and has been widely applied to aqueous and non-aqueous microemulsions.

$$I_{TS}(q) = \frac{I_0}{a + bq^2 + cq^4}. \qquad \textbf{(I-25)}$$

In the case of an absolute scale the constant I_0 is given by $8\pi c\left\langle \phi(1-\phi)\Delta\rho^2 \right\rangle / \xi$. The corresponding correlation function can be achieved by *Fourier* transformation and finally delivers equation I-26

$$g_{TS}(r) = \exp\left(\frac{-r}{\xi}\right)\left[\frac{\sin(\pi r/d)}{2\pi r/d}\right] \qquad \textbf{(I-26)}$$

where the domain size d (periodicity of the polar or non-polar domains, equation I-27) and the correlation length ξ (equation I-28) represent two characteristic length scales. The stability condition $(4ac\text{-}b^2)>0$ with $a>0$, $b<0$, and $c>0$ must be fulfilled for the parameters.

$$d = 2\pi\left[\frac{1}{2}\sqrt{\frac{a}{c}} - \frac{1}{4}\frac{b}{c}\right]^{-1/2} \qquad \textbf{(I-27)}$$

$$\xi = \left[\frac{1}{2}\sqrt{\frac{a}{c}} + \frac{1}{4}\frac{b}{c}\right]^{-1/2} \qquad \textbf{(I-28)}$$

The position of the maximum q_{max} can be calculated from the two length scales according to equation I-29.

$$q_{max} = \left[\left(\frac{2\pi}{d} \right)^2 - \frac{1}{\xi^2} \right]^{1/2} \qquad \textbf{(I-29)}$$

The analytic expression proposed by *Teubner & Strey* (equation I-25) can be used to fit the experimental data directly. Alternatively, the data can be plotted as $I_0/I(q)$ versus $(q\text{-}q_{max})^2$, where a figure close to a parabola is found (equation I-30).

$$I_{TS}(q) = \frac{I_0}{(1 - I_0 / I_{max})(q^2 / q_{max}^2 - 1)^2 + I_0 / I_{max}} \qquad \textbf{(I-30)}$$

$I_{max} = I(q_{max})$ is the maximum scattering intensity.

Additional information from the *Teubner-Strey* fit can be extracted from the ratio d/ξ, which provides information about the polydispersity of the microstructure present. A high value corresponds to a high polydispersity and *vice versa*. A further important variable, the amphiphilic factor f_a (equation I-31), can be calculated from the fitting parameters.[89, 114]

$$f_a = \frac{b}{(4ac)^{1/2}} \qquad \textbf{(I-31)}$$

The amphiphilic factor approaches unity for the disorder line where the system loses its quasiperiodic order. $f_a = -1$ corresponds to the liquid crystalline lamellar phase. Both values limit the range where microemulsions can be found.[120] The factor seems to range between -0.9 and -0.7 for well-structured bicontinuous microemulsions, which was also found by *Teubner & Strey*.[114]

Dilution lines and theoretical models

Microstructures can be seen as a dispersion of spheres without ambiguity. Dilution lines are necessary because other microstructures cannot be ascertained by studying only one sample. Several samples have to be measured along one dilution line and the results have to be compared to predictive models from literature to ensure the existence of a certain microstructure.

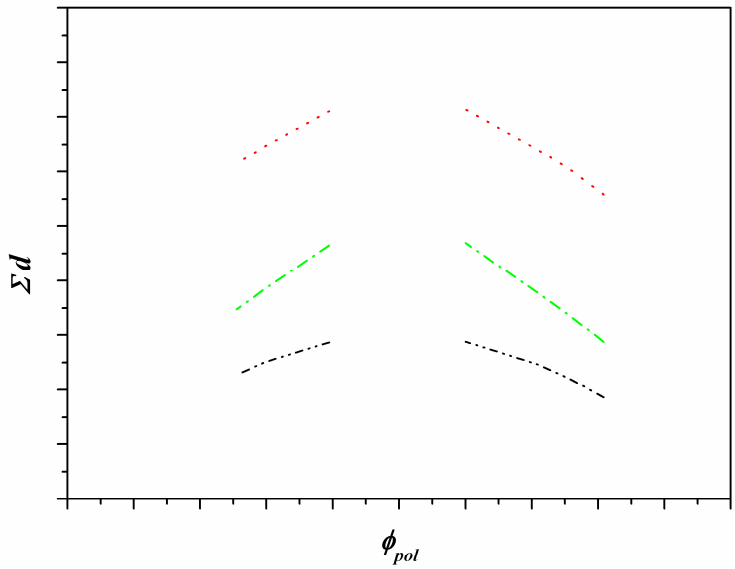

Figure I-12. Schematic illustration of a dilution plot including the cubic random cell model (black), the model of o/w and w/o microstructure, respectively (green), and the model of repulsive spheres (red).

The so-called dilution plot[121] (Figure I-12) has to be constructed as follows: the value of specific area Σ multiplied by the domain size d obtained from *Teubner-Strey* evaluation is plotted against the polar volume fraction ϕ_{pol}. Theoretical models that can be used to compare the experimental data will be discussed in the following.

Cubic random cell model (CRC)

This model is valid for bicontinuous structures in a polar volume fraction range of $0.18<f_{pol}<0.82$[122] and assumes that the structure can be described by a set of cubes of the size d^* filled with water or oil. It was first described by *Jouffroy et al.*[123] The size is given by equation I-32, but also can be set equal to the domain size d obtained from *Teubner-Strey* evaluation.

$$d^* = \frac{2\pi}{q_{max}} \qquad \textbf{(I-32)}$$

Finally, for cubic random cells equation I-33 should hold.

$$\Sigma d = 6\phi_{pol}(1-\phi_{pol}) \qquad \textbf{(I-33)}$$

Zemb could show that the factor of 6 is not correct and the precise value is 5.84,[124] a change that does not have any influence on the final results and therefore can be neglected.

Spheres of water in oil or oil in water, respectively

The relation that holds in this case can be expressed as[112]:

$$\Sigma d = 4.84\phi^{1/3} \qquad \textbf{(I-34)}$$

where the volume fraction of the inner phase should be used.

Repulsive spheres

For repulsive spheres a slightly different equation holds in comparison to w/o or o/w spheres.[112] Equation I-35 shows the relation that has to be taken into account to evaluate the microstructure.

$$\Sigma d = 4.32\phi^{2/3} \qquad \textbf{(I-35)}$$

Again, the volume fraction of the potential inner phase has to be used.

The model of disordered and connected structures: locally cylinders or lamellae

Connected cylinders can be represented by "molten" hexagonal or cubic phases that have lost long range order while connected lamellae are a disordered state of a smectic phase.[112]

Disordered lamellae is the likely microstructure if spontaneous curvature is low compared to d^*, while connected cylinders is the likely microstructure at high surfactant content and high curvature.

A complete set of microstructure begins with a set of *Vornoï* polyhedra constructed on seed points of density n (cm^{-3}). Instead of filling each cell by water or oil like in simple microemulsion models mentioned before. The cells are splitted according to volume fraction and either cylinders perpendicular to cell faces or some flat pentagons or hexagons on the faces of cells are constructed.[112]

In general CRC models give a good approximation for flexible films. If strong curvature constants come into play, gradual transformation of a microstructure from droplets to locally connected cylinders and finally disordered lamellae (sponge or vesicles) are the relevant microstructures.

Checking the presence of connected microstructures starts when the three parameters volume fraction ϕ, specific area Σ, and packing parameter p are determined. The density n of *Poisson* points equivalent to the scattering peak position d^* and the connectivity Z can be calculated by solving three implicit equations:

$$\phi = \left[\frac{4\pi}{3} R^3 - \frac{1}{3} Z r^3 \left(\Omega \rho^3 - \pi \sqrt{(\rho^2 - 1)} \right) \right] n + \pi R^2 Z \left[\frac{8.15 n^{2/3}}{13.4} - nr \sqrt{(\rho^2 - 1)} \right] \qquad \textbf{(I-36)}$$

$$\Sigma = \left[(4\pi - \Omega Z) R^2 n + 2\pi Z r \left(\frac{8.15 n^{2/3}}{13.4} - nr \sqrt{(\rho^2 - r)} \right) \right] \qquad \textbf{(I-37)}$$

where $\rho = R/r$ and $\Omega = 2\pi(1 - \sqrt{(\rho^2 - 1)})$. The packing parameter *p* is an imposed value for the constraint of the average film curvature and is given by:

$$p = \frac{\phi(R + l, Z, n) - \phi(R, Z, n)}{l\Sigma(R, Z, n)} \qquad \textbf{(I-38)}$$

For solving this equation a program written in BASIC is available from *Zemb*. This allows to predict the peak position shift versus composition and to prove the existence of connected structures.[112, 121, 124-126]

II. Experimental Section

1. Methods

1.1 Analytical Methods

^{1}H-NMR and ^{13}C-NMR spectra were recorded on a FT-NMR-spectrometer of the type *Bruker Avance* 300 (^{1}H: 300 MHz; ^{13}C: 75 MHz) at ambient temperature. Results are reported as follows: chemical shift in ppm from internal $CHCl_3$ (7.26 ppm) as standard on the δ_H scale, multiplicity (s = singlet, d = doublet, t = triplet, q = quartet, qt = quintet, and m = multiplet), integration and coupling constant (Hz). ^{13}C chemical shifts are reported in ppm from internal $CHCl_3$ (77.2 ppm) as standard on the δ_H scale.

Mass spectrometry was performed on a *Varian* MAT 311A, *Finnigan* MAT 95 or *Thermoquest Finnigan* TSQ 7000 at the Central Analytical Laboratory (Universität Regensburg).

The water content of all products was determined by coulometric *Karl-Fischer* titration using an *Abimed* MCI analyser (Model CA-02).

Differential scanning calorimetry (DSC) measurement of [emim][$etSO_4$] was performed on a *Mettler* DSC 30 by using aluminium crucibles. The heating rate was 10 °C/min. The glass transition temperature was determined by using the half-step temperature of the transition.

Decomposition temperature of [emim][$etSO_4$] was measured on a thermogravimetric analyser from *Perkin-Elmer* TGA 7. The heating rate was 10 °C/min, applying a continuous nitrogen flow. The decomposition temperature was determined by onset analysis of mass loss.

Gas chromatography (GC) analysis of $C_{10}E_4$ was performed on a HP 6890 analyser equipped with an autosampler and a flame ionization detector (FID). A HP-5 column and high-purity helium carrier gas were used. Injection temperature: 250 °C. Detection temperature: 300 °C. Program: 5 min isothermal at 125 °C, temperature range 25 °C/min up to 250 °C, isothermal 25 min at 250 °C.

1.2 Phase Diagrams

Ternary Phase Diagram

The ternary phase diagram was recorded at 25 ± 0.2 °C according to a procedure reported by *Clausse et al.*[127] Different ratios of surfactant to limonene were prepared in 5 wt% steps between (0 and 100) wt% of the surfactant. The IL was added dropwise under nitrogen flow. The weight fractions at which transparency-to-turbidity occurred were derived from precise weight measurements. As the system showed very slow kinetics and tended to form stable clear emulsions that separate after several hours, the time of adding a drop to the initial solution had to be increased to several hours. The procedure was repeated starting from surfactant/[emim][$etSO_4$] mixtures adding limonene and starting from [emim][$etSO_4$]/limonene mixtures adding surfactant. This procedure resulted in trustworthy phase diagrams, mirroring the exact position of the single phase region.

„Fish"-Cut

The pseudo-binary phase diagrams were achieved at a constant [emim][$etSO_4$] to limonene mass ratio (1:1) with the variables temperature and surfactant content. This so-called "fish"-cut was recorded by adding surfactant to the 1:1 (m/m) mixture of the two solvents in order to obtain surfactant mass fractions within (2 - 35) wt%. The samples were first heated at 60 °C and subsequently cooled in an ice bath to homogenize the mixtures. Finally, the samples were equilibrated in a thermostated (± 0.2 °C) sample holder and heated slowly, allowing the resulting phases to be counted. The equilibration time was set between 12 and 24 hours due to long segregation times.

Segregation Temperatures

The segregation temperatures were recorded using a precise cryostat (± 0.02 °C) FP40 from *Julabo* for temperature control. Microemulsions with varying compositions along the experimental path have been prepared and subsequently cooled down. Segregation temperatures may be understood as transition of transparency to turbidity or freezing of one of the components. The accuracy in the value of the segregation temperature was evaluated to be better than ± 0.5 °C.

1.3 Surface Tension Measurements

Surface tension measurements were carried out on a *Krüss* processor tensiometer K100MK2. The sample holder was equipped with a precision thermostating system with an uncertainty of ± 0.1 °C. For surfactant/water measurements a double dosing system (*Methrom* Liquino 711) was used which allows an automatic recording of surface tension versus surfactant concentration. For surfactant/IL measurements the dosing equipment was not adaptive. However, a sample holder is available with a maximum sample volume of 2 mL. The sample environment for surfactant/IL measurements was Argon.

1.4 Conductivity

Conductivity measurements were performed on an in-house built apparatus described by *Barthel et al.*, equipped with a precision thermostat, symmetrical *Wheatstone* bridge with *Wagner* earth, sine generator, and resistance decade.[128] The temperature was kept constant to ± 0.003 °C. Triton X-100, Triton X-114 and $C_{10}E_4$ based microemulsions were measured at 25 °C along a certain experimental path, while the surfactant concentration was kept constant. For $C_{10}E_4$ based microemulsions the conductivity additionally was measured at 0 °C and -15 °C. A set of six three-electrode capillaries with cell constants ranging from 2 m^{-1} to 1161 m^{-1} was used. Cell constants were determined with aqueous KCl solutions according to a procedure described by *Wachter et al.*[129] Resistances *R* were aligned at frequencies *v* between 480 Hz and 10 kHz. The resistance value at infinite frequency used to calculate the conductivity was obtained by linear extrapolation of the curve *R* versus (1/*v*).[129] The relative uncertainty of the electrical conductivities was estimated to be less than 0.5 %. The cell constants *C* for the six capillaries used within this work are summarized in Table II-1.

Table II-1. Cell constants of the utilized capillaries for measuring conductivities.

Cell number	C [m^{-1}]
1	2.084
2	24.61
3	53.6
4	224
5	470
6	1161

Cell constants are temperature dependent as they are affected by the expansion coefficient of platinum (electrode material) and *Pyrex* glass (cell material). The temperature dependence can be expressed as:

$$B(T) = B(298.15\ K)(1 + \beta(T - 298.15\ K)) \qquad \textbf{(II-1)}$$

where β is the temperature coefficient (equation II-2).

$$\beta = \frac{1}{B(298.15\ K)} \frac{\mathrm{d}B}{\mathrm{d}T} \qquad \textbf{(II-2)}$$

Hence, the temperature coefficient depends on the type of capillary that is applied. *Robinson & Stokes*[130] as well as *Barthel* and coworkers[129] described this correlation. A β value of $-3.5 \cdot 10^{-6}\ K^{-1}$ was found for capillary cells. This value changes the conductivity values only within the uncertainty limits. Therefore, temperature dependences of cell constants were not taken into account.

1.5 Viscosity

Dynamic viscosities were measured on a *Bohlin Instruments* rheometer CVO 120 under argon atmosphere and controlled temperature (± 0.5 °C). A cone plate system (CP40/4°) with shear rates of (10 - 400) cm^{-1} was used. Measurements were performed for all microemulsions along the experimental path at 25 °C and for the temperature stable samples in a temperature range of (10 - 60) °C. *Newtonian* behaviour for all microemulsions along the experimental path at different temperatures was found. Consequently, the usage of a capillary viscometer was justified.

Kinematic viscosities for Triton X-100 based microemulsions were measured with a modified automated AVS/G capillary viscometer (*Schott*) as described in literature.[131] The viscosity measurements were conducted in two micro-*Ubbelohde* capillaries (*Schott Instruments*, type 537 20 / II and III), which were placed in a Dewar flask that was connected to a high precision thermostat[128, 132] with a circulation pump. The overall temperature uncertainty of this setup was less than 0.003 °C. The samples were kept under dry nitrogen throughout the measurements by means of an in-house built setup-modification. The capillaries' constants were confirmed with certified viscosity standard oil (50 BW, *ZMK-Analytik*, relative uncertainty 0.32 %) at various temperatures, with a flow time reproducibility of better than ± 0.05 %. The viscosities are average values of 3 to 10 single runs and the estimated uncertainty

of presented viscosity data was less than 0.5 % with respect to the accuracy of the thermostat. The cell constants *K* of the two capillaries can be found in Table II-2.

Table II-2. Cell constants of the two utilized capillaries for measuring kinematic viscosities.

Cell type	K [mm^2/s^2]
53720 / II	0.094530
53720 / III	0.99620

Kinematic viscosities for Triton X-114 and $C_{10}E_4$ based microemulsions were measured on a falling sphere viscometer AMVn from *Anton Paar*. Triton X-114 based microemulsions were measured from 40 °C down to 5 °C. $C_{10}E_4$ based systems from 30 °C down to 5 °C. Four capillaries with differing diameters were used (4.0 mm^2 for viscosities ranging from 80-2500 mPas, 3.0 mm^2 for viscosities ranging from 20-230 mPas, 1.8 mm^2 for viscosities ranging from 2.5-70 mPas, and 1.6 mm^2 for viscosities ranging from 0.3-10 mPas).

1.6 Density

Temperature dependent density measurements were performed on a vibrating tube densimeter DMA 5000 M from *Anton Paar*. Measurements at 25 °C were measured on an *Anton Paar* DMA 60 instrument equipped with a precision thermostat. The uncertainty in densities was estimated to be less than 0.1 kg/m^3. Densities were used to calculate volume fractions from mass ratios as well as for calculations of dynamic viscosities from measured kinematic viscosities.

1.7 Small Angle X-Ray Scattering (SAXS)

SAXS measurements were carried out at the institute ICSM (CEA, Marcoule, France).

Small and wide angle X-ray scattering data were obtained using a XENOCS setup. The X-ray beam originates from a Mo GENIX source. The K_α radiation ($\lambda = 0.71$ Å) is selected using a multilayered curved mirror (one reflexion) focusing the beam towards infinity. The size of the beam (< 1 mm) in front of the sample is defined by scatterless slits provided by *FORVIS*. Sample and empty cell transmissions are determined using an offline pin-diode that can be inserted downstream the sample. The sample distance to the detector 2D MAR345 is 750 mm. A *q*-range between (0.02 - 2.5) $Å^{-1}$ was covered. Quartz capillaries from *Hilgenberg*

(Malsfeld, Germany) are used as sample containers with a wall thickness of 0.01 mm and a total thickness of 2 mm; usual corrections for background (empty cell and detector noise) subtractions and intensity normalization using *Lupolen*^{TM} as standard were applied. Figure II-1 illustrates a schematic image of the equipment used.

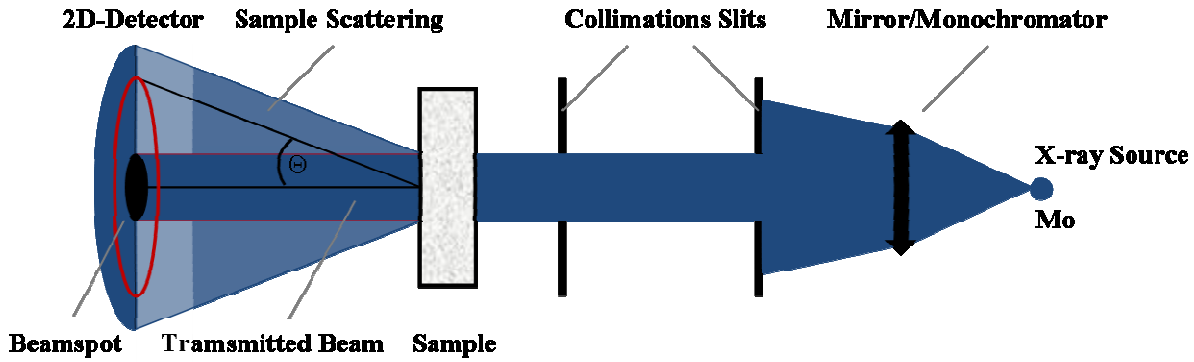

Figure II-1. Illustration of the used SAXS equipment at the institute ICSM, CEA, Marcoule, France.

The samples were measured at room temperature and additionally in a temperature range from 40 °C down to -10 °C for temperature stable compounds. Temperature control was guaranteed by a connected heating/cooling system which allows a temperature regulation with an uncertainty of ± 0.1 °C.

2. Chemicals

(*R*)-(+)-Limonene (97 %, 98 %*ee*/GC) was obtained from Sigma-Aldrich, dried over molecular sieves (3 Å) and redistilled before usage. The water content determined by Karl Fischer Titration was less than 100 ppm. Triton X-100 and Triton X-114 were purchased from Fluka and dried under vacuum at 80 °C for 4 days, yielding a final water content of less than 20 ppm for Triton X-100 and less than 40 ppm for Triton X-114. Diethylsulfate (Aldrich, 98 %) was used as received. 1-Methylimidazole (Roth, ≥99 %) was refluxed over KOH plates and distilled off afterwards, stored over molecular sieves and redistilled prior to use. Tetraethylene glycol (99 %) and 1-bromodecane (98 %) were obtained from Sigma-Aldrich and used as received.

Solvents, unless otherwise mentioned were of analytical grade. Water was used from a Millipore system. Chemical structures of (*R*)-(+)-limonene, Triton X-100 and Triton X-114 are given in Figure II-2.

(*R*)-(+)-limonene

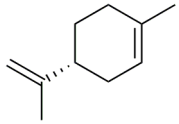

Triton X

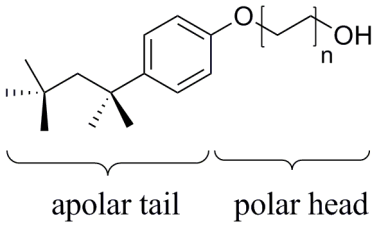

Triton X-100: n = 9-10
Triton X-114: n = 7-8

Figure II-2. Chemical structure of (*R*)-(+)-limonene, Triton X-100 and Triton X-114 surfactants.

3. Synthesis

1-Ethyl-3-methylimidazolium ethylsulfate ([emim][etSO_4]) (Figure II-3) was prepared according to a literature procedure by the reaction of equimolar amounts of 1-methylimidazol and diethylsulfate in toluene.[133] To an ice cooled solution of 1-methylimidazole (1.0 eq., 80 mL, 1.0 mol) in 300 mL toluene, diethylsulfate (1.0 eq., 131 mL, 1.0 mol) was added dropwise over a period of 5 hours under nitrogen atmosphere. The solution was stirred over night at ambient temperature. The finally obtained IL was insoluble in toluene. The product was washed three times with toluene (200 mL) and dried under high vacuum at 40 °C for 4 days.

^{1}H-NMR (300 MHz, $CDCl_3$): δ_H = 9.39 (s, 1H, NC**H**N), 7.49 (d, 2H, *J* = 1.6 Hz, NC**H**C**H**N), 4.24 (q, 2H, *J* = 7.4 Hz, NC$\mathbf{H}_2CH_3$), 4.02 (q, 2H, *J* = 7.1 Hz, $CH_3C\mathbf{H}_2SO_4^-$), 3.94 (s, 3H, NC$\mathbf{H}_3$), 1.48 (t, 3H, *J* = 7.4 Hz, C$\mathbf{H}_3CH_2SO_4^-$), 1.21 (t, 3H, *J* = 7.1 Hz, $NCH_2C\mathbf{H}_3$).

^{13}C-NMR (300 MHz, $CDCl_3$): δ_C = 137.1, 123.8, 122.0, 63.3, 45.1, 36.3, 15.5, 15.2.

MS (EI-MS); *m/z* (%): 111.0 [M^+], 347.1 [$(2M^+ + X^-)^+$], 819.4 [$(4M^+ + 3X^-)^+$], 1055.5 [$(5M^+ + 4X^-)^+$], 124.9 [X^-], 361.0 [$(2X^- + M^+)^-$], 597.2 [$(3X^- + 2M^+)^-$], 833.3 [$(4X^- + 3M^+)^-$], 1069.4 [$(5X^- + 4M^+)^-$].

Water content (Karl-Fischer titration): 25 ppm (m/m).

Glass transition temperature (DSC): T_g = -80 °C.

Decomposition temperature (TGA-onset): T_d = 356 °C.

1-ethyl-3-methylimidazolium ethylsulfate
[emim][etSO_4]

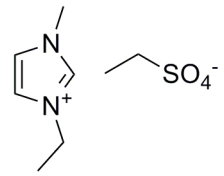

Figure II-3. Chemical structure of [emim][etSO_4].

Tetraethyleneglycol monodecylether ($C_{10}E_4$) (Figure II-4) was prepared by reaction of 1-bromodecane and tetraethyleneglycol. Excess tetraethyleneglycol (173 mL, 1.0 mol) and an aqueous solution of 50 wt% NaOH (1 eq., 8 g, 0.2 mol) were heated up to 100 °C. 1-Bromodecane (1eq., 42 mL, 0.2 mol) was added dropwise under continuous stirring over a period of 5 hours. The reaction mixture was stirred for 24 hours at that temperature, cooled down, and extracted three times with n-hexane. The combined organic phases were washed with brine and dried over Na_2SO_4. After evaporation of n-hexane the crude product was obtained. A subsequent fractional distillation finally delivered the product ($p = 1 \cdot 10^{-3}$ mbar, T_b = 140-145 °C) in high purity as colourless oil.

^{1}H-NMR (300 MHz, $CDCl_3$): δ_H = 3.58 (m, 16H, O-(C**H**$_2$-C**H**$_2$-O)$_4$-H), 3.39 (t, 2H, J = 6.8 Hz, CH_3-$(CH_2)_7$-CH_2-C**H**$_2$-O), 2.82 (s, 1H, O**H**), 1.52 (qt, 2H, J = 6.8 Hz, CH_3-$(CH_2)_7$-C**H**$_2$-CH_2-O), 1.21 (m, 14H, CH_3-(C**H**$_2$)$_7$-CH_2-CH_2-O), 0.82 (t, 3H, J = 6.6 Hz, C**H**$_3$-$(CH_2)_7$-CH_2-CH_2-O).

^{13}C-NMR (300 MHz, $CDCl_3$): δ_C = 77.6, 77.1, 76.7, 72.6, 71.5, 70.6, 70.5, 70.0, 61.6, 31.9, 29.6, 29.5, 29.5, 29.3, 26.1, 22.6, 14.1.

MS (CI-MS, NH_3); *m/z* (%): 352.2 (100.00) [MNH_4^+], 335.2 (12.88) [MH_4^+].

Water content (Karl-Fischer titration): 30 ppm (m/m).

GC analysis: purity ≥99 %, t_r = 14.69 min.

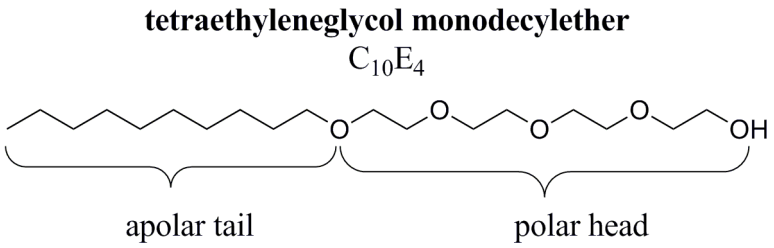

Figure II-4. Chemical structure of tetraethyleneglycol monodecyl ether ($C_{10}E_4$).

III. Results and Discussion

1. Critical Aggregation Concentrations of Non-Ionic Surfactants in [emim][etSO$_4$]

1.1 Introduction

The self-assembly of surfactant molecules is a key characteristic for several applications like nanoparticle synthesis, drug delivery, and separation processes. Not only is the formation of aggregated surfactant structures in water of importance, but also in non-aqueous solvents like ionic liquids (ILs). Micelle formation of alkyltrimethylammonium bromides, alkylpyridinium bromides and octylphenol ethoxylate (TX-100) in EAN was first reported almost 30 years ago.[38-39, 84] In addition to micellar structures in binary IL/EAN mixtures, liquid crystals of lipids in EAN have been identified.[85] However, there has been a renewed strong research interest in this field. ILs as solvents to promote self-assembly have been reviewed in 2005[134] and more recently in 2007[16] and 2008.[17] Some general conclusions can be drawn from the data available in the literature. The critical micelle concentration (cmc) is significantly higher in ILs compared to water. For example *Evans et al.* found that the cmc of conventional surfactants in EAN is between 5 and 10 times higher compared to the cmc in water.[84] *Greaves et al.* studied the self-assembly behaviour of amphiphiles in 22 different protic ILs,[4] where 14 of those were found to promote self-assembly of amphiphiles. The concept of the *Gordon* parameter, which represents a measure of the cohesive energy density of a solvent and hence the driving force of a solvent as promoter for self-assembly was applied to these systems. In the past, it was generally accepted that no amphiphilic aggregation exists for solvents with a *Gordon* parameter below 1.3 J/m^3.[135] Nowadays, ethylammonium butyrate with a value of 0.576 J/m^3 is the solvent with the lowest *Gordon* parameter reported to promote self-assembly of amphiphiles.[136] This phenomenon is not restricted to protic ILs. It has been documented for several aprotic ILs as well.[86-88]

The main part of this work deals with the formulation and characterization of microemulsions using an aprotic ionic liquid, [emim][etSO$_4$] as polar phase and limonene as oil phase. Three non-ionic surfactants were studied, Triton X-100 (HLB = 13.5), Triton X-114 (HLB = 12.4), and $C_{10}E_4$ (HLB = 10.5). First of all, the possibility to form aggregated structures in

[emim][$etSO_4$] was investigated by means of surface tension measurements. HLB is the abbreviation for hydrophilic lipophilic balance and can be calculated for each surfactant according to:

$$HLB = 20\frac{M_H}{M} \qquad \textbf{(III-1)}$$

where M_H denotes the molar mass of the hydrophilic part of the molecule and M the molar mass of the whole molecule. The HLB value is a measure of the degree to which a surfactant is hydrophilic or lipophilic. HLB values are given on a arbitrary scale of 0 to 20. An HLB of 0 corresponds to a completely hydrophobic molecule and an HLB of 20 to a completely hydrophilic molecule.

Critical micellar concentrations of Triton X-100 have extensively been studied in various ionic liquids, but are scarce for Triton X-114 and $C_{10}E_4$. In this context it should be stressed that $C_{10}E_4$ is a pure surfactant synthesized in the lab and the other two surfactants are commercially available. In Table III-1 cmcs for Triton X-100 in various ionic liquids documented in the literature are summarized.

Table III-1. Cmc for Triton X-100 in different ionic liquids.

solvent	method	cmc [mol/L]	reference
EAN	surface tension	$5.9\cdot10^{-3}$	*Evans et al.*[84]
[bmim][BF_4]	surface tension	0.33	*Gao et al.*[137]
[bmim][PF_6]	surface tension	0.76	*Gao et al.*[137]
[emim][Tf_2N]	near infrared spectroscopy	0.133	*Tran et al.*[138]

However, no data could be found for the surfactants TX-114 and $C_{10}E_4$ in ionic liquids. The more generalized term critical aggregation concentration (cac) will be used for data presented here, because the size and shape of these self-assembled aggregates has not been studied in detail.

1.2 Comparison of Cacs in Water and IL

As already mentioned, the *Gordon* parameter *G* is a measure for the ability to allow the formation of associated structures and can be calculated according to equation III-2:

$$G = \frac{\sigma}{V_m^{1/3}} \qquad \textbf{(III-2)}$$

where σ is the surface tension and V_m is the molecular volume of the solvent. [emim][etSO$_4$] exhibits a *Gordon* value of G = 0.176 J/m^3 (σ = 46.963 mN/m and V_m = 0.019 m^3/mol).

As the aggregation phenomena were measured by surface tension measurements, some general aspects should be mentioned. It is well known that surfactant molecules arrange to form a monolayer at the air-liquid interface, when added to aqueous solutions. Once the surface of the liquid is saturated with surfactant monomers, micelles begin to form in the bulk solution. This point is referred to as the critical micellar concentration (cmc) or the critical aggregation concentration (cac). The same definitions hold for ionic liquid based systems. When adding surfactant to a solvent that promotes self-assembly, the amphiphile is accumulated at the air-solvent interface, whereat the hydrophobic tails of the surfactant molecules are inclined to be projected out into the air. This decreases the surface tension of the solution. With increasing surfactant concentration the interface will be accumulated with surfactant molecules and further surface tension will be reduced. At and above the cac the surface is saturated with monomers. Hence, the excess surfactant molecules will form aggregated structures in the bulk solution, *e.g.* in form of micelles. Thus, surface tension will stay almost constant above the aggregation concentration. As a consequence, cacs can be reflected by surface tension measurements. The main difference between IL-based and aqueous solutions is the initial surface tensions of the continuous phase. The neat ILs exhibit significantly lower values (40 -50 mN/m) than pure water (72 mN/m). Figure III-1 shows the experimentally determined cacs for the surfactants Triton X-100, Triton X-114, and $C_{10}E_4$ in water and [emim][etSO$_4$]. The IL [emim][etSO$_4$] itself exhibits a surface tension of 46.96 mN/m, identical to a value of 46.96 mN/m found in literature.[133] Measurements were performed for Triton X-100 and Triton X-114 at 25 °C and for $C_{10}E_4$ at 20 °C as the latter exhibits a cloud point slightly above 20 °C.

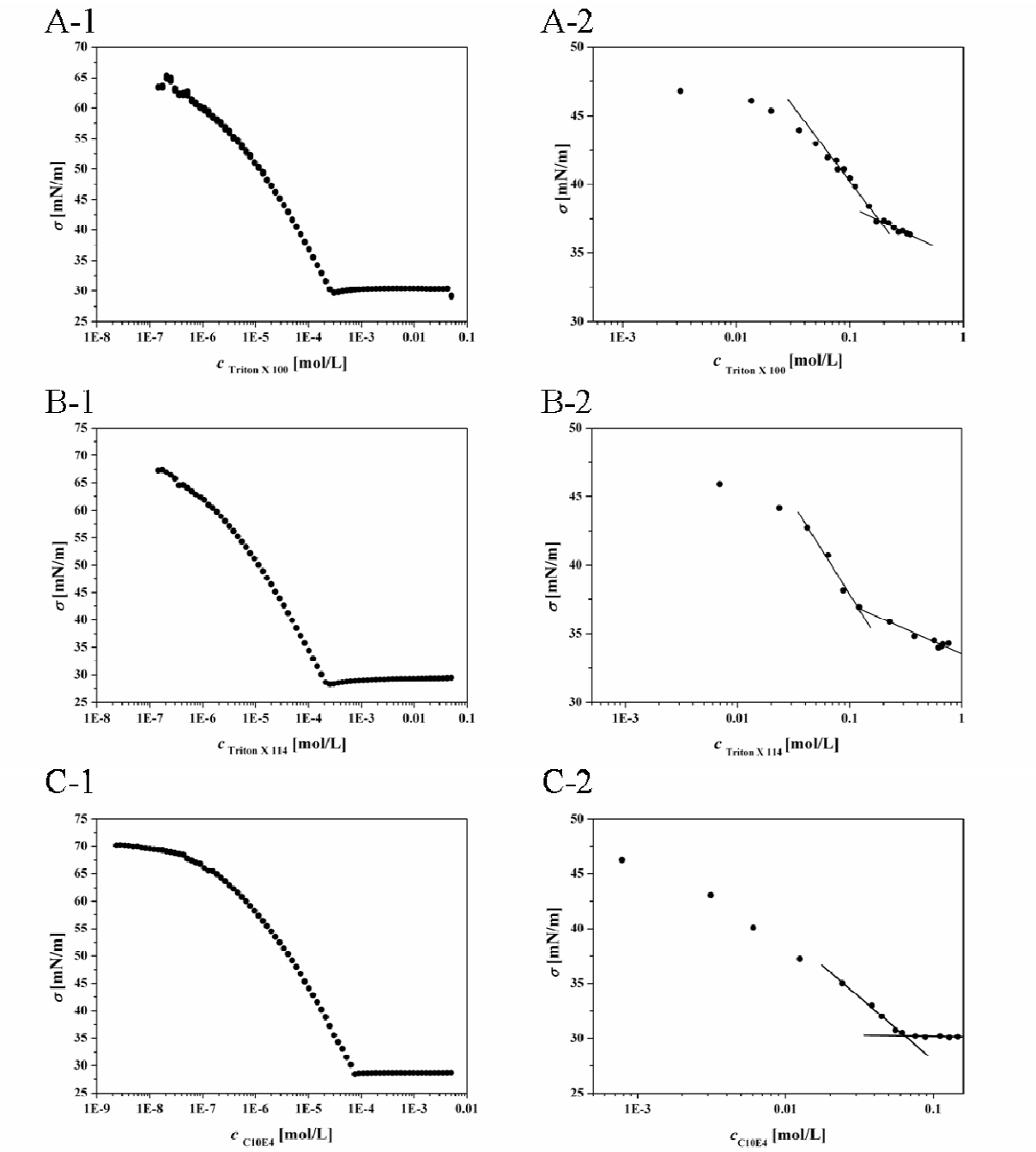

Figure III-1. Surface tension measurements for Triton X-100 (A), Triton X-114 (B), $C_{10}E_4$ (C) in water (left, 1) and in [emim][etSO$_4$] (right, 2). Measurements for TX-100 and TX-114 based systems were carried out at 25 °C and for $C_{10}E_4$ at 20 °C.

Surfactant aggregates are highly cooperative and are driven by the hydrophobic effect resulting from the lipophilic tail of the surfactants that dislikes water. Consequently, the system tends to decrease the amount of unfavourable interactions between the tails and water and forms micelles where the hydrophobic tails are not in contact with the water molecules. Compared to water-based surfactant systems, the solvophobicity between the ILs and the hydrophobic tail of the used surfactants is significantly lower. This is indicated by the high cacs obtained in ionic liquids. In the case of [emim][etSO$_4$] the inferred cacs of Triton X-100

were 669 times, of Triton X-114 559 times and of $C_{10}E_4$ 614 times higher than the corresponding cacs obtained in water. *Gao et al.* supposed that the lower solvophobicities in ILs denote that the driving force of micellar formation is weak and implicates a slow association of surfactant molecules in ILs.[137] Further, the relatively high viscosity of ILs support the theory of slow micellation processes as well. The cacs determined within this thesis are summarized in Table III-2.

Further, cacs decrease from Triton X-100 over Triton X-114 to $C_{10}E_4$ in water and IL. This dependency can be related to the decrease in hydrophobicity of the surfactant. Triton X-100 exhibits a hydrophilic lipophilic balance (HLB) of 13.5, Triton X-114 of 12.4 and $C_{10}E_4$ of 10.6. The lower the HLB value the more hydrophobic is the surfactant. $C_{10}E_4$ is less soluble in [emim][etSO$_4$] and water and therefore tends to form aggregated structures at lower concentrations than Triton X-100 and Triton X-114.

Table III-2. Determined cacs from surface tension measurements.

surfactant	cac in water [mol/L]	cac in IL [mol/L]]
Triton X-100	$2.88 \cdot 10^{-4}$	0.19
Triton X-114	$2.15 \cdot 10^{-4}$	0.12
$C_{10}E_4$	$8.80 \cdot 10^{-5}$	0.054

High cmcs were also observed for sodium dodecyl sulfate (SDS) and the non-ionic surfactants Brij 35 (polyoxyethylene-23-lauryl ether), Brij 700, docSS (dioctyl sulfosuccinate), and SB3-10 (caprylyl sulfobetaine) in [bmim][Cl] and [bmim][PF$_6$].[86] Moreover, the aggregation behaviour of a series of alkyl poly(oxyethylene glycol) ethers in [bmim][BF$_4$], and [bmim][PF$_6$] also demonstrated a higher aggregation concentrations.[88]

1.3 Conclusion

In general, the observations made within this work are consistent with the data of previous studies: the critical aggregation (or micellar) concentrations of surfactants in ILs are significantly higher than the corresponding cacs/cmcs in water. The higher concentrations that are required to form micellar aggregates in ILs are due to the nature of the solvent. The application of an IL results in a lower solvophobicity between solvent and surfactant resulting in a slow aggregation process. Additionally, the *Gordon* parameter of 0.176 J/m^3 could be determined for the solvent [emim][etSO$_4$]. Although this value is much lower than the

reported ones for PILs, the self-assembly of three non-ionic surfactants, namely Triton X-100, Triton X-114 and $C_{10}E_4$ could be demonstrated by surface tension measurements. However, the aggregation concentration of TX-100 in [emim][$etSO_4$] is considerably higher than the corresponding value in EAN but significantly lower than the one in [bmim][BF_4] and [bmim][PF_6]. The higher value compared to water might be related to the absence of a three-dimensional hydrogen-bond network in [emim][$etSO_4$]. Further, the cac values depend on the hydrophobicity of the surfactant. The lower the HLB value the lower the corresponding cac in water and [emim][$etSO_4$] whereat the cacs in the ionic liquid are about 600 times higher.

2. [emim][etSO$_4$] as Polar Phase for Low-Temperature-Stable Microemulsions Including Triton X-100 as Surfactant

2.1 Introduction

Ionic liquids (ILs) in microemulsions have attracted remarkable attention in the past years. Nevertheless, the emphasis rarely lay on their extraordinary properties, such as the wide liquid range,[34] and the resulting possibilities in forming self-assembled structures under unusual conditions, such as high or low temperatures. The substitution of water in traditional microemulsions by polar solvents like ethylene glycol,[139] formamide,[89] and ILs[16-18] has been reported already and it is crucial to know if microemulsions can be formed, and to which category they belong.

Per definition ILs consist solely of ions and are liquid at temperatures below 100 °C. In this context the subclass of room temperature ionic liquids (RTILs) is of particular interest. ILs can be either polar and miscible with water or be apolar and immiscible with water. They can therefore replace either oil or water in traditional microemulsions. The extraordinary properties of ILs have attracted the interest of many disciplines like electrochemistry,[140]organic chemistry,[3] and analytical chemistry.[16-17, 141]

The possibility of self-assembly in ILs has been widely reported during the last decades.[16-18] An overview already has been given in section III.1.

This chapter deals with non-aqueous microemulsions including the often utilized surfactant Triton X-100 (octylphenol ethoxylate). Several studies on RTIL-based microemulsions including the amphiphile TX-100 can be found in literature. The non-ionic surfactant Triton X-100 has been proved to be able to dissolve water and oil,[142-144] water and IL,[145-148] or oil and IL.[24, 95-96, 117] Most work based on this surfactant and ILs in microemulsions deal with RTILs such as 1-butyl-3-methylimidazolium tetrafluoroborate ([bmim][BF_4]) to replace water and 1-butyl-3-methylimidazolium hexafluorophosphate ([bmim][PF_6]) to substitute oil, respectively. In this context, current research is focused on the characterization of the ternary phase diagram recorded at ambient temperature. When the IL replaces water, the emphasis mostly is located on IL-in-oil (IL/o) microemulsions. Conductivity measurements,[96] small angle X-ray scattering (SAXS),[149] small angle neutron scattering (SANS),[117] dynamic light scattering (DLS),[95, 148] freeze fracture transmission electron microscopy (FF-TEM),[24] and UV-VIS spectroscopy[95, 150] measurements have been performed to characterize these microemulsions. Surprisingly, most studies do not benefit from the high temperature ranges

that can be achieved using ILs in microemulsions. As mentioned before, the group of Prof. *Kunz* demonstrated that non-aqueous microemulsions with IL as polar phase are stable from room temperature[27] up to 150 C.[28-30] Therein, EAN-in-oil structures stabilized by the surfactant [C_{16}mim][Cl] and the cosurfactant 1-decanol have been investigated. Besides, *Gao et al.* studied changes on microstructure in IL-based microemulsions as a function of temperature.[32] They reported the effect of temperature on [bmim][BF_4]-in-cyclohexane and [bmim][BF_4]-in-toluene reverse microemulsions characterized by DLS, FF-TEM, and two-dimensional rotating frame Overhauser (2D ROESY spectroscopy analysis) experiments. They concluded the existence of an IL/o structure up to 60 °C with an increase in an apparent droplet size derived from dynamic properties with raising temperature. *Gao et al.*[32] supposed that the change in curvature arises from the temperature dependence of the solubility of the hydrophobic chain in the organic solvent while the electrostatic interaction between $[bmim]^+$ and EO is relatively temperature independent. Compared to aqueous microemulsions with non-ionic surfactants, where temperature sensitivity occurs from the interaction between water and EO groups, the microstructure of microemulsions with [bmim][BF_4] is much less susceptible to changes in temperature.[32]

The Hildebrand solubility parameter provides a measure of the interactions of the molecules in a solvent. It should be stressed in this context that the parameter is much lower for ionic liquids than for water, which is usually applied in microemulsions as polar phase. Although, the exact value for [emim][$etSO_4$] is not reported in literature, values for imidazolium based ionic liquids could be found that range from (25-30) $MPa^{1/2}$ which are significantly lower than for water (48 $MPa^{1/2}$).[151]

The formulation of o/IL structures stable from ambient temperature down to at least -20 °C will be presented in the following. For this purpose, ingredients with low crystallization temperatures are required. Therefore, the IL [emim][$etSO_4$] was chosen as polar phase exhibiting a glass transition temperature of -80 °C. Furthermore, limonene with a melting point of -96 °C was applied as apolar phase along with the surfactant Triton X-100 as amphiphile. The following investigation presents a detailed study of the system from 40 °C down to -10 °C. All characterization measurements were carried out along an experimental path, where the amount of surfactant was kept constant at 38 wt%. The IL concentration was increased along the experimental path while simultaneously decreasing the limonene concentration.

2.2 Results and Discussion

2.2.1 Phase Diagrams and Phase Behaviour at 25 °C

The ternary phase diagram of the system [emim][etSO$_4$], limonene, and Triton X-100 is illustrated in Figure III-2. A wide single phase region can be observed. Hence, a considerable large range in volume fraction can be investigated along a dilution line with constant surfactant concentration of 38 wt% TX-100.

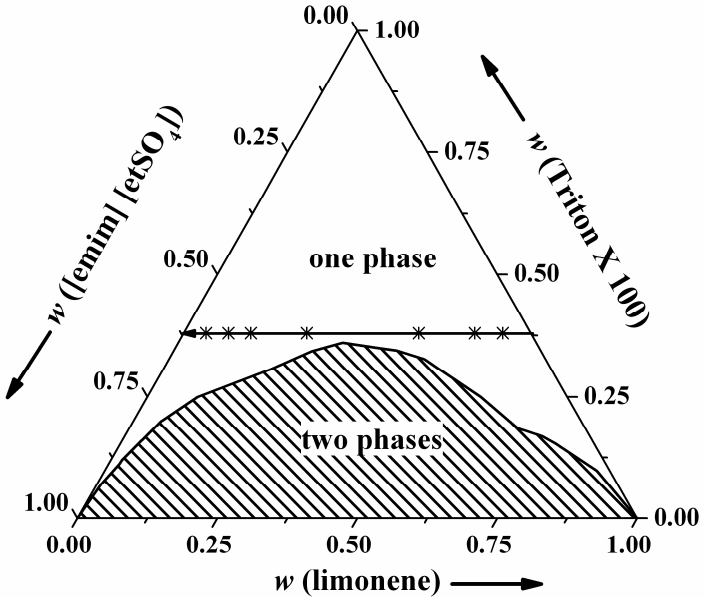

Figure III-2. Ternary phase diagram of [emim][etSO$_4$], limonene, Triton X-100 at 25 °C. The arrow marks the experimental path. A cross highlights the sample investigated by SAXS.

In addition to the ternary phase diagram, the "fish"-cut is shown in Figure III-3. A three phase body occurs in a temperature range between 28.8 °C and 31.5 °C. The phase inversion temperature at which the surfactant is perfectly balanced between oil and IL phase with a mean curvature close to zero was found to be at 30 °C. Below this temperature the curvature can be considered as positive and the surfactant film is curved towards oil. Therefore, at low temperatures and low surfactant concentrations an oil/IL microemulsion with excess oil phase [2] (Winsor I) is formed. At high temperatures the curvature changes from positive to negative versus zero mean curvature and an IL/oil microemulsion with an excess IL phase was found [$\bar{2}$] (Winsor II). The lowest surfactant concentration at which a three phase region [3] is formed is 11 wt% Triton X-100 whereas the lowest surfactant concentration to form a single phase microemulsion [1] is about 24 wt% Triton X-100. The latter is also called the efficiency of a surfactant.

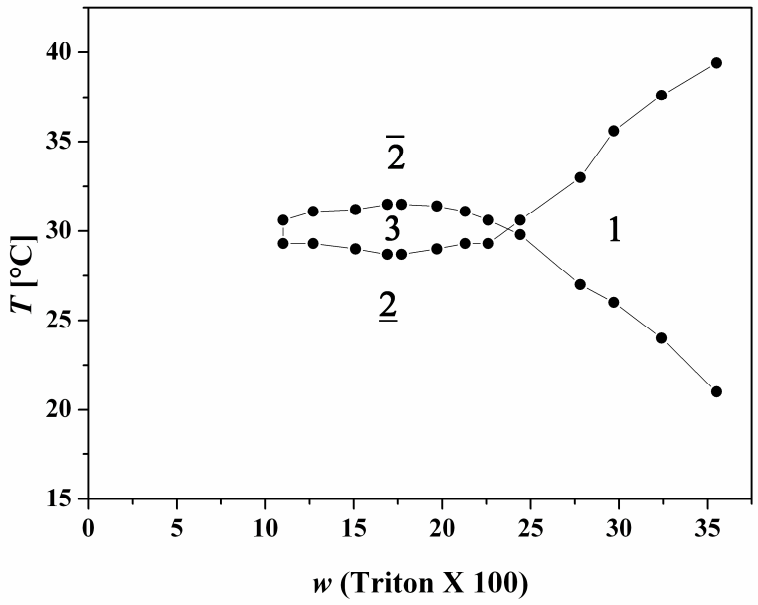

Figure III-3. "Fish"-diagram at constant IL/oil mass ratio of 1:1. 1: single phase microemulsion, "fish-tail"; 3: three phase system, "fish–head"; $\bar{2}$: two phase system, oil/IL microemulsion and excess oil phase, $\underline{2}$: IL/oil microemulsions and excess IL phase.

Investigations of transport properties of microemulsions, such as electrical conductivity and viscosity provide important information about their internal dynamics: flexible microemulsions have a monotonic behaviour of conductivity that can be described by a single power law. In contrast, rigid ones present a maximum in conductivity, due to local microstructure as in liquid crystals. Moreover, isolated non-coalescing water droplets are easily identified by means of very low conductivity values. Similar observations hold also for non-aqueous microemulsions with ionic liquids as polar phase.[95-96]

As the spectra will be given as a function of volume fraction ionic liquid (ϕ_{IL}) and not weight fraction, Table III-3 provides both values for a better overview. The volume fraction can be calculated if the densities of the microemulsion and the components are known. The volume fraction of the polar phase (ϕ_{pol}) corresponds to the volume of EO groups (V_{EO}) plus the volume of [emim][etSO$_4$] (V_{IL}) divided by the volume of the microemulsion (V). In contrast, the volume fraction of [emim][etSO$_4$] (ϕ_{IL}) corresponds to V_{IL} divided by V.

Table III-3. Weight fraction of IL in characterized microemulsions and resulting volume fractions for the three ingredients at 25 °C.

wt%IL	2	6	8	10	14	18	22	26	30
ϕ_{IL} [%]	1.5	4.6	6.1	7.6	10.8	14.2	17.7	21.3	24.9
$\phi_{TX\text{-}100}$ [%]	33.2	33.4	33.4	33.7	34	34.1	34.7	35.2	35.6
$\phi_{Limonene}$ [%]	65.3	62	60.5	58.7	55.1	51.7	47.6	43.5	39.5
wt%IL	34	38	42	45	50	54	58	60	62
ϕ_{IL} [%]	28.7	32.6	36.6	39.7	45	49.9	53.6	56.1	58.6
$\phi_{TX\text{-}100}$ [%]	36.2	36.8	37.4	38.1	39	39.3	40.5	41.1	41.4
$\phi_{Limonene}$ [%]	35	30.6	26	22.3	16	10.8	5.9	2.8	0

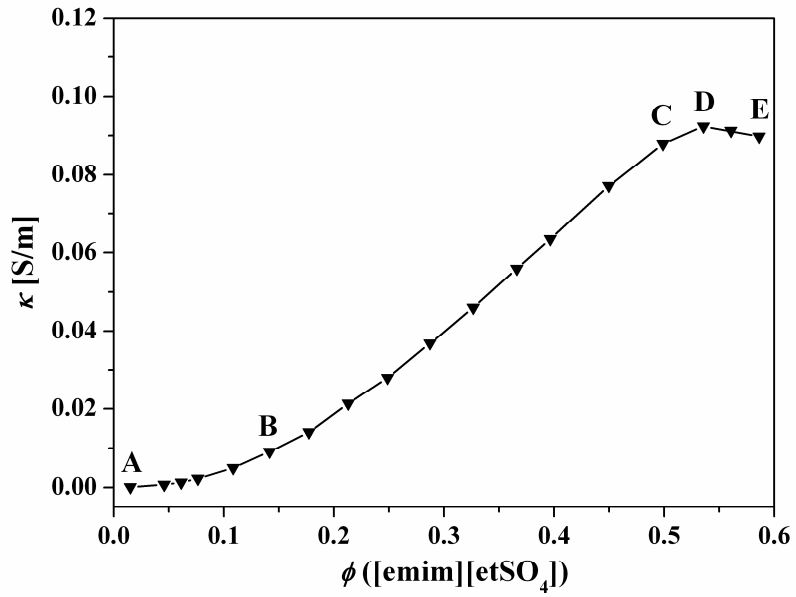

Figure III-4. Conductivity measured at 25 °C along the experimental path marked in Figure III-2. A, B, C, D, and E mark the detectable subareas.

Conductivity measurements (Figure III-4) indicate different domains with increasing amount of [emim][$etSO_4$]. From point A to B the conductivity remains quite low and increases slightly with increasing amount of RTIL, ($1.3 \cdot 10^{-4}$- $5.0 \cdot 10^{-3}$) S/m. Although the conductivity is low, its value is still much higher compared to the conductivity of a neat non-polar solvent, which is in the range of (10^{-12} - 10^{-16}) S/m. The ionic liquid is insoluble in pure limonene and

vice versa. For example, the conductivity of IL saturated limonene remains $8.0 \cdot 10^{-10}$ S/m, reflecting the accuracy of the previous statement. Hence, an increase in conductivity can only be attributed to the formation of some kind of microstructure. Consequently, between point A and B two possible microstructures have to be considered. First a droplet-like IL/o structure, *i.e.* IL droplets stabilized by surfactant in a continuous oil matrix is possible. With increasing IL-content the size of the droplets increases. The conductance of such IL/o microstructures at low ionic liquid volume fractions can be interpreted according to the charge fluctuation model of *Eicke et al.*[97] This model assumes spherical droplets with radius *r* that move independently from each other. In a thermal equilibrium these droplets are in sum uncharged as the number of positively charged $[emim]^+$ cations is equal to the number of negatively charged $[etSO_4]^-$ counter ions. However, due to spontaneous fluctuations, charged droplets will form that carry an excess charge *z*, yielding an increased conductivity compared to the pure apolar solvent. Notwithstanding, a conductivity in the order of 10^{-4} S/m even at low IL-content appears to be extraordinarily high for a simple IL/o droplet structure. The second possible scenario is the existence of interconnected structures even at low IL volume fractions. Interconnected structures or droplet clusters allow an effective transport of charge carriers and can explain the relatively high values of the specific conductivity. Although conductivity measurements do not eliminate the possibility of IL/o droplet formation, a rather interconnected structure appears to be more likely to exist, which is further supported by the SAXS data discussed afterwards.

As can be observed in Figure III-4, the existence of interconnected systems can be assumed between point A and B, while the volume fraction, the degree of interconnection, and hence the conductivity rises continuously up to point C with limonene as continuous phase. At point C ($\phi = 0.50$), the monotonous increase in conductivity breaks up and the conductivity between point C and D increases only slightly. This can be attributed to the formation of a bicontinuous structure where the transport properties do not change significantly. The following decrease in conductivity between D and E suggests that the IL is now forming the continuous phase. A decrease in conductivity can be assigned to a decrease in the mobility of charge carriers. The subtraction of a co-solvent, in the present case limonene, decreases the mobility of charge carriers due to an increased presence of ion pairs in the solution.

Viscosity can be a useful tool to confirm the characterization of local microstructures as well. It has been shown by *Cates & Candau*[110] that locally cylindrical and random flexible films exhibit a high fluidity, while locally lamellar and other rarer structures such as "molten" cubic phases are forming extremely viscous microemulsions. Similar to conductivity measurement,

equations for percolation have been suggested. However, a quantitative verification is only possible, if the viscosity η of the polar compound is sufficiently different from η of the oil,[111] which can be excluded in the present system. Along the experimental path, all samples exhibit *Newtonian* behaviour within the measured shear rate (Figure III-5). The observed linear dependence indicates the presence of a *Newtonian* fluid. The dynamic viscosity can be obtained by calculating the slope of the linear curve.

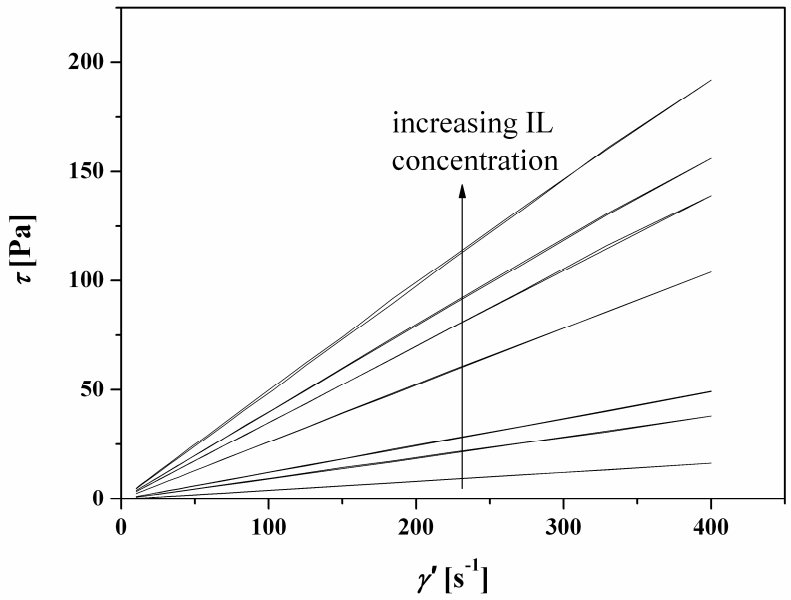

Figure III-5. Shear stress vs. shear rate at 25 °C obtained by measurements on a *Bohlin Instruments* rheometer for microemulsions with concentrations along the experimental path.

Unfortunately, the cone plate system (*Bohlin* rheometer), used to determine dynamic viscosities, was not suitable for the whole investigated concentration range and temperature range. This was indicated by high irregularities in the determined absolute values of the dynamic viscosities, resulting from the insufficient temperature control (± 0.5 °C). Nevertheless, the presence of *Newtonian* fluids could be proved and the exact values for the dynamic viscosities were determined by measurements of kinematic viscosities and densities. The dynamic viscosities are obtained by multiplication of the two values according to equation III-3.

$$\eta = \rho_m \cdot \nu \qquad \textbf{(III-3)}$$

where η denotes the dynamic viscosity, ρ the density, and v the kinematic viscosity.

The finally calculated mean value of the dynamic viscosity increases monotonic up to point C with increasing amount of room temperature ionic liquid as shown in Figure III-6. At point C

($\phi = 0.50$) the slope changes and indicates a change in microstructure, consistent with the conductivity data.

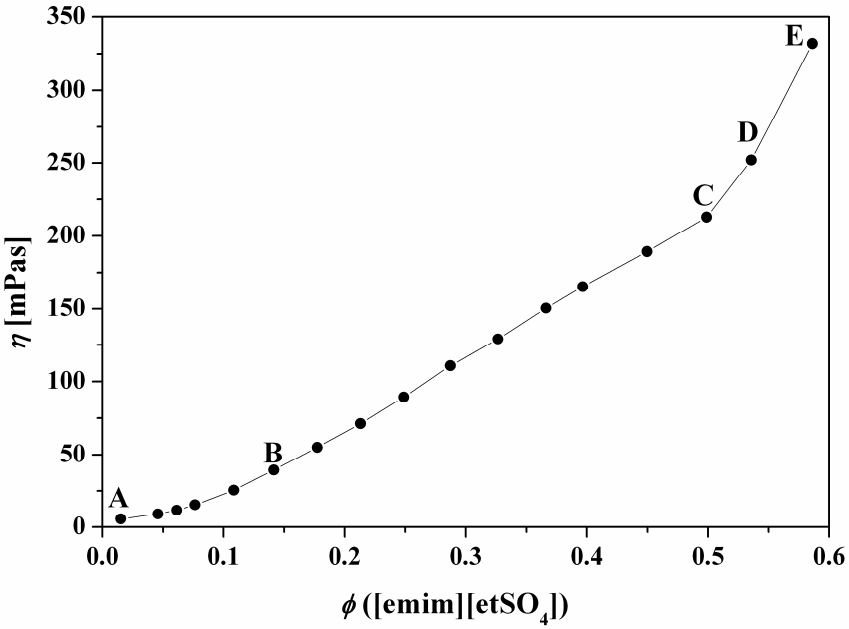

Figure III-6. Dynamic viscosities at 25 °C in dependence on volume fraction [emim][$etSO_4$]. The points A, B, C, D, and E mark the same points as in Figure III-4.

2.2.2 Lower Segregation Temperatures and Viscosity Measurements as a Function of Temperature

The segregation temperatures obtained are shown in Figure III-7. Distinct temperature stabilities can be observed for microemulsions containing a high content of IL (point C to E, see Figure III-6). Moderate temperature-stability can be found between point A and B and strong temperature dependence can be detected for the intermediate region between point B and C. The changes in temperature-stability occur at similar points where both conductivity and viscosity change. Nevertheless, interpretations on the kind of microstructure cannot be deduced from segregation temperatures alone. The segregation mechanism results in a separation of the solution in two phases followed by the freezing of the surfactant.[152] By contrast, o/IL microemulsions do not exhibit phase segregation down to -20 °C.

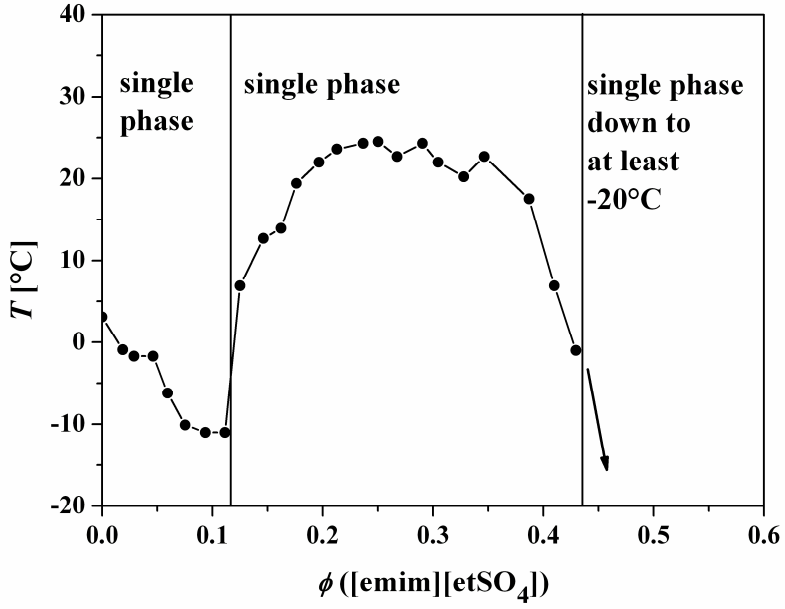

Figure III-7. Lower "Phase Segregation Temperatures" for microemulsions having a composition along the experimental path shown in Figure III-2. Samples between $\phi = 0.43$ and $\phi = 0.58$ do not show a segregation down to at least -20 °C.

The kinematic viscosity of microemulsions including 50 wt% [emim][$etSO_4$], 54 wt% [emim][$etSO_4$], and 58 wt% [emim][$etSO_4$] was measured between (0 and 40) °C. The same compositions were also investigated with SAXS experiments down to -10 °C. The dynamic viscosities were calculated from kinematic viscosities and measured densities at the appropriate temperature. The *Newtonian* behaviour over a wide temperature range (Figure III-8) was verified by measurements on a cone-plate system as reported for 25 °C.

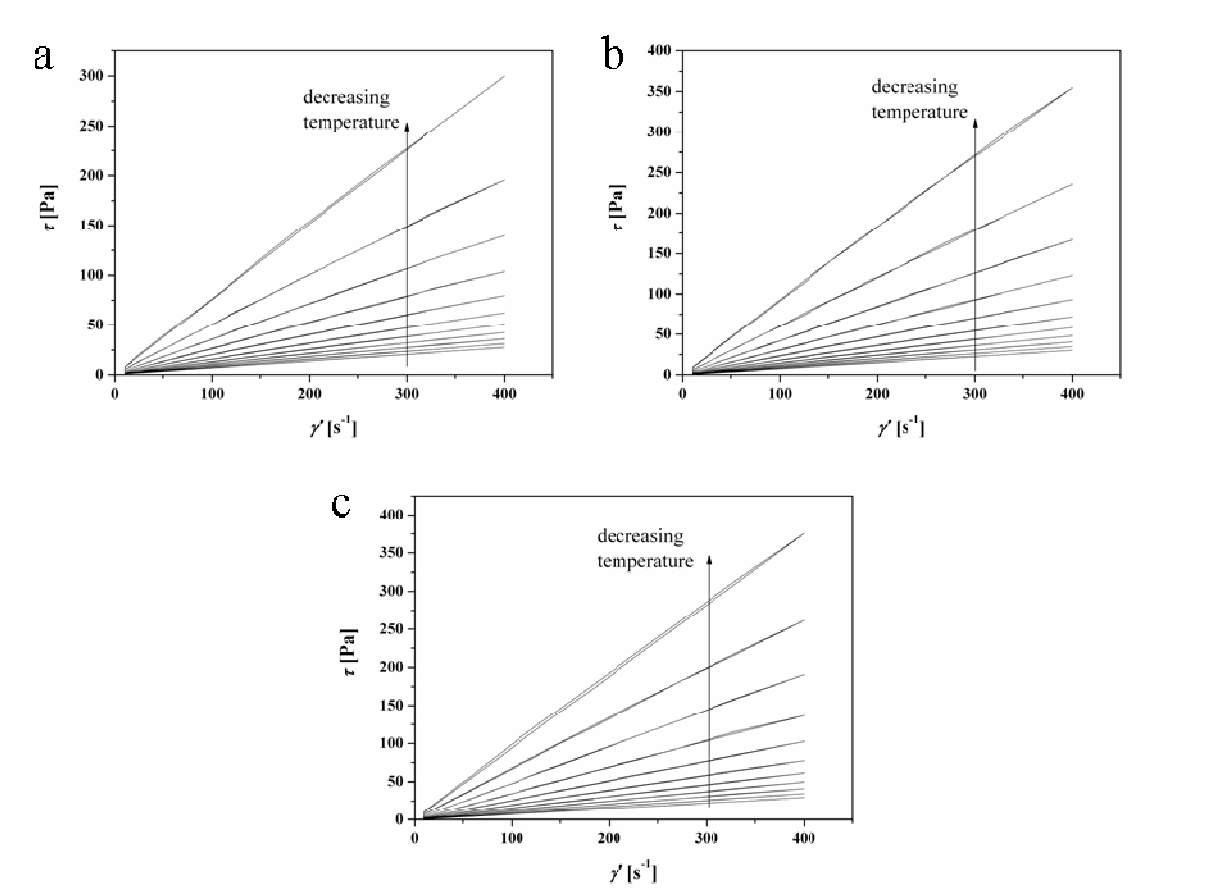

Figure III-8. Shear stress vs. shear rate at (10, 15, 20, 25, 30, 35, 40, 45, 50, 55, 60) °C plotted for microemulsions including 50 wt%IL (a), 54 wt%IL (b), and 58 wt%IL (c).

The results for viscosity measurements are presented in Figure III-9. At 0 °C the dynamic viscosity already reaches a value of more than 1 Pas which is in the same order of magnitude as the viscosity of glycerine[41] at ambient temperature (1.763 Pas at 20 °C). Nevertheless, magnetic stirring is possible down to -20 °C and enables applications of these microemulsions in these temperature ranges.

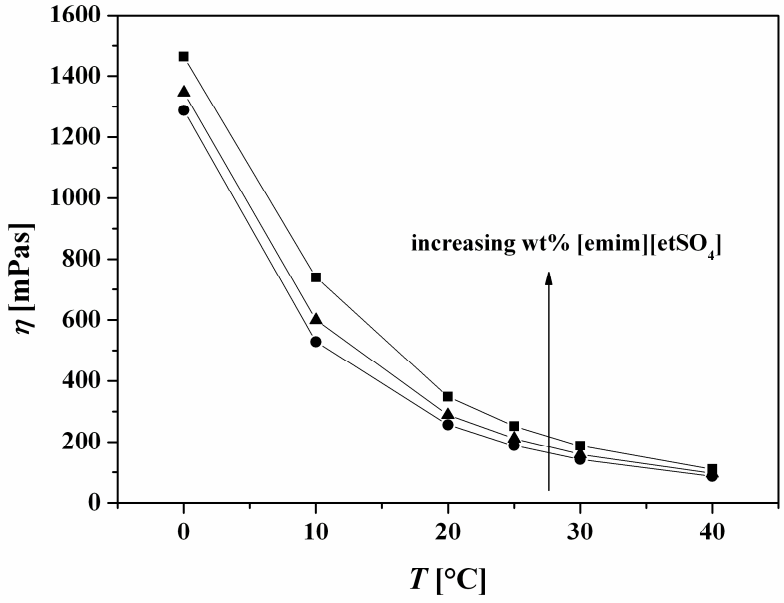

Figure III-9: Dynamic viscosities for microemulsions with 50 wt% (●), 54 wt% (▲), 58 wt% (■) [emim][$etSO_4$] measured in a temperature range from 0 °C to 40 °C. The data points were connected by a solid line to guide the eye.

2.2.3 Small Angle X-Ray Scattering

SAXS measurements have been performed along the mentioned experimental path at 25 °C and additionally for the three compositions, 58 wt%, 54 wt%, and 50 wt% [emim][$etSO_4$] at temperatures of 40 °C, 30 °C, 15 °C, 10 °C, 5 °C, 0 °C, -5 °C, and -10 °C. The SAXS spectra exhibit a single broad correlation peak followed by a q^{-4} decay at large q values similar to SAXS spectra of aqueous microemulsions. The first step in data evaluation is to extract three parameters from the broad maxima, one of them being the characteristic cell distance d. This also represents the frequency in the correlation function.[115] This three parameter fit formula (equation III-4) from *Teubner & Strey* (TS) indicates some apparent domain size as well as the ratio between size and "persistence" length, indicative of stiffness/flexibility balance. Consequently, *Freiberger et al.*[153] could show that TS can be even applied in the particulate regime, then giving access to inter-droplet distances d. The *Teubner-Strey* fit and the experimental data along the experimental path at 25 °C (Figure III-10) and for three compositions at temperatures from 40 °C down to -10 °C (Figure III-11) are visualized in the following.

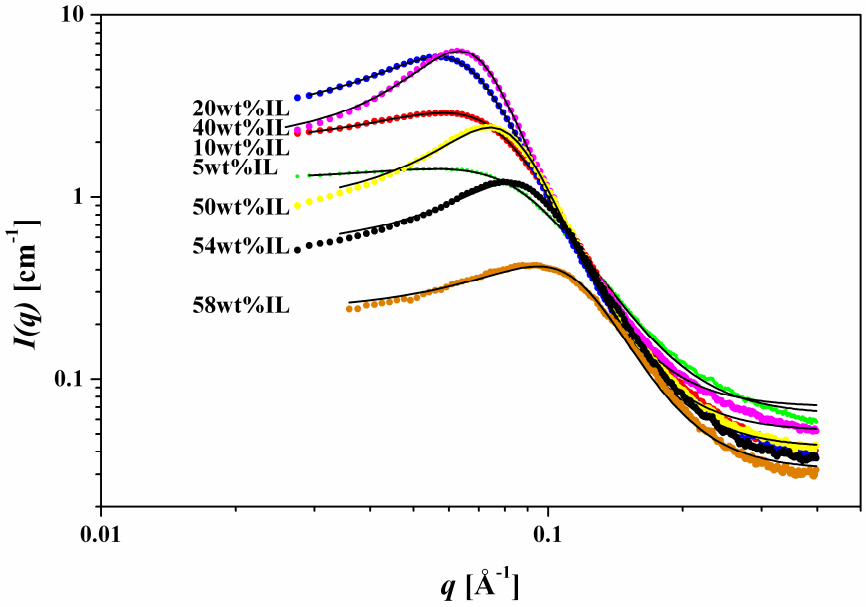

Figure III-10. Experimental SAXS data and Teubner-Strey Fit (solid lines) at 25 °C. 5 wt%IL (green), 10 wt%IL (red), 20 wt%IL (blue), 40 wt%IL (magenta), 50 wt%IL (yellow), 54 wt%IL (black), 58 wt%IL (orange).

$$I(q) = \frac{1}{a_2 + c_1 q^2 + c_2 q^4} + I_0 \qquad \textbf{(III-4)}$$

According to equation III-5 and III-6, two characteristic length scales were extracted from the Teubner-Strey-Fit, the correlation length ξ and the domain size d.

$$\xi = \left[\frac{1}{2}\left(\frac{a_2}{c_2} \right)^{1/2} + \frac{1}{4}\frac{c_1}{c_2} \right]^{-1/2} \qquad \textbf{(III-5)}$$

$$d = 2\pi \left[\frac{1}{2}\left(\frac{a_2}{c_2} \right)^{1/2} - \frac{1}{4}\frac{c_1}{c_2} \right]^{-1/2} \qquad \textbf{(III-6)}$$

Additionally, the amphiphilic factor f_a can be calculated from the fitting data using equation III-7.

$$f_a = \frac{c_1}{(4 a_2 c_2)^{1/2}} \qquad \textbf{(III-7)}$$

These equations have been already given in the Fundamentals of this work, but are of main importance for this chapter and are therefore repeated once more. The extracted length scales for the measurements along the experimental path at 25 °C are summarized in Table III-4.

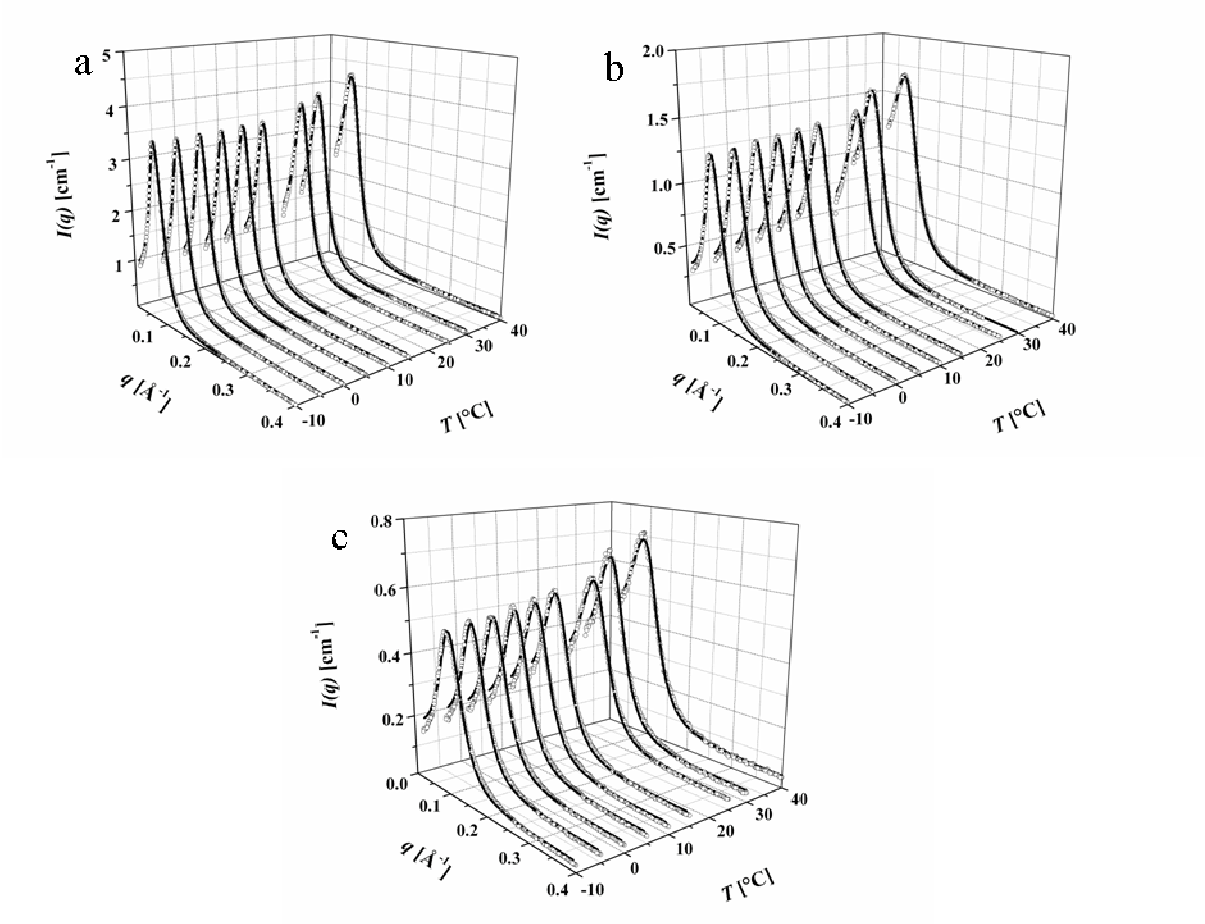

Figure III-11. Experimental SAXS data (○) and Teubner-Strey-Fit (solid line) for 58 wt% [emim][etSO4] (a), 54 wt% [emim][etSO4] (b), and 50 wt% [emim][etSO4] (c) at different temperatures varying from 40 °C down to -10 °C.

For IL weight fractions between (5 and 20) wt%, which represent points in the regime A-B, the domain size increases with increasing RTIL-content, consistent with an increase in size for IL/o microstructures. At higher IL weight fraction, where limonene can be assumed to be the internal phase ((50 - 58) wt% corresponds to the C-E regime), the domain size decreases. This results from o/IL structures whose size decreases with decreasing limonene content. The size of the domain swells as well with increasing temperature. However this effect is not significant, as it can be seen in Table III-5. This is in agreement with the results reported by *Warr et al.* for EAN[25] or PAN[33] based systems, where in general higher surfactant chain length were necessary to induce temperature dependent phase changes or intruding lamellar phases compared to aqueous systems. Additionally, these results confirm the results found by *Gao et al.*[32], where Triton X-100 based non-aqueous reverse microemulsions also showed less pronounced temperature dependence compared to their aqueous counterparts.

Table III-4. Characteristic length scales and amphiphilic factor from the Teubner-Strey model, the DOC lamellae model, and the DOC cylinder model for [emim][$etSO_4$] microemulsions at 25 °C.

						DOC Lamellae				DOC Cylinder		
wt%IL	ϕ_{pol}	Σ[cm²/cm³]	d_{TS} [Å]	ξ [Å]	f_a [-]	Ψ	t	d_{DOC} [Å]	v/l_a	Z	d_{DOC} [Å]	v/l_a
58	0.81	$4.07 \cdot 10^6$	59.3	22.1	0.69	0.25	37.4	60.0	0.95			
54	0.76	$3.82 \cdot 10^6$	70.2	30.9	0.77	0.30	37.1	70.9	0.95			
50	0.71	$3.64 \cdot 10^6$	79.4	39.5	0.81	0.30	36.9	75.3	0.95			
40	0.60	$3.50 \cdot 10^6$	94.8	51.5	0.84	0.30	33.0	80.4	0.96			
20	0.39	$3.26 \cdot 10^6$	101.7	41.0	0.73	0.35	35.5	56.7	1.02	3.0	83.4	1.15
10	0.30	$3.73 \cdot 10^6$	92.2	28.3	0.58	0.30	35.6	49.1	1.02	3.0	64.0	1.24
5	0.25	$4.08 \cdot 10^6$	84.0	20.0	0.38	0.25	34.8	44.8	1.02	3.0	54.3	1.30

Table III-5. Values of domain size d_{TS}, correlation length ξ, and amphiphilic factor f_a derived from Teubner-Strey Fits for 58 wt% [emim][etSO$_4$], 54 wt% [emim][etSO$_4$], and 50 wt% [emim][etSO$_4$] at various temperatures.

T [°C]		40	30	25	15	10	5	0	-5	-10
58 wt%	d_{TS} (Å)	65.8	62.4	59.3	58.6	57.2	56.2	55.2	54.3	53.6
IL	ξ (Å)	21.3	22.8	22.1	24.0	24.6	25.6	26.1	26.5	27.1
	f_a	-0.61	-0.68	-0.69	-0.74	-0.76	-0.78	-0.79	-0.81	-0.82
	Σd	2.70	2.53	2.44	2.60	2.63	2.58	2.58	2.55	2.57
54 wt%	d_{TS} (Å)	81.5	76.0	70.2	68.9	67.5	66.3	65.1	64.1	63.1
IL	ξ (Å)	25.7	27.9	30.9	32.1	33.5	34.5	35.8	37.0	37.9
	f_a	-0.59	-0.77	-0.77	-0.79	-0.81	-0.83	-0.85	-0.86	-0.87
	Σd	3.12	3.01	2.71	2.82	2.80	2.79	2.77	2.74	2.75
50 wt%	d_{TS} (Å)	89.9	83.7	79.4	78.1	77.0	76.1	75.4	75.0	74.8
IL	ξ (Å)	34.7	38.1	39.5	43.1	44.1	44.5	44.9	45.1	44.9
	f_a	-0.71	-0.78	-0.81	-0.85	-0.86	-0.86	-0.87	-0.87	-0.87
	Σd	3.10	2.96	2.74	2.81	2.80	2.79	2.77	2.74	2.75

The amphiphilicity factor f_a obtained from the Teubner-Strey fit is limited to the values 1, corresponding to the disorder line and -1, corresponding to the lamellar instability line. Structured microemulsions can be formed between these limits.[120] Well structured bicontinuous microemulsions can be found between -0.7 and -0.9 according to Teubner and Strey.[115] The values obtained from the TS-fits decrease with decreasing temperature from -0.61 to -0.82 for 58 wt% [emim][etSO$_4$], from -0.59 to -0.87 for 54 wt% [emim][etSO$_4$], and from -0.71 to -0.87 for 50 wt% [emim][etSO$_4$]. Consequently, a bicontinuous structure at 50 wt% [emim][etSO$_4$] over the whole investigated temperature range can be assumed. However, with increasing IL-content just bicontinuous structures are more likely to exist between (-10 and 25) °C. Furthermore, f_a indicates that microemulsions including (20 - 54) wt%IL preferentially form bicontinuous microstructures. These conclusions drawn from the extracted amphiphilicity factor give first hints concerning the microstructure at different

compositions. However, it is counterintuitive to expect transition from o/IL to bicontinuous structures with decreasing temperature. Consequently, the dimensionless dilution plot can be applied for a convenient picture about the microstructure present at a given composition. The dilution plot, which is illustrated in Figure III-12, allows verifying the microstructure suggested from the values of the amphiphilicity factor.

It has been determined that microstructures seem to be bicontinuous in an average volume fraction range. To progress further with the present experimental data, the construction of a dimensionless dilution plot, Σd vs. ϕ_{Pol} (shown in Figure III-12) is required. Using "dilution laws" as introduced by *De Gennes & Taupin*[124] can help to distinguish between flexible and stiff microemulsions. Flexible microemulsions will follow the *De Gennes & Taupin* law[122, 124] while other bicontinuous locally cylindrical or locally lamellar (alias bi-liquid foams) exhibit other dilution lines. The extreme case of flexible microemulsions is obtained with SDS-pentanol or linear non ionic surfactants as model systems.[154] Stiff microemulsions have been identified by *Rushforth et al.*[155] in the water-rich domain and by *Barnes et al.*[156] in the oil rich domain. Theoretical models can be found in literature[121] and all can be calculated analytically, but the specific area Σ is required for producing dimensionless dilution plots.

Therefore, the information contained in the scattering data has been analyzed by means of the *Porod* limit, experimental invariant and finally specific area Σ (equation III-8).[27]

$$\Sigma = \frac{\lim_{q\to\infty}(Iq^4)\pi\phi_{pol}(1-\phi_{pol})}{\int_0^\infty I(q)q^2dq} \qquad \textbf{(III-8)}$$

$\lim_{q\to\infty}(Iq^4)$ denotes the *Porod* limit and $\int_0^\infty I(q)q^2dq$ represents the experimental invariant Q_{exp}.

The theoretical Invariant Q_{theo} can be estimated by means of the scattering length density difference Δρ and the volume fractions through the relation $Q_{theo} = 2\pi^2(\Delta\rho)^2\phi_{pol}(1-\phi_{pol})$. In the present case the values for Q_{exp} and Q_{theo} differ about 30 %. This probably indicates a high solubility of Triton X-100 in one solvent, most likely in the ionic liquid, resulting in an approximated value of $\Delta\rho$. In 2009 *Anjum et al.*[144] published a detailed study to the phase behaviour of the system water, Triton X-100, and the hydrophobic IL, [bmim][PF_6]. Several "fish cuts" were recorded at different mass ratios of IL and water. With increasing amount of IL the "fish"-head was shifted to higher surfactant concentrations leading to the conclusion of an extraordinarily high solubility of the surfactant Triton X-100 in the IL. Considering the present investigation together with studies published by *Atkin et al.*[25, 33] and the higher cmc

values reported for surfactants in ILs compared to the corresponding aqueous systems, a high solubility of non-aggregated surfactant molecules in ILs appears to be very likely. Consequently, the specific area was calculated in dependence of the experimental invariant because it mirrors the real situation in the sample and is hence the more reliable value.

Several models have been calculated for comparison. The cubic random cell (CRC) model holds for bicontinuous structures and is valid for volume fractions between 0.18 and 0.82 and corresponds to the *De Gennes & Taupin* law for flexible microstructures.[124] The model assumes a set of cubes filled randomly with IL and oil to describe the microstructure. The analytic expression for this model can be written as[112]

$$\Sigma d = 6\phi_{pol}(1-\phi_{pol}) \qquad \textbf{(III-9)}$$

Actually, the numerical factor has been recalculated to be 5.83 and not 6,[124] an insignificant difference, which cannot be detected experimentally.

The Σd value for w/o or o/w spheres, equivalent to IL/o or o/IL spheres, can be predicted by equation III-10.[112]

$$\Sigma d = 4.84\phi^{1/3} \qquad \textbf{(III-10)}$$

However, the volume fraction is linked to the specific area for repulsive spheres by equation III-11.[112]

$$\Sigma d = 4.32\phi^{2/3} \qquad \textbf{(III-11)}$$

For $\phi_{Pol} > 0.5$ the experimental data were in-between repulsive spheres and o/w spheres. Taking into account the estimated error of 15 % in Σd, the data could be additionally interpreted in terms of IL/o or o/IL spheres, respectively. However, the adaptability of other models that could better describe the experimental data has also been checked.

The adaptability of the model of disordered open connected (DOC)-lamellar microstructure[157] has been verified to describe the experimental values. The DOC model is based on a *Voronoï* cell tessellation of space, yielding a complete set of microstructures ranging from isolated spheres via connected cylinders to disordered lamellae. With the fixed input parameters ϕ_{pol} and Σ, and the assumption of a surfactant chain length of 8.5 Å, and a fixed effective surfactant parameter p_0, the asymmetry parameter Ψ and the predicted d value d_{DOC} for DOC lamellar structures has been obtained. Therein, p_0 is defined as $p_0 = V / (a\ l)$ where V is the volume of the apolar part of the surfactant film, a the area of film per surfactant, and l the film thickness.[158] For the connected cylinder microstructure with the input parameters ϕ_{pol}, specific area and curvature mirrored by the value of the surfactant parameter p_0, no physical reasonable values for the connectivity Z could be extracted. In general, the connectivity Z can

be found between $0 < Z < 1.2$ when the conductivity is low, for $1.2 < Z < 4$ the polar network of coalescent droplets is infinite.[159] Therefore, the connectivity was fixed at 3.0. For a fixed connectivity, the granularity of the microemulsion is determined. For explicit analytic expressions, the reader is referred to refs 126 and 127. For IL weight fractions within (50 - 58) wt% that corresponds to the regime C-E and to volume fractions 0.71 to 0.82, the experimental data agree reasonably well with the DOC lamellar model. In contrast, it was not possible at all to describe the experimental points with the DOC-cylinder model. The microstructure of connected cylinders can be observed at high curvatures and high surfactant content, while the disordered lamellar structure is likely if the spontaneous curvature is low compared to d.[112, 120] By further going from right to left in the dilution plot, the values in the dimensionless Σd scale do not decrease with increasing oIL-content and cannot be described by any of the models. Consequently, the existence of microemulsions with a flexible interfacial film can be excluded in the case of $0.3 < \phi_{pol} < 0.4$, corresponding to (10 - 20) wt%IL. On the contrary, the data suggest that curvature cannot be reversed towards the IL phase. Hence, at mean RTIL-content (10 - 40) wt% (ϕ_{pol} = 0.3 - 0.6) the interfacial film is still curved towards the limonene phase.

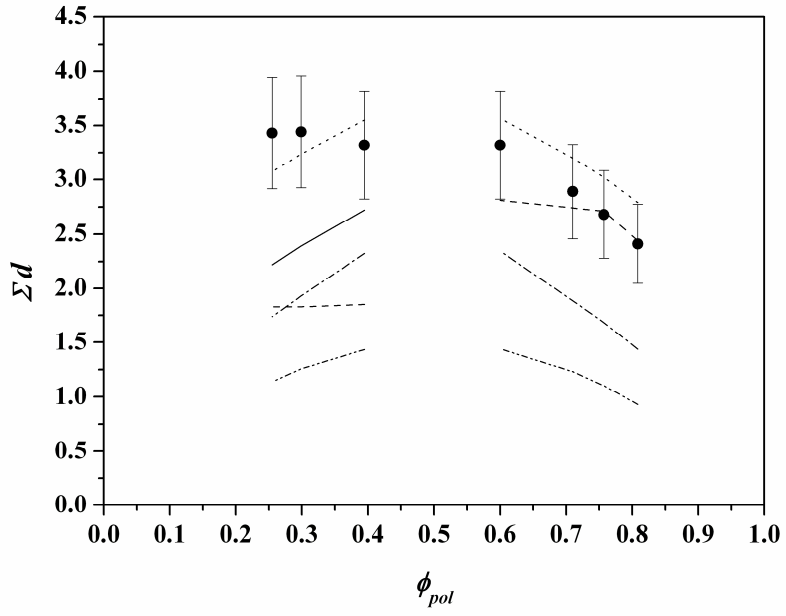

Figure III-12. Dilution plot: experimental data at 25 °C (●) including an assumed error of 15 %, CRC model (—·—), IL/o or o/IL (·····), repulsive spheres (—··—), DOC lamellae (----), DOC cylinder (—).

Comparable observations have already been made for aqueous microemulsions by *Barnes et al.*[157] where the ternary system DDAB/tetradecane/water was studied and the curvature was tilted towards the oil even at low water contents. In the present case the formation of

asymmetric sponge phases or liquid-foam like structures are reasonable explanations. These structures exist down to IL concentrations of 5 wt% consuming a high surface.

The results for scattering measurements as a function of temperature are not shown in the dilution plot for the sake of clarity. However, the values are included in Table III-4. The temperature effect on Σd can be summarized as follows: above 25 °C the value increases and fits better to the model of o/IL microemulsions at 40 °C. Below 25 °C the change is not significant and therefore, the conclusion that the microstructure does not change drastically with decreasing temperature is appropriate.

2.3 Conclusion

It was shown that microemulsions which are stable far below 0 °C do exist and evidences were found that indicate a “bicontinuous” structure in a large temperature range. Dilution plots show that the film is not flexible. Isolated droplets or flexible random microemulsions are not formed. None of the available models is consistent with all data presented. The microstructure which accommodates best to the data at high IL concentrations is a locally lamellar structure. This can be ascribed to a bi-liquid foam structure or an oil-swollen sponge phase, in present case an asymmetric sponge that has been described by *Roux et al.* in 1992[160] and by *Wolf et al. in* 2010.[161]

Since the dilution plot does not follow the "universal" *De Gennes-Taupin* plot, the bending constant associated to this surfactant, separating oil and IL must be ≥ 1 kT. To determine if the bending constant is as high as 10 kT, dilution of lamellar phases should be made. These are time-consuming scattering experiments that were not performed. The access to SAXS or SANS equipments is usually limited. However, the spontaneous packing parameter associated to the phase diagram and microstructure can be assumed to be close to one.

While conductivity measurements alone were not sufficient to distinguish between several possible microstructures, scattering experiments shined light on the present microstructure. At low IL-content, (5 – 20) wt%, biliquid-foam like (or locally lamellar alias asymmetric sponge) structures are most likely to exist. At high IL-content above 50 wt%IL (above point D) the data fit reasonably well to the connected locally lamellar structure. Further, these microemulsions offered the best visually observed temperature-stability down to -20 °C. The results indicate that the effect of temperature is not very pronounced, regarding both the domain size obtained from TS and the dimensionless dilution plot reflecting the microstructure present. Further, the moderate viscosities at low temperatures renders these systems applicable, *e.g.* as reaction media, at low temperature. Nevertheless, the formulation

of low-temperature-stable systems with even lower viscosities and wider liquid ranges should build a future task. These microemulsions with a polar continuous phase could be used over a wide temperature range. To the best of our knowledge, this is the first work reporting such temperature-stability of o/IL microemulsions. This system represents a model system for the formulation of low-temperature-stable microemulsions and surely can be further improved.

3. Microemulsions with Triton X-114 - Effect of Surfactant Hydrophobicity on the Phase Behaviour of Ionic Liquid Based Microemulsions

3.1 Introduction

In the last chapter the characteristics of microemulsions composed of 1-ethyl-3-methyl-imidazolium ethylsulfate ([emim][etSO$_4$])/limonene/Triton X-100 (TX-100) with the purpose to develop low-temperature-stable microemulsions have been discussed. These systems have high potential for several applications such as reaction media or lubricants.

In this part of the thesis, the effect of surfactant amphiphilicity with respect to phase behaviour, microstructure and thermal stability will be focused. Consequently, all other conditions, *i.e.* the ionic liquid and the apolar phase have been kept identical. The IL [emim][etSO$_4$] as polar phase and limonene as oil phase appear to be extraordinary promising for the formulation of systems that are stable even far below the freezing point of water due to their very low glass transition temperature (-80 °C) and low melting point (-96 °C), respectively. The only change that is made is the replacement of Triton X-100 by Triton X-114 (TX-114).

The difference between the two surfactants is the number of ethylene oxide (EO) groups. TX-100 comprises in average 9.5 EO groups, TX-114 only 7.5 EO groups, resulting in an increased hydrophobicity of the TX-114 surfactant. The HLB of TX-100 is 13.5, while 12.4 for TX-114.

The two surfactants, Triton X-100 and Triton X-114, are predestined for studying the effect of surfactant amphiphilicity on the formulation of microemulsions and their present microstructure as the two compounds exhibit exactly the same chemical structure expect the number of EO groups.

This again changes the phase behaviour in a crucial manner: formation of a three phase state slightly above room temperature and increased surfactant efficiency. Experiments are presented that enable the determination of the present microstructure along an experimental path and temperature range. The results will be compared to the TX-100 based system. Additionally, as reported before for TX-100 based microemulsions, the TX-114 system is also suitable for the formulation of “cold” microemulsions well below 0 °C, partly down to -35 °C. This goes far beyond the temperature range that could be achieved for TX-100 based microemulsions. Finally, a general concept for the formulation of low-temperature-stable microemulsions can be established.

3.2 Results and Discussion

3.2.1 Structural Changes along the Dilution Line at Ambient Temperature

Compared to the previous study of [emim][$etSO_4$], limonene, and TX-100, the ternary phase diagram with TX-114 exhibits a significantly enlarged single phase region (Figure III-13). Already at 25 °C this surfactant is more efficient than TX-100. Consequently, a better surfactant was found to solubilise limonene and [emim][$etSO_4$] at least at ambient temperature. The experimental path for single phase characterization was chosen to be at 36 wt% Triton X-114. Structural changes along the experimental path at 25 °C will be first discussed before heading for the temperature effects (next section).

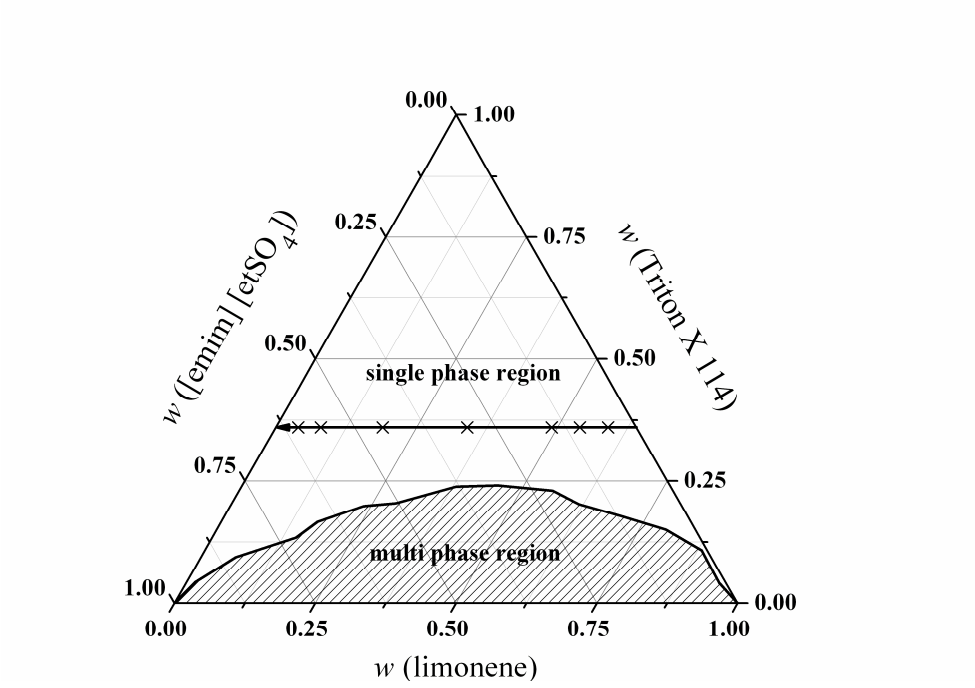

Figure III-13. Ternary phase diagram at 25 °C for the system: [emim][$etSO_4$], limonene, Triton X-114. The black arrow marks the experimental path that was chosen for further experiments. Crosses highlight the compositions that were further investigated by SAXS measurements.

In general, the conductivity of o/w, w/o, and bicontinuous microemulsions is significantly different and therefore allows a discrimination between the possible microstructures. A monotonic behaviour of conductivity suggests the presence of flexible microemulsions while rigid ones present a maximum in conductivity. Additionally, w/o droplets can be easily differentiated according to their very low conductivity values. For IL-based microemulsions similar observations have been made.[95-96]

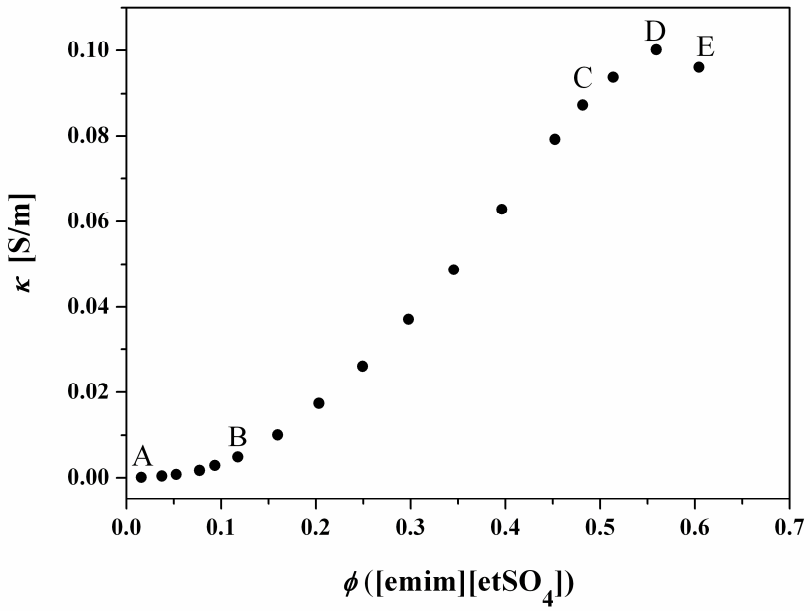

Figure III-14. Conductivity along the dilution line at 25 °C; A, B, C, D mark the concentrations where a change in microstructure could be possible.

Figure III-14 illustrates the conductivity along the experimental path at 25 °C, which in general is very similar to the previous reported system with Triton X-100. The almost stable, low conductivity at high oIL-content (between point A and B) could suggest the existence of IL/o droplets. Nevertheless, the conductivity is much higher (10^{-4} S/m) than the conductivity usually observed for reverse micelles in limonene that is mainly dominated by the conductivity of the oil phase (10^{-8} S/m). A possible explanation for this behaviour was given in the previous study of TX-100 microemulsions. Locally connected structures, *e.g.* biliquid foams could exist rather than separated droplets. Evaluation of scattering data will shed light on this statement. First, the remaining conductivity curve remains to be discussed. Above point B the conductivity rises continuously and allows the assumption of an enlargement of connected structures. Above point C the increase in conductivity with increasing IL-content is less pronounced than between point B and C. Consequently, a change in microstructure occurs. Point D represents a maximum in conductivity. The value decreases slightly between point D and E, while at point E only IL and surfactant is present in the solution. The lower conductivity could be explained by a high solubility of surfactant molecules in the conducting IL phase, where possibly most TX-114 molecules are dissolved as monomers in the IL phase and not at the interface, resulting in a decreased conductivity.[95] Adding limonene leads to a preferred micelle formation and to a slight increase in conductivity. The shape of the conductivity curve exhibits many similarities compared to the curve obtained for TX-100

microemulsions. Therefore, one could conclude that other features found before for TX-100 microemulsions also could be present in this system. This prior investigated system for example indicated the presence of an interfacial film, which is located in between rigid and flexible films. SAXS experiments at 25 °C along the dilution line can give an answer to the question of rigid or flexible microemulsions. Before going into detail on this question, some general evaluations from scattering data will be discussed. The experimental data were fitted according to the formula proposed by *Teubner & Strey* (equation III-4).[115]

The domain size d_{TS} (equation III-5), the correlation length ξ (equation III-6), and the amphiphilic factor f_a (equation III-7) have been extracted.

Since f_a tends to 1 for disordered systems and to -1 for a lamellar phase, f_a can provide important information about the microstructure present.[120] The results from *Teubner-Strey* analyses are summarized in Table III-6, the scattering curves with the corresponding fits are visualized in Figure III-15.

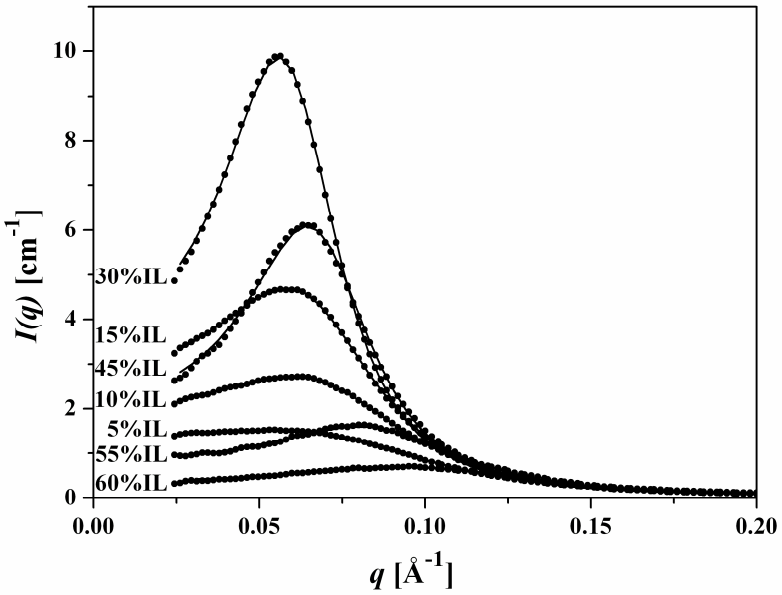

Figure III-15. Experimental SAXS data and TS-fit at ambient temperature for 7 sample compositions along the dilution line.

Table III-6. Results from SAXS data evaluation with *Teubner-Strey*-formula for measurements at 25 °C and sample 1 to sample 7.

Sample	wt%IL	ϕ_{IL}	ϕ_{pol}	d_{TS} [Å]	ξ [Å]	f_a
1	5	0.037	0.230	84.1	19.1	-0.34
2	10	0.077	0.273	87.7	25.2	-0.53
3	15	0.118	0.320	94.8	31.5	-0.63
4	30	0.251	0.463	104.6	46.2	-0.77
5	45	0.398	0.624	91.5	42.7	-0.79
6	56	0.516	0.752	70.6	26.4	-0.69
7	60	0.559	0.798	59.1	21.6	-0.68

According to *Teubner & Strey*, well structured bicontinuous systems should be found between -0.7 and -0.9.[115] From the seven samples measured at ambient temperature the three samples between (5-15) wt% yield values between -0.34 and -0.63. Consequently, no well structured bicontinuous microemulsions are present. This is completely in agreement with the conductivity results, which suggest potentially connected IL/o microstructures up to point B (ϕ_{IL} = 0.12, corresponds to 15 wt%IL). The interpretation also correlates with the low IL-content and high limonene content that is present in the samples (1-3). The determined domain size d_{TS} as well underlines this assumption as the value increases from (5-15) wt%IL (84 Å-95 Å) arguing strongly for a swelling of reverse micelles. Mainly, comparable results have been found for TX-100 microemulsions. Both systems seem to exhibit several similarities. Further, samples including 30 wt%IL (ϕ_{IL} = 0.25) and 45 wt%IL (ϕ_{IL} = 0.40) result in values of f_a = -0.77 and f_a = -0.79. The samples lie in the B-C range of the dilution line and the values of the amphiphilic factor as well as the conductivity measurements indicate the extension of connected structures in this domain. A bicontinuous structure is most likely present according to almost equal amounts of oil and IL phase in these samples. Finally, two samples remain to be discussed, 56 wt%IL (ϕ_{IL} = 0.52) corresponding to a point between C and D and 60 wt%IL (ϕ_{IL} = 0.56) corresponding to point D. Amphiphilic factors of -0.69 and -0.68 are received, respectively. These values are slightly below the border of a well structured bicontinuous microemulsion proposed by *Teubner & Strey*.[115] This and the fact that the modulus of the amphiphilic factor decreases from sample 5 (45 wt%IL) to sample 7 (60 wt%IL) combined with a simultaneous decrease in d_{TS} indicates a change in

microstructure, most likely the formation of o/IL droplets. This would be in agreement with high IL-contents/low limonene contents. In addition, it would underline the results obtained from conductivity measurements, which as well suggest a change in microstructure at concentrations above point C. Furthermore, the determined amphiphilic factors, domain sizes (Table III-5), and correlation lengths (Table III-5) are in the same order of magnitude as the obtained values for TX-100 microemulsions. To draw more conclusions one has to extract even more information from SAXS measurements using a dilution plot. The plot gives the possibility to distinguish between rigid and flexible microemulsions, but is only meaningful if experiments were carried out along a dilution line,[112] as it is the case for this system. The product of specific area (Σ) and domain size (d_{TS}) is plotted *versus* the volume fraction of the polar phase (ϕ_{pol}) to construct the dilution plot. Thus, the specific area has to be obtained as follows: first one has to extract the *Porod* limit and the experimental invariant, and then calculate the polar volume fractions. Finally equation III-7 can be used to obtain Σ.

The obtained values for *Porod* limit, theoretical (Q_{theo}) and experimental (Q_{exp}) invariant are summarised in Table III-7. Q_{theo} and Q_{exp} fit extraordinary well; the maximum deviation was 14 %. This indicates that the made assumptions about composition are correct.

Table III-7. Extracted experimental invariant Q_{exp}, calculated theoretical invariant Q_{theo}, *Porod* limit and specific surface Σ for the seven concentrations measured at 25 °C.

Sample	**wt%IL**	ϕ_{pol}	Q_{exp} [$cm^{-4}/10^{21}$]	Q_{theo} [$cm^{-4}/10^{21}$]	Σ [$cm^2/cm^3/10^6$]	***Porod* limit** [$cm^{-5}/10^{27}$]
1	5	0.230	1.60	1.83	4.65	13.4
2	10	0.273	1.84	2.14	4.34	12.8
3	15	0.320	2.28	2.39	3.90	13.0
4	30	0.463	2.74	2.82	3.42	12.0
5	45	0.624	2.47	2.60	3.48	11.7
6	56	0.752	1.80	1.90	4.16	12.8
7	60	0.798	1.45	1.54	4.61	13.2

The resulting dilution plot is visualized in Figure III-16. Together with the experimental data, model systems that can be found in literature are plotted.

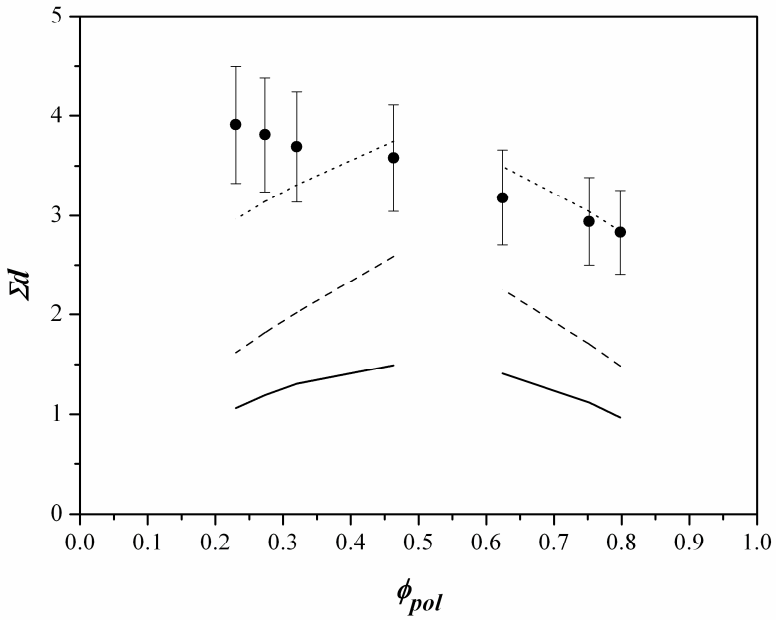

Figure III-16. Dilution plot: experimental data at 25 °C (●) including an assumed error of 15 %, CRC model (─), IL/o or o/IL (·····), repulsive spheres (─··─).

As can be observed in Figure III-16, the experimental values fit well to o/IL droplets for high IL-concentrations (samples 6, 56 wt%IL and sample 7, 60 wt%IL). This result displays one important difference between the previous work on TX-100 microemulsions and the present work on TX-114 microemulsions. TX-100 microemulsions could be well described in this concentration range by the model of disordered open connected (DOC)[125] lamellae. In the present case we can disclaim the application of the DOC models as our data can be well described by the theoretical model of o/IL spheres. By going further to lower IL concentrations in the dilution plot, samples 4 (45 wt%IL) and 5 (30 wt%IL) provide Σd_{TS} values slightly below the theoretical value for o/IL or IL/o droplets. This means that less surface is consumed and indicates a structural change for the two samples compared to samples 6 and 7. This is consistent with the data obtained from conductivity and the values for the amphiphilic factor that indicate the presence of a well structured bicontinuous microemulsion in this concentration range. The next samples (1-3) exhibit values that are even above the predicted ones for IL/o droplets. If the microstructure would change to separated IL/o droplets, the value of Σd_{TS} would decrease below $\phi_{polar} = 0.5$. The effect of non-decreasing Σd_{TS} could be already observed for Triton X-100 microemulsions, but was not as pronounced as in this case. One can conclude that separated IL/o structures are not likely according to the shape of the dilution plot that indicates that the interfacial film does not curve towards the IL phase. Therefore, biliquid-foam (or locally lamellar alias asymmetric sponge)-

like structures are most likely to exist. This as well would explain the relatively high conductivities at very low IL-content. Furthermore, the non decreasing Σd_{TS} values do not follow the dilution law of *De Gennes & Taupin* that is valid for flexible films. Hence, a rigid or intermediate surfactant film can be assumed for the present system. Same observations have been already made for TX-100 microemulsions. The differences and similarities observed for the two systems at 25 °C can be now summarized. Similarities can be found in the microstructure at low and intermediate IL-contents and differences in the microstructure at high IL-contents. Intermediate weight fractions of IL lead quite surely in both cases to well-structured bicontinuous microemulsions. Low IL concentrations lead to structures that are hard to determine, where separated IL/o droplets can be excluded according to conductivity and SAXS data. Most likely structures are locally connected for both systems studied. At high IL-content structural differences can be seen as o/IL droplets can be found for TX-114 and a DOC lamellae structure for TX-100 microemulsions. It is not probable that the small discrepancy is due to differences in the surfactant concentration along the experimental path, which is 38 wt% (0.61 mol/kg) for the TX-100 and 36 wt% (0.67 mol/kg) for the TX-114 system.

3.2.2 Structural Changes of o/IL Microstructure as a Function of Temperature

Additionally to the characterization at ambient temperature the system has also been analyzed in respect of temperature-stability. The major target is to find microemulsions that do not separate by cooling. Hence, segregation temperatures have been determined. The results are plotted in Figure III-17. The experiment clearly demonstrated that this system features low-temperature-stability. Along the experimental path each sample shows at least no segregation down to -4 °C. That means that the cooled samples do still form single-phase microemulsions and none of the included components freezes during the cooling process. Compared to the previous studied microemulsions with Triton X-100, the resulting segregation temperatures are much lower. This is a big improvement in concerns of low-temperature-stable microemulsions. Once again microemulsions with a high amount of IL exhibit the best temperature-stability down to at least -35 °C. At room temperature these compositions, 56 wt%IL (ϕ_{IL} = 0.52) and 60 wt%IL (ϕ_{IL} = 0.56) have been shown to correspond to an o/IL microstructure. The temperature dependent changes on these structures remain to be discussed.

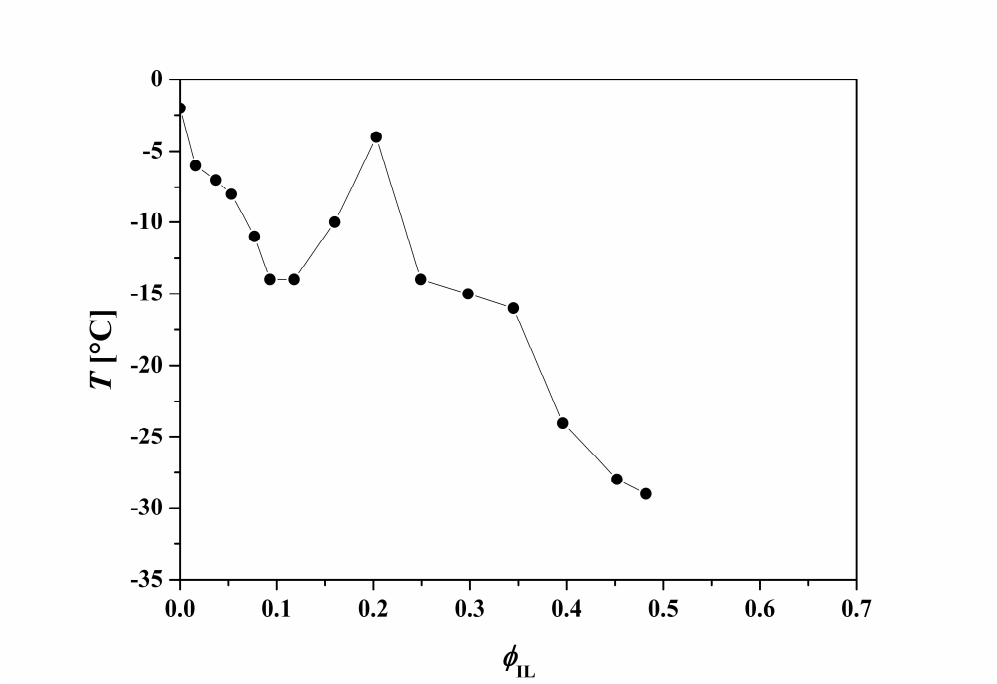

Figure III-17. Segregation temperatures recorded along the experimental path marked in the ternary phase diagram. The data points were connected to guide the eye.

SAXS has been measured as a function of temperature (-10 - 40) °C and fitted to the formula of *Teubner & Strey*. The spectra are show in Figure III-18.

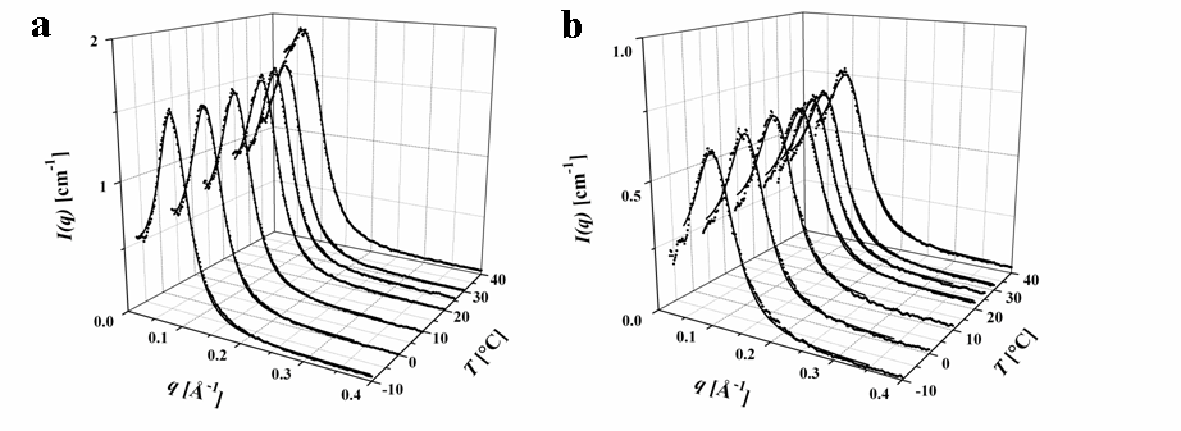

Figure III-18. SAXS spectra: experimental data (●) and Teubner Strey fit (—) for samples 6 (a) and 7 (b) at -10 °C, 0 °C, 10 °C, 20 °C, 25 °C, 30 °C, and 40 °C.

From the *Teubner-Strey* fit domain size and correlation length can be extracted. The domain size slightly decreases for sample 6 (56 wt%IL) from 81.6 Å at 40 °C to 63.4 Å at -10 °C and for sample 7 (60 wt%IL) from 63.1 Å at 40 °C to 53.1 Å at -10 °C. The change in domain size is not very pronounced and could be also related to a decrease in mobility at low temperatures. However, the amphiphilic factor decreases for both samples below 25 °C to a

value of -0.7 and even further by cooling down to -10 °C. Nevertheless, in this case the value has to be handled with care. A change from o/IL to a bicontinuous structure with decreasing temperature would be suggested by an exclusive consideration of the amphiphilic factors (Table III-8). This however is completely against all observations made before for structural changes in microemulsions and our observations that are discussed in the following section ("fish"-cut).

Table III-8. Results from *Teubner-Strey* evaluation of SAXS data for sample 6 and sample 7 and results for specific surface Σ at various temperatures.

	Sample 6 (56 wt%IL)				**Sample 7 (60 wt%IL)**			
T **[°C]**	d_{TS} **[Å]**	ξ **[Å]**	f_a	Σd_{TS}	d_{TS} **[Å]**	ξ **[Å]**	f_a	Σd_{TS}
-10	63.4	32.1	-0.82	2.64	53.1	23.8	-0.78	2.37
0	65.3	30.1	-0.79	2.78	54.7	24.0	-0.77	2.53
10	67.7	28.6	-0.75	2.82	56.8	23.8	-0.75	2.57
20	69.9	26.4	-0.70	2.84	58.1	22.2	-0.70	2.70
25	70.6	26.4	-0.69	2.94	59.1	21.6	-0.68	2.72
30	73.4	24.6	-0.63	3.21	60.9	21.2	-0.65	2.81
40	81.6	20.8	-0.44	3.54	63.1	20.1	-0.60	2.86

Nevertheless, the change in the amphiphilic factor at least indicates a change in microstructure. All results from *Teubner-Strey* evaluation are summarized in Table III-8 together with the resulting Σd_{TS} values. Those as well indicate structural changes. The formation of locally connected structures like sponge phase, disordered lamellae or connected cylinders at low temperatures could be possible. The Σd_{TS} value decreases with decreasing temperature and finally, lies in between theoretical values for o/IL droplets and repulsive spheres. Consequently, a change from a flexible interfacial film to a rigid interfacial film could occur with decreasing temperature. For TX-100 based systems this structure could be well described by the model of disordered open connected (DOC) lamellae. The application of the DOC model however does not make sense unless a dilution line is investigated and thus was not applied in the present case. TX-100 microemulsions exhibited comparable changes as a function of temperature. The characteristics of an intermediate interfacial surfactant film

were observed for TX-100 based microemulsions already at ambient temperature as discussed in section 3.1 of this chapter. At temperatures above 25 °C the domain size increases further up to 40 °C, the Σd_{TS} parameter increases also and can only be attributed to an o/IL microstructure for both samples. This effect was also observed for TX-100 microemulsions. Therefore, one can now conclude that o/IL microstructures are most likely present for TX-114 based microemulsions at (relatively) high temperatures and DOC lamellae could be the preferred structure at low temperatures.

In addition to microstructure, the viscosity of the present system is of main importance if one implicates the possible applications. Kinematic viscosities have been measured as a function of temperature from 40 °C down to 5 °C. Dynamic viscosities were obtained from the multiplication of kinematic viscosities by the corresponding densities. Prior to this calculation, the existence of *Newtonian* fluids was verified by measurements on a cone-plate system as described for the Triton X-100 based system. The results for dynamic viscosities are illustrated in Figure III-19. The values obtained for the TX-114 microemulsions are in the same order of magnitude as the values obtained for TX-100 based systems at 5 °C, (1000 – 1200) mPas.

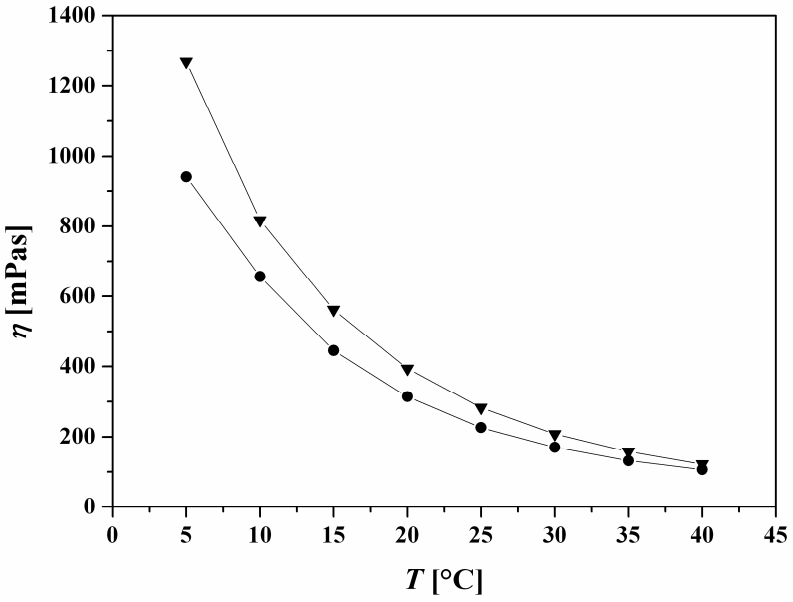

Figure III-19. Viscosity measurements as a function of temperature. Sample 6 (56 wt%IL) (●). Sample 7 (60 wt%IL) (▼). The data points were connected to guide the eye.

3.2.3 "Fish"-Cut at $\alpha = 0.5$

The "fish"-cut at $\alpha = 0.5$ is shown in Figure III-20. A three phase body is observed at temperatures between 24.6 and 27.1 °C, ΔT being 2.5 °C.

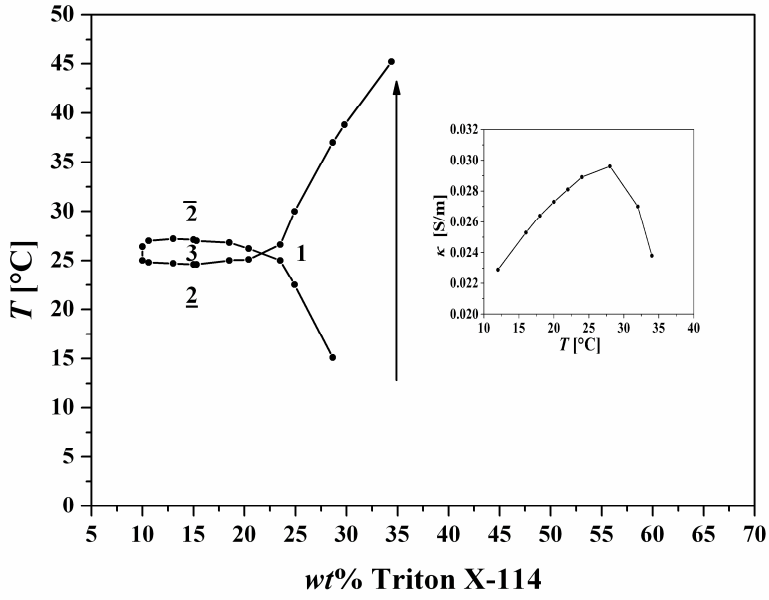

Figure III-20. "Fish"-cut at α = 0.5 and conductivity results at 35 wt% Triton X-114 between 12 and 35 °C. The data points were connected to guide the eye.

With increasing temperature a phase change occurs from *Winsor* I (2) over *Winsor* II ($\bar{2}$) to *Winsor* III (3) as previously described for non-ionic surfactant based aqueous[80] microemulsions and microemulsions including PILs.[25, 33] The phase inversion temperature (PIT), corresponding to the temperature where the minimal amount of surfactant is needed to form a one phase microemulsion could be extracted to be 25.7 °C. For TX-100 microemulsions the value was 30.1 °C. The maximum surfactant efficiency is about 22 wt%. This is an improvement of 2 % compared to the Triton X-100 microemulsions. Additionally, lowest temperature where a three phase body occurs was lowered from 28.0 to 24.6 °C. These changes in phase behaviour can be attributed to the difference in hydrophobicity of the surfactants, while TX-100 exhibits a HLB-value of 13.5 and TX-114 a value of 12.4. The formation of surfactant structures in the hydrophobic oil is therefore preferred at lower temperatures. Conductivity measurements can additionally give information on the structural characteristics of the one phase region. Conductivity at 35 wt% Triton X-114 and in a temperature range between 12 °C and 35 °C shows a clear maximum around the phase inversion temperature followed by a sharp decrease in conductivity. The shape of these conductivity measurements indicates the existence of highly structured systems along the measured temperature range. Two opposite effects influence the appearance of this curve: first the effect of increasing temperature rises the conductivity according to an increased mobility of effective charge carriers. Second the structural change from o/IL microemulsions at low

temperatures over bicontinuous structures to IL/o microstructures would result in a relatively high starting conductivity that increases up to the PIT and decreases above the PIT to a lower value than the starting value. The observed shape of our curve hence allows the conclusion of highly structured systems.

3.3 Conclusion

This work has shown the effect of the surfactant Triton X-114 on the phase behaviour of the ionic liquid [emim][etSO$_4$] and limonene. Previous work with Triton X-100, featuring a slightly higher HLB value than Triton X-114 have shown the curiosity of microemulsions that exhibit intermediate characteristics between rigid and flexible systems at ambient temperature. TX-114 microemulsions can be at high IL concentrations defined as o/IL microstructure. Both systems show many similarities, o/IL microstructure is in both cases the one with the best stability towards low temperatures. That means the samples do not separate while they are cooled down. Another similarity can be found in the present microstructure, both systems display features for connected structures at low IL-content. Finally, the temperature dependence on microstructure of the temperature stable systems was comparable. However, o/IL droplets could be identified at ambient temperature for TX-114 microemulsions at high IL concentrations and DOC lamellae was the present structure for TX-100 microemulsions. At temperatures below 25 °C, both systems gave hints for connected structures and at high temperatures for o/IL droplets. Another difference is the position of the "fish" at $\alpha = 0.5$ as slightly above 25 °C a three phase body could be observed. This change can be attributed to changes in surfactant hydrophobicity. The most important difference between both systems is possibly the temperature range in which the systems are applicable. The TX-114 microemulsions with high amount of surfactant exhibit temperature-stability down to -35 °C that clearly exceeds the obtained values from -20 °C for TX-100 systems. Consequently, this allows one to draw the conclusion that an even lower HLB-value of the surfactant may lead to even lower temperatures accessible. Further, an interesting feature of the o/IL microstructure that seems to undergo a change from o/IL droplets to intermediate structures with decreasing temperature has been found. This observation holds for both surfactants. Unfortunately, the viscosity could not be reduced by replacing Triton X-100 through Triton X-114 as the two formed microemulsion systems exhibit similar viscosities. Indeed, this would be of importance when applications come into play and therefore a system should be found that exhibits low-temperature-stability and moderate viscosities.

4. Microemulsions with $C_{10}E_4$ - Formulation of Microemulsions Suitable for Applications as Reaction Media

4.1 Introduction

In the two previous chapters the possibility to formulate low-temperature-stable microemulsions was demonstrated. First experiments with Triton X-100 and Triton X-114 led to the assumption that surfactants with lower HLB values could be more efficient in solubilising [emim][$etSO_4$] and limonene at room temperature and temperatures well below 0 °C. Triton X-100 exhibits an HLB value of 13.5 and Triton X-114 an HLB value of 12.4. Consequently, the next step comprises the application of a surfactant with a lower HLB value.

Triton X-100 and Triton X-114 are commercially available low-cost surfactants. However, they feature a distribution in EO groups with a mean value of 9.5 for Triton X-100 and 7.5 for Triton X-114. One of the final goals of this thesis is the utilization of low-temperature-stable microemulsions as reaction media. To realize this aim a pure surfactant with defined number of EO groups should be implemented instead of the Triton X-type surfactants. The simplest non-ionic surfactants are ethoxylated alcohols of the type C_iE_j. However, pure surfactants of this type are very expensive (1 mL about 100 Euros). Unfortunately, microemulsions contain a relatively high amount of surfactant. In the two systems already reported, an experimental path was characterized comprising 36 wt% or 38 wt% surfactant, respectively. Consequently, a purchase of these surfactants for a detailed study on the microstructure of microemulsions is almost impossible.

Tetraethyleneglycol monodecylether ($C_{10}E_4$) was chosen as amphiphile after first experiments with a corresponding technical surfactant (same HLB) led promising results in formulating low-temperature-stable microemulsions. These preliminary results are not presented here as this work focuses on the most promising systems that have been investigated. $C_{10}E_4$ can be synthesized simply from inexpensive starting materials. Further, $C_{10}E_4$ exhibits an HLB of 10.6, being definitely below the HLB of Triton X-114 (12.4). Therefore, there exists a high potential in the formulation of low-temperature-stable microemulsions implementing this surfactant. The ternary phase diagram, conductivity, viscosity, and SAXS measurements will be reported in the following. Additionally, the application of these microemulsions as reaction media and results from preliminary experiments will be presented.

4.2 Results and Discussion

4.2.1 Ternary Phase Diagram

The resulting ternary phase diagram for the system [emim][$etSO_4$], limonene, and $C_{10}E_4$ is illustrated in Figure III-21. The surfactant is less efficient than Triton X-100 and Triton X-114 at room temperature. The implementation of a more hydrophobic surfactant leads to a system where the multi phase region is more pronounced than in the previous studies. Nevertheless, these results do not automatically implicate that low-temperature-stable microemulsions cannot be obtained by using this surfactant. In the case of the $C_{10}E_4$ based systems, no "fish"-cut was recorded. At $\alpha = 0.5$ the system is definitely "above" the "fish" at room temperature and down to -10 °C.

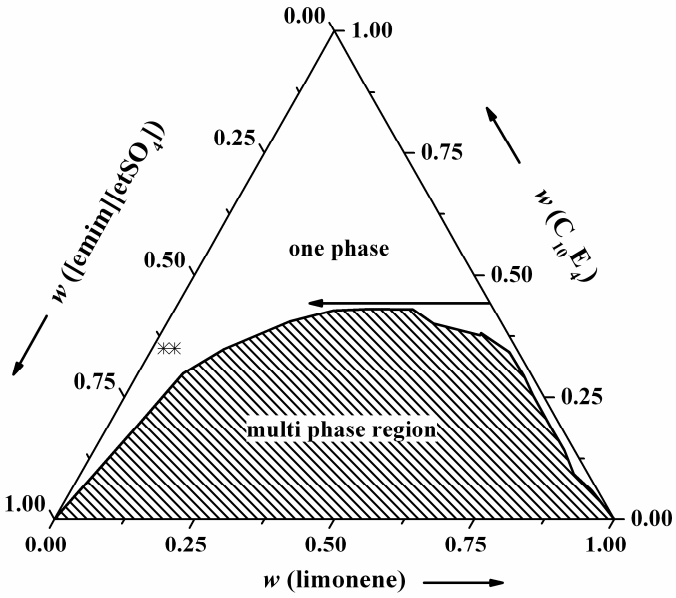

Figure III-21. Ternary phase diagram for [emim][$etSO_4$], limonene, and $C_{10}E_4$. The black arrow marks the investigated experimental path at ambient temperature. A cross highlights the microemulsion compositions that were investigated by SAXS measurements.

4.2.2 Characterisation along the Experimental Path

Along the experimental path the surfactant concentration is kept constant at 45 wt% $C_{10}E_4$. This corresponds to the dilution with the lowest possible surfactant concentration in the single phase region of the ternary phase diagram.

As already reported for the two microemulsion systems including Triton X-100 and Triton X-114, conductivity measurements provide important information about the transport properties and microstructure present. As the system exhibits remarkable temperature-stability along the experimental path (Figure III-22), conductivity was measured not exclusively at 25 °C (Figure III-23), but also at 0 °C (Figure III-26) and -15 °C (Figure III-27).

One important difference to the previously studied systems is visualized in Figure III-22. Herein, segregation temperatures are illustrated, measured along the experimental path at 45 wt% surfactant. Microemulsions with comparable amounts of limonene and [emim][$etSO_4$] are stable down to -20 °C. Segregation points identify the temperature at which the samples separate or freeze. In contrast to these microemulsions, the systems including Triton X-100 and Triton X-114 exhibit the best stability if high amounts of ionic liquid and low amounts of limonene are present in the formulation.

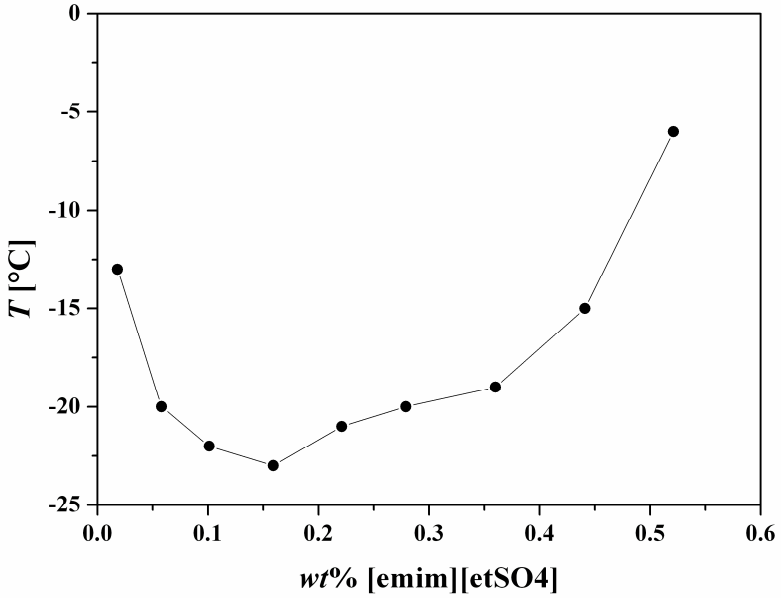

Figure III-22. Segregation temperatures for $C_{10}E_4$ based microemulsions with compositions along the experimental path.

The conductivity at 25 °C along the experimental path is illustrated as function of [emim][$etSO_4$] volume fraction in Figure III-23.

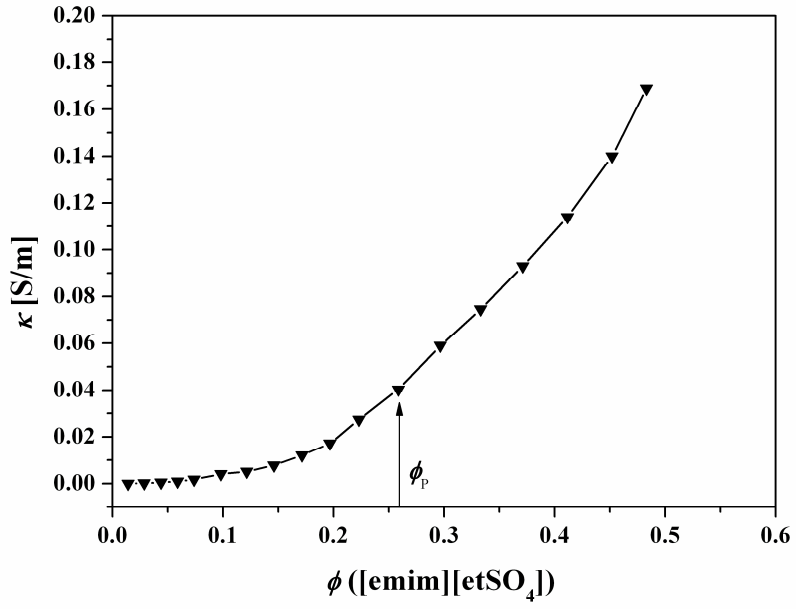

Figure III-23. Conductivity measured along the experimental path at 25 °C. ϕ_P denotes the determined percolation threshold. The line was drawn to guide the eye.

Conductivity values are almost zero at low IL-content and increase over several orders of magnitude when the IL-content is increased. The low conductivity at low IL-content (10^{-6}S/m) can be correlated to the existence of IL/o droplets. The conductivity of those structures is mainly governed by the conductivity of the neat oil phase (10^{-8} S/m).[97] Furthermore, typical percolation behaviour can be assumed. After the percolation threshold (ϕ_P), conductivity values increase over several orders of magnitude to a final value of 0.18 S/m. Therefore, ϕ_P can be determined by plotting log(κ) versus the volume fraction of [emim][$etSO_4$] (Figure III-24), fitting the curve with a fourth order polynomial and setting the second derivate to zero.[106] Shortly, this corresponds to the determination of the inflection point of the curve. The resulting percolation threshold is ϕ([emim][$etSO_4$]) = 0.26.

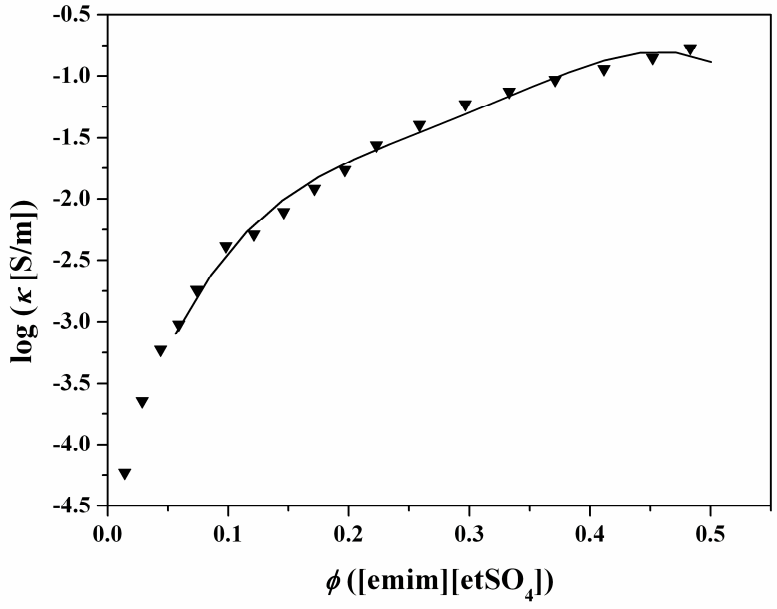

Figure III-24. log($\kappa(\phi)$) plot for the determination of the percolation threshold for $C_{10}E_4$ microemulsions at 25 °C. Measured data is depicted by triangles and the solid curve corresponds to the fourth order polynomial fit.

The percolation behaviour can be further characterized by the determination of two characteristic parameters μ and s. Two models exist to explain the percolation phenomenon, static or dynamic. Dynamic percolation[102-103, 107] describes droplets that are in motion. The increase in conductivity is related to rapid fusion-fission processes among the dispersed droplets. Static percolation describes the idea of an isolating solution with solid conductors and is based on the appearance of a bicontinuous structure.[105] To distinguish between both models a plot according to Figure III-25 is required ($\ln\kappa$ versus $\ln(|\phi-\phi_P|)$).

According to the most widely used dynamic percolation model, two pseudo phases can be assumed: one in which charge is transported by the diffusion of microemulsion globules and the other phase in which charge carriers itself diffuse in the reverse micellar cluster.[105] According to this theory two separate asymptotic power laws can be used to describe the conductivity behaviour above and below the percolation threshold along the dilution line.

$$\ln\kappa = \ln\kappa_1 + \mu\ln(|\phi-\phi_P|) \qquad \text{(above percolation threshold)} \qquad \textbf{(III-12)}$$

$$\ln\kappa = \ln\kappa_2 - s\ln(|\phi-\phi_P|) \qquad \text{(below percolation threshold)} \qquad \textbf{(III-13)}$$

The two characteristic parameters μ (equation III-12) and s (equation III-13) can be determined from Figure III-25. Computer simulations determined parameters of μ = 1.94 and s = 1.2 for dynamic percolation and μ = 2 and s = 0.6-0.7 for static percolation.[107-108]

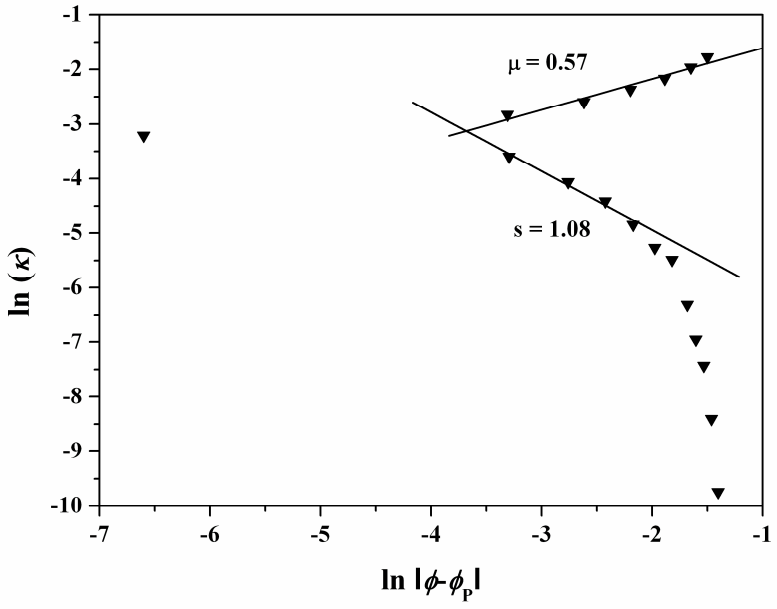

Figure III-25. Plot for the determination of the two characteristic parameters μ and s.

The resulting parameters are $\mu = 0.57$ and $s = 1.08$ in the case of these non-aqueous microemulsions containing $C_{10}E_4$. The parameter μ is not suitable for a clear differentiation between static and dynamic percolation as the values are to similar for both models. In contrast, the parameter s is suitable to distinguish between both percolation phenomena. The value of 1.08 for s fits more to the phenomena of dynamic than for static percolation. In general, a value of s below 1 indicates static percolation and a value above 1 dynamic percolation whereas μ lies usually between 1 and 2.[162] A value of $\mu = 0.57$ is below the typical values.

Conductivity data at 0 °C (Figure III-26) and -15 °C (Figure III-27) are presented in the following two figures. A very low conductivity at low IL-content indicates the existence of IL/o droplets. Limonene forms the continuous phase. The conductivity values do not increase over several orders of magnitude as observed at 25 °C. This can be correlated to the decreased mobility of the charge carriers at low temperatures. Nevertheless, above $\phi_{IL} = 0.2$ a slight increase in conductivity can be observed for measurements at 0 °C. This indicates the formation of connected structures. At high IL-contents conductivity values do not decrease as it was observed for Triton X-100 and Triton X-114 based systems. This observation indicates the presence of flexible interfacial films. The same holds for the conductivity results at 25 °C.

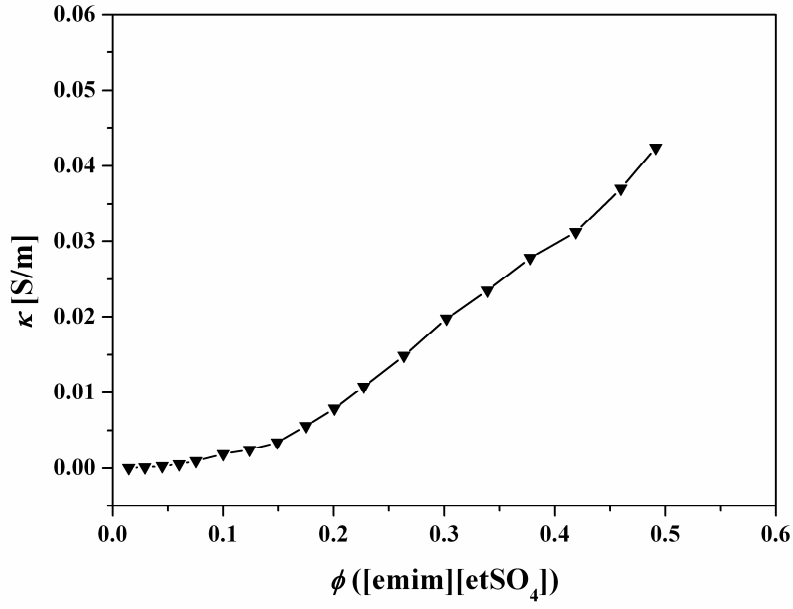

Figure III-26. Conductivity data for $C_{10}E_4$ based microemulsions at 0 °C. The line was drawn to guide the eye.

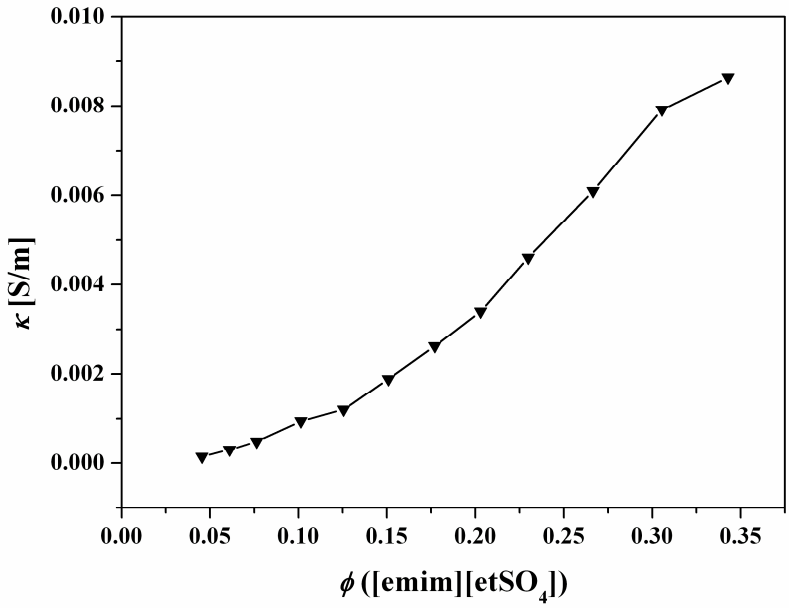

Figure III-27. Conductivity data for $C_{10}E_4$ microemulsions at -15 °C. The line was drawn to guide the eye.

At -15 °C the slope of the curve is even less steep than at 0 °C and 25 °C. A continuous increase in conductivity can be observed. The slope of the curve does not change significantly along the experimental path. A limited concentration range could be measured due to some samples that freeze or separate when they are cooled down to -15 °C. Subareas cannot be doubtlessly defined at this temperature.

Viscosity is of importance when applications come into play. Additionally, viscosities can also give information about transport properties and the microstructure present. Consequently, the dynamic viscosities have been determined along the experimental path (45 wt% $C_{10}E_4$) in a temperature range from (5-30) °C (Figure III-28). Dynamic viscosities were derived from kinematic viscosities and densities after the existence of *Newtonian* fluids was confirmed (same procedure as for Triton X-100 microemulsions). The values for the dynamic viscosities are significantly lower than in the previous measured systems including Triton X-100 and Triton X-114. At 5 °C the microemulsions formed with Triton X-100 exhibited a dynamic viscosity of (1300-1500) mPas and Triton X-114 a dynamic viscosity of (900-1500) mPas. These are values, which have been obtained for systems that include a high content of [emim][$etSO_4$]. Therefore, these values can be only compared to $C_{10}E_4$ microemulsions with comparable amounts of ionic liquid. A microemulsion with 45 wt% $C_{10}E_4$, 52 wt% [emim][$etSO_4$], and 3 wt% limonene exhibits a viscosity of 280 Pas at 5 °C. The goal to formulate microemulsions that can be applied below 0 °C and that show a relatively low viscosity could be met. Consequently, these microemulsions with the simple surfactant $C_{10}E_4$ are easier to handle and exhibit a higher potential for future applications than their competitive systems including Triton X-100 and Triton X-114. The decreased viscosity could result from the difference in viscosity from the surfactants, 20 mPas for $C_{10}E_4$, 290 mPas for Triton X-100, and 282 mPas for Triton X-114 at ambient temperature.

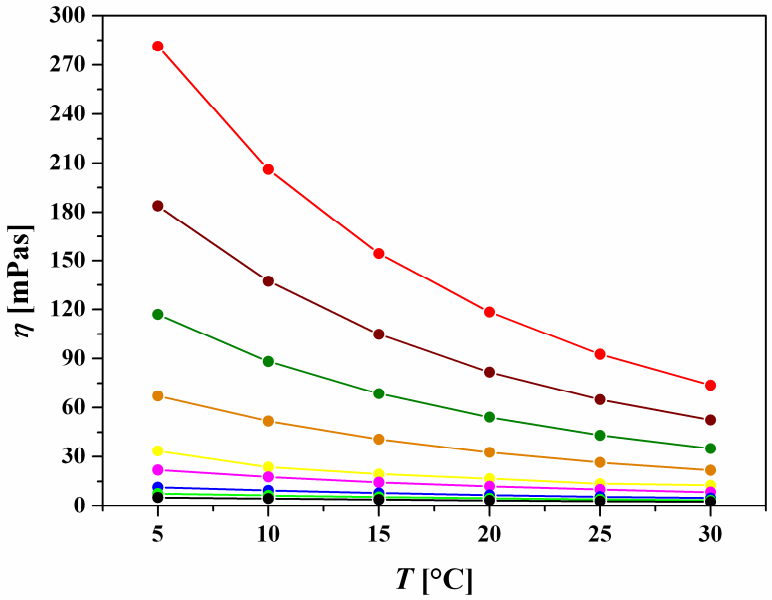

Figure III-28. Dynamic viscosities measured in a temperature range of (30-5) °C for microemulsions along the experimental path containing 45 wt% $C_{10}E_4$. Black: 2 wt%, bright green: 6 wt%, blue: 10 wt%, magenta: 16 wt%, yellow: 22 wt%, orange: 28 wt%, green: 36 wt%, brown: 44 wt%, red: 52 wt% [emim][$etSO_4$]. The data points were connected to guide the eye.

Dynamic viscosities at 25 °C as function of ionic liquid content are shown in Figure III-29. Significant differences in viscosities between surfactant-limonene and surfactant-ionic liquid mixtures could give information on the microstructure present. However, Figure III-29 illustrates a continuous increase in viscosity along the experimental path without characteristic changes in the slope of the curve. Indeed, typical percolation behaviour cannot be observed. Further curves at other temperatures have not been plotted here as they exhibit similar shape and no information on microstructure can be extracted.

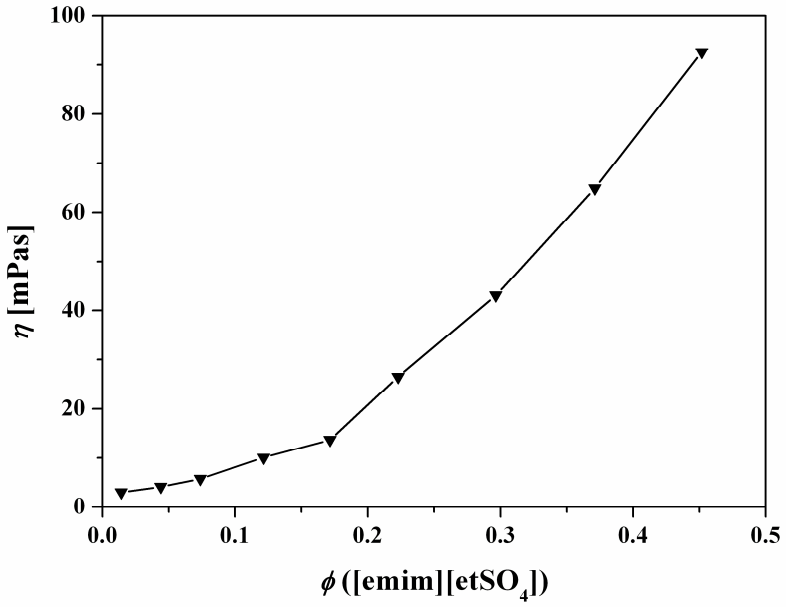

Figure III-29. Dynamic viscosities along the experimental path for microemulsions containing $C_{10}E_4$ at 25 °C as a function of IL-content. The line was drawn to guide the eye.

4.2.3 SAXS Investigations

The system has been investigated by means of conductivity and segregation temperatures along the experimental path. For further applications of the system, *e.g.* as chemical nanoreactors, two samples with a less surfactant concentration have been chosen (35 wt%IL). The samples were investigated with SAXS (Figure III-30). The segregation temperatures of these samples were -12 °C. Small angle X-ray scattering (SAXS) has been measured at temperatures of 30 °C, 25 °C, 10 °C, 0 °C, and -10 °C. The experimental data were fitted according to *Teubner & Strey* (equation III-3).[115] The results from TS-fit and the experimental data are shown in Figure III-30.

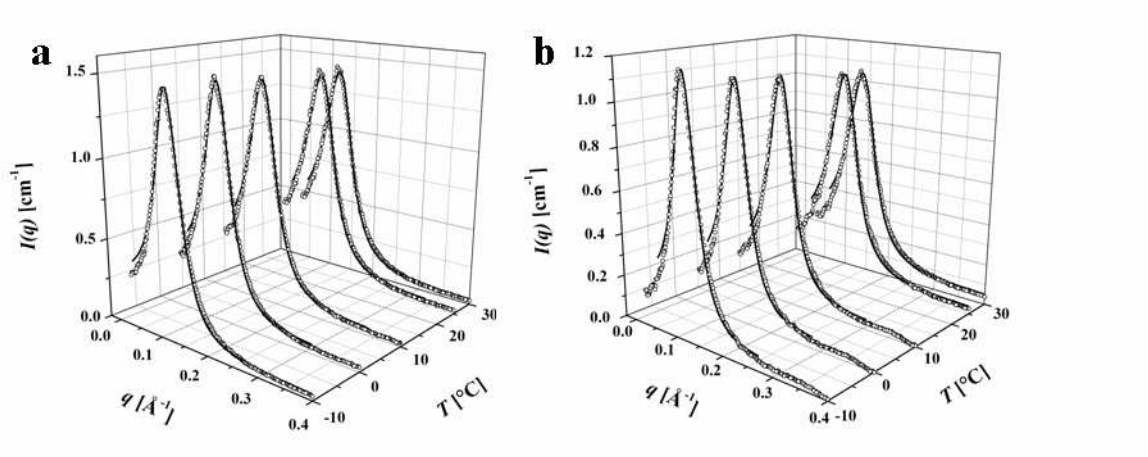

Figure III-30. SAXS spectra of $C_{10}E_4$ based microemulsions. 63 wt% [emim][$etSO_4$], 2 wt% limonene, 35 wt% $C_{10}E_4$ (b). 61 wt% [emim][$etSO_4$], 4 wt% limonene, 35 wt% $C_{10}E_4$ (a).

The three characteristic values, two length scales (domain size d_{TS} and persistence length ξ) and the amphiphilic factor f_a were extracted from the fits according to *Teubner & Strey*. The results are summarized in Table III-9.

Table III-9. Extracted parameter from *Teubner-Strey* evaluation of $C_{10}E_4$ based microemulsions.

	Sample 1 (61wt%IL)			**Sample 7 (63wt%IL)**		
***T* [°C]**	**d_{TS} [Å]**	**ξ [Å]**	**f_a**	**d_{TS} [Å]**	**ξ [Å]**	**f_a**
-10	49.1	30.5	-0.91	45.1	34.5	-0.88
0	49.8	29.4	-0.90	44.9	32.6	-0.86
10	50.3	27.5	-0.89	47.9	31.5	-0.84
25	51.4	25.4	-0.87	47.5	26.8	-0.81
30	51.3	25.4	-0.86	47.1	26.3	-0.81

The domain size remains almost constant with decreasing temperature. In contrast, the domain size calculated for Triton X-100 and Triton X-114 systems increased clearly with decreasing temperature. d_{TS} changes from 51.3 Å (30 °C) to 49.1 Å (-10 °C) for the microemulsion including 61 wt%IL and from 47.1 Å (30° C) to 45.1 Å (-10 °C) for the microemulsion containing 63 wt%IL. The variation is about 2 Å in both cases and therefore can be neglected. Consequently, $C_{10}E_4$ based microemulsions have been formulated whose domain size does not change in the measured temperature range of 40 °C. These observations

underline the choice of these systems for low temperature applications, *e.g.* as reaction media for catalysis or nanoparticle synthesis. The calculated amphiphilic factor for these microemulsions exhibits values between -0.8 and -0.91 for both systems. This is theoretically in the range of well structured bicontinuous microemulsions as proposed by *Teubner & Strey*.[115] This value has to be taken with care as it does not ensure the absence of separated micelles. From this point of research, no exact conclusion about the present microstructure of these two samples can be drawn. Further investigations of dilution lines with SAXS could provide the desired information about the microstructure. Alternatively, microscopy methods like FF-TEM and Cryo-TEM measurements are helpful tools for this purpose.

Viscosities have been measured for these microemulsion compositions as well. The dynamic viscosities were derived from measured kinematic viscosities and measured densities. Prior to this, the existence of *Newtonian* fluids was confirmed by measurements on a cone-plate system as described for Triton X-100 microemulsions before. The results of dynamic viscosities for the two samples are shown in Figure III-31. The values are quite low at 5 °C and allow the conclusion that these systems are suitable for further applications, *i.e.* as reaction media.

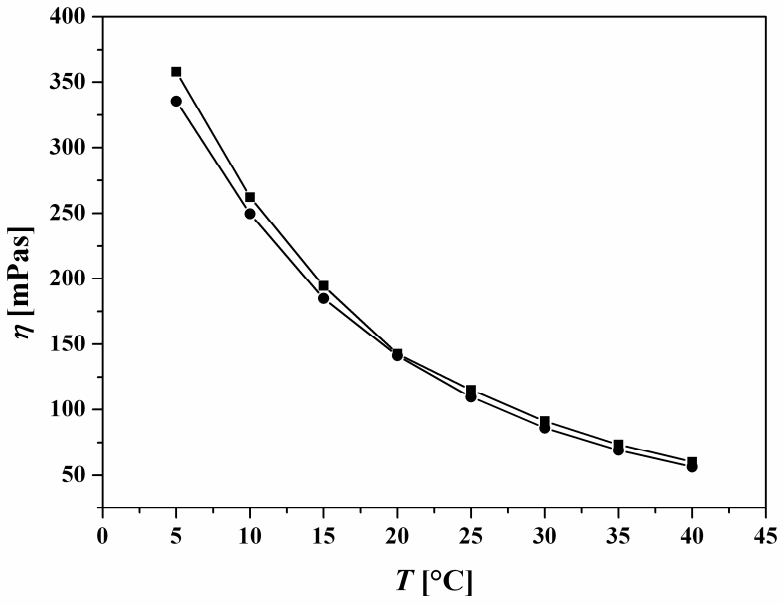

Figure III-31. Measured dynamic viscosities for the compositions: 61 wt% [emim][$etSO_4$], 35 wt% $C_{10}E_4$, 4 wt% limonene (●), and 63 wt% [emim][$etSO_4$], 35 wt% $C_{10}E_4$, 2 wt% limonene (■). The lines were drawn to guide the eye.

4.3 Preliminary Experiments for Applications of Low-Temperature-Stable Microemulsions as Nanoreactor

Synthesis of Ru-nanoparticles in o/IL microemulsions with subsequent hydrogenation of the oil phase:

Preliminary experiments have been realized at the Institut de Chimie de Lyon, Lyon University, *Dr. Catherine C. Santini*. In this context *Dr. Santini and Dr. Campbell* are gratefully acknowledged for performing these experiments.

Ru-particles are synthesized from organo-metallic complexes using hydrogen. The reaction takes place in the apolar cores of the o/ IL microemulsions. The *in situ* synthesis of Ru-particles is followed by catalytic hydrogenation of the substrate limonene. The principle is illustrated in Figure III-32 and was already studied in pure imidazolium based ionic liquids with an alkyl chain length of n = 4-8.[163] The nanoparticle synthesis and the reaction of limonene were tested at 0 °C. First results showed that the organo-metallic precursor was highly soluble in the apolar cores of the microemulsions (25 g/L). Two microemulsion compositions were used: first sample (referred to as sample 1) containing 35 wt% $C_{10}E_4$, 63 wt% [emim][$etSO_4$], and 2 wt% limonene, second sample (referred to as sample 2) containing 35 wt% $C_{10}E_4$, 61 wt% [emim][$etSO_4$], 4 wt% limonene. These samples build model systems. In future the substrate limonene can be substituted by toluene or benzene. The aim is to study the selectivity of catalytic hydrogenation reactions of aromatic rings.

The results of the Ru-particle synthesis and the hydrogenation of limonene in IL based microemulsions can be summarized as follows:

- The Ru-particles have been synthesised under 4 bars of H_2 at 0 °C for 4 days. In sample 1 no size control could be observed, the particle size varied between 10 and 100 nm (transmission electron microscope (TEM) images: Figure III-33). The synthesis in sample 2 produced exclusively particles around 10 nm (TEM images: Figure III-34).
- After the reaction the resulting black suspensions have been analysed by GC. Sample 1: 83 % of the present limonene has been hydrogenated, 21 % para-1-menthene and 62 % menthane (cis- and trans-) were the main products. Sample 2: 67 % of the limonene has been hydrogenated, 38 % para-1-menthene, and 29 % menthane (cis- and trans-) have been the main products. In both samples traces of other menthene isomers were detected (double bond at other positions on the ring).

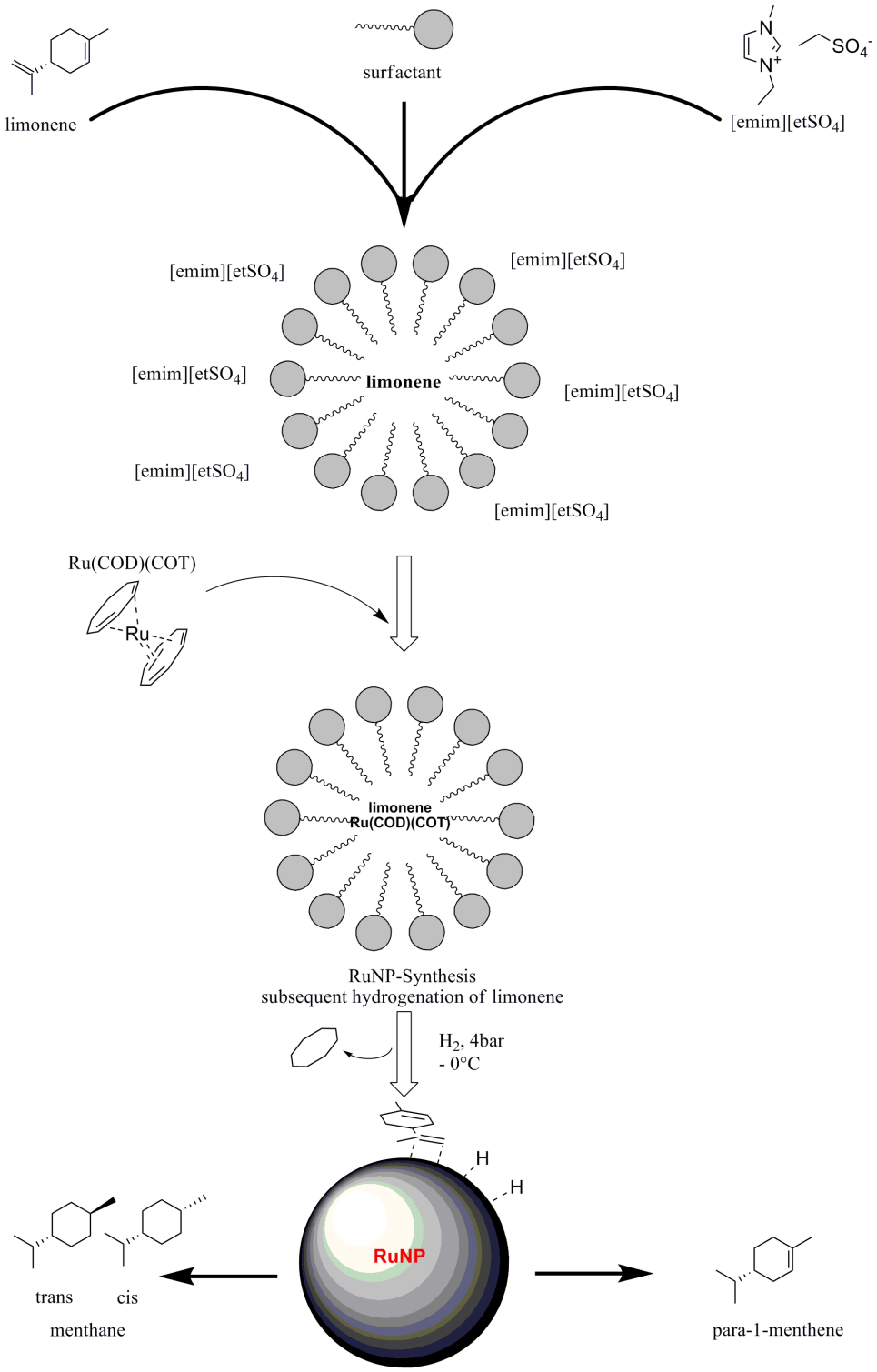

Figure III-32. Schematic illustration of the reaction process: formation of Ru-nanoparticles in o/IL microemulsions followed by a subsequent hydrogenation of limonene.

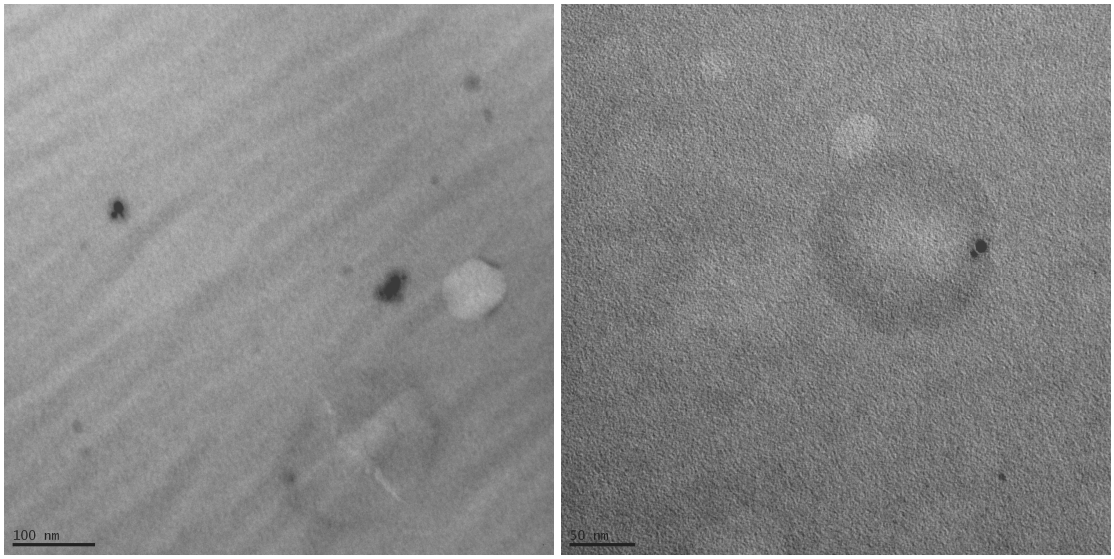

Figure III-33. TEM pictures of Ru-particles synthesized in sample 1 (35 wt% $C_{10}E_4$, 63 wt% [emim][$etSO_4$], 2 wt% limonene).

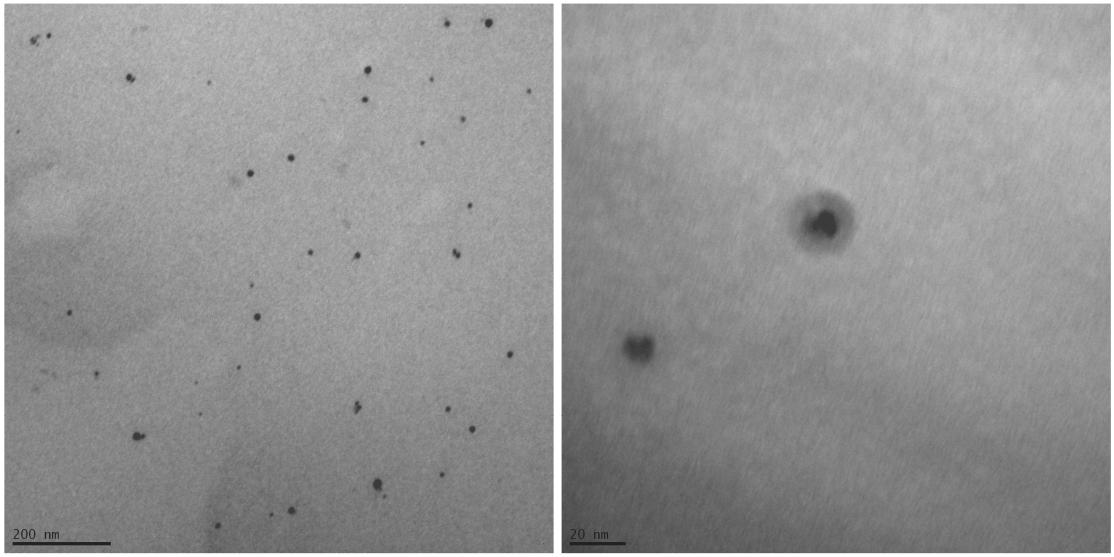

Figure III-34. TEM picture of Ru-particles synthesized in sample 2 (35 wt% $C_{10}E_4$, 61 wt% [emim][$etSO_4$], 4 wt% limonene).

These first experiments have shown that catalytically active Ru-particles can be synthesized in the present microemulsions. However, further experiments at different temperature, reaction times, and finally with different microemulsions are necessary for a correct estimation of the present results. The insufficient size control of the particles built could be due to possible flexible films that exist in this type of microemulsion. Surfactants with linear short alkyl chains often form flexible, deformable films with a bending constant of the order 1 kT.[71] Nevertheless, more experiments are required to confirm this theory. Bending constants for example can be calculated by contrast variation experiments in small angle neutron scattering (SANS).

Epoxidation of limonene in o/IL microemulsions in the presence of m-CPBA:

The epoxidation of limonene should proof the reaction media capability of o/IL microemulsions. For this reason a reaction was chosen that does not contain many reactants, which could destroy the structured microemulsion.

Limonene has been epoxidised in the presence of *m*-CPBA (*meta*-chloroperoxybenzoic acid).[164] The reaction takes place in the apolar cores of the o/IL microemulsions (2 or 4 wt% limonene, 35 wt% $C_{10}E_4$, [emim][$etSO_4$] as continuous phase). The reaction equation is presented in Scheme III-1.

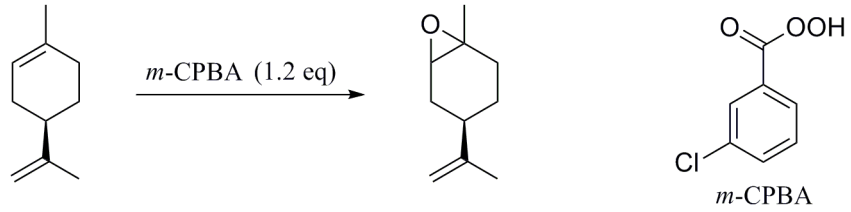

Scheme III-1. Schematic illustration of the epoxidation of limonene with *m*-CPBA.

The utilization of *m*-CPBA has several benefits. Only one reactant is needed to perform the conversion to the desired product. The reaction occurs in a very fast rate and produces almost exclusively the desired product. Therefore, only a small excess of reagent is needed. The microemulsion seemed to be stable over the whole reaction process, which means that no phase separation occurred. Since *m*-CPBA is an electrophilic epoxidation reagent it epoxidises only the electron richer double bond in the six-membered ring, not the sterical more accessible double bond on the side chain.

The reaction process could be easily followed by means of characteristic proton signals of starting material and product in ^{1}H-NMR (Figure III-35). None of the reaction components shows a proton signal in the same ppm range. This allows the determination of product/starting material ratios without further isolation of the product. These ratios are summarised in Table III-10.

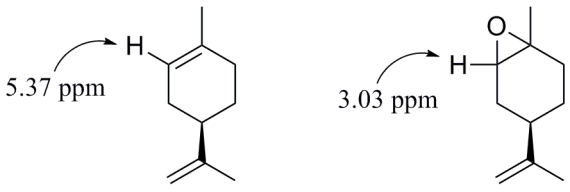

Figure III-35. Essential ^{1}H-NMR shifts of limonene and 1,2-limonene oxide.

Table III-10. Product/starting material ratio derived from NMR-analysis.

t	45 min	1.5 h	3.5 h
RT	1/0.6	1/0.2	1/0
0 °C	1/2	1/0.7	1/<0.02

The resulting 1,2-limonene oxide is a useful starting material for several natural product syntheses. For example, the first step of the synthesis of (*Z*)-(1'*S*,3'*R*,4'*S*)(-)-2-(3',4'-Epoxy-4'-methylcyclohexyl)-6-methylhepta-2,5-diene, a main component of the sex pheromone of the male green stinkbug *Nezara viridula* (Brazil), is the epoxidation of (*S*)-limonene (Scheme III-2).[165] The southern stinkbug is mainly distributed throughout the tropical and neotropical regions of the world and is a major pest of cotton, citrus, and cereal.

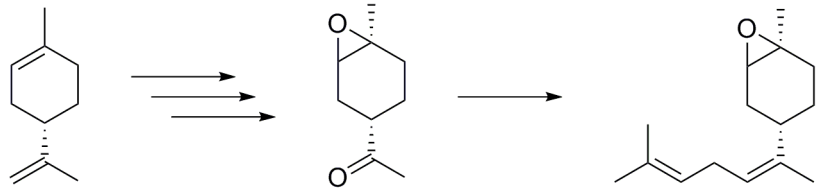

(*Z*)-(1'*S*,3'*R*,4'*S*)(-)-2-(3',4'-Epoxy-4'-methyl cyclohexyl)-6-methylhepta-2,5-diene

Scheme III-2. Limonene as starting material for the synthesis of (Z)-(1'S,3'R,4'S)(-)-2-(3',4'-Epoxy-4'-methylcyclohexyl)-6-methylhepta-2,5-diene.

In addition, the epoxide works as starting material for importing building blocks of vitamin D analogues (Scheme III-3).[166] For instance, 1α,25-dihydroxy vitamin D_3 is known as a strong calcium and phosphorus regulator, but also plays an important role in the regulation of malignant cell proliferation, implied in cancers and other hyperproliferation diseases, cellular differentiation and immunology. Unfortunately, doses required in treatments cause hypercalcaemia side effects that limit its application as a valuable therapeutical agent. Owing to these properties, preparation of vitamin D analogues has attracted the interest of numerous synthetic groups.

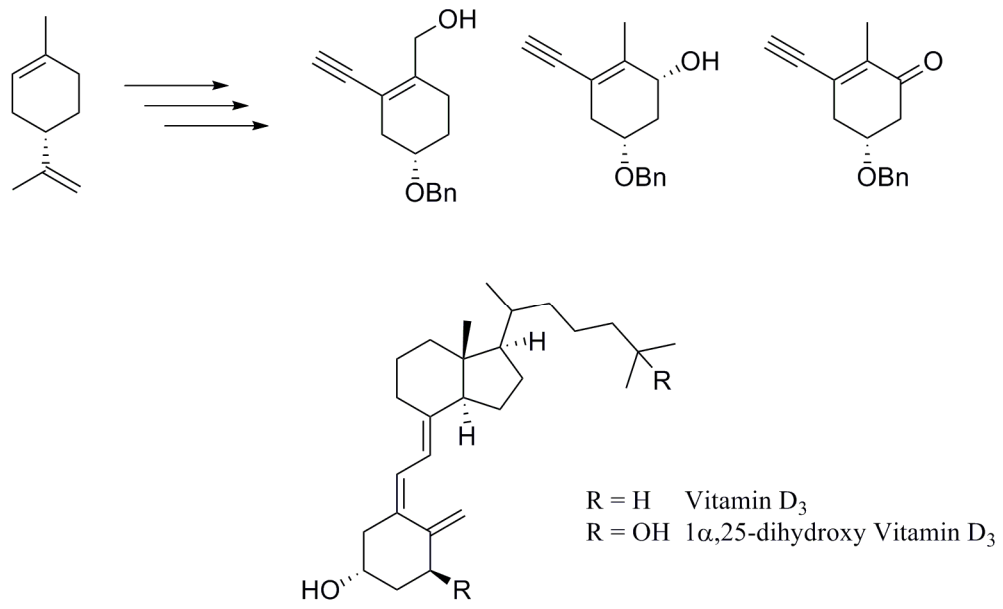

Scheme III-3. Limonene as starting material for building blocks for the synthesis of vitamine D analogues.[166]

4.4. Conclusion

Microemulsions have been formulated including the ionic liquid [emim][$etSO_4$] as polar phase, the oil limonene as apolar phase and the non-ionic surfactant $C_{10}E_4$ as amphiphile. The aim of this project was the establishment of a structured system that exhibits low-temperature-stability and is suitable for potential applications. Further requirements were moderate viscosities and the incorporation of a pure surfactant. The latter is mainly of importance when the microemulsions should serve as reaction media. A high number of substances are present in commercial available non-ionic surfactants due to an EO distribution that cannot be avoided in large-scale productions. However, this distribution fact complicates the utilization of such systems as reaction media. Consequently, the $C_{10}E_4$ system was established and characterized. $C_{10}E_4$ was chosen as its HLB is 10.6 and previous experiments suggested a low HLB for the successful formulation of low-temperature-stable microemulsions. Furthermore, this surfactant can be synthesized easily in the lab. At 25 °C the one phase region of the ternary phase diagram is not as large as for the previously studied systems containing Triton X-100 and Triton X-114. Nevertheless, segregation temperatures measured for samples along the experimental path (45 wt% $C_{10}E_4$) revealed good stabilities as intermediate IL concentrations. Conductivity and viscosity measurements were performed at room temperature and temperatures down to -15 °C and 5 °C, respectively. Comparison with the Triton X-100 and Triton X-114 systems reveals several differences. First, segregation temperatures have different characteristics. In contrast to $C_{10}E_4$ based systems, Triton X

surfactants are most stable at high IL-content. The conductivity characteristics are significantly different as well. In contrast to $C_{10}E_4$, TX-100 and TX-114 microemulsions seem to exhibit too high viscosities as percolation could be observed. High viscosities lead to lower conductivities. Therefore, the increase in conductivity values is not significant enough to be identified as percolation. $C_{10}E_4$ microemulsions indeed have lower viscosities and consequently typical percolation behaviour is observed. The threshold was calculated from the inflection point of the curve $\log(\kappa(\phi_{IL}))$. Additionally, $C_{10}E_4$ microemulsions with 35 wt%IL were characterized by means of SAXS and viscosity measurements. The composition was chosen in regard of applications as reaction media. Preliminary results of the application of $C_{10}E_4$ based microemulsions as reaction media have been presented. On the one hand, the o/IL microemulsion can act as template for the synthesis of Ru-nanoparticles with subsequent hydrogenation of limonene. On the other hand, it serves as reaction media for the epoxidation of limonene. Both reactions have been carried out in o/IL microemulsions preliminary results have been presented.

.

V. Conclusions and Outlook

Three differing microemulsion systems have been established, all suitable for low temperature applications. One ionic liquid, namely [emim][$etSO_4$] was used as polar phase. The apolar phase was represented by the natural oil limonene. The choice for the ionic liquid and the oil resulted from the low glass transition temperature and melting point of the substances, respectively. Three surfactants were studied, Triton X-100, Triton X-114 and $C_{10}E_4$. All three systems show in particular low-temperature-stability. Triton X-100 systems are most stable at high IL-content and Triton X-114 systems show the same behaviour. In contrast, the system formulated with $C_{10}E_4$ is most stable if intermediate amounts of ionic liquid and oil are present. The microemulsions were all investigated by means of low-temperature-stability, conductivity, viscosity, and small angle X-ray scattering. The two microemulsion systems including Triton X-100 and Triton X-114 exhibit elevated viscosities at low temperatures. Consequently, the goal was to find microemulsions with higher fluidity. $C_{10}E_4$ is a suitable surfactant for this purpose. Indeed, preliminary results with $C_{10}E_4$ based microemulsions showed the high potential of these systems for future applications according to low viscosities and the observed temperature-stability. The main difference between the three systems is that $C_{10}E_4$ is a pure surfactant with a less viscosity and therefore more suitable for applications as reaction media. Model reactions have been carried out in these microemulsions: the synthesis of Ru-particles with a subsequent hydrogenation of limonene and the epoxidation of limonene in o/IL microemulsions. Preliminary results showed the high potential of these systems to be used as reaction media. In future, these experiments can be investigated in more detail. Moreover, several other reactions with limonene are possible:

- ***Reaction of (R)-Limonene with S-Thioacids:***

  Thio-products derived from limonene can be used as flavours or flotation-agents. The reaction of *S*-thioacids with (*R*)-limonene is a very attractive route to 9-(*p*-menthenyl) *S*-thiocarboxylates.[167] As in the case of related monoterpene sulfides, the products offer great potentials as starting materials for a multistep preparation of bisabolanes. The reaction is presented in Scheme IV-1. Usually, the reaction occurs under elevated temperatures and in organic solvents. The reaction could be also performed in limonene/IL microemulsions. The effect of this media on the reaction process could be

studied as well as temperature effects. This could lead to a different selectivity compared to the reaction at elevated temperatures.

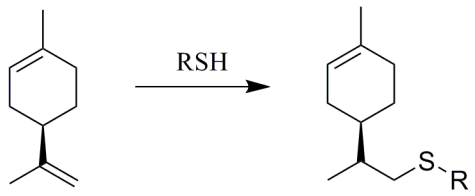

Scheme IV-1. Schematic illustration of the reaction of limonene and R-SH.

- ***Limonene and R-OH: $FeCl_3$ catalyzed functionalization of monterpenes***

The coupling of monoterpenes with alcohols using $FeCl_3$ as catalysis has been reported by *Yadav et al.* for monoterpenes like limonene, isolimonene, α-pinene and β-pinene.[168] The corresponding ethers were obtained in high yields. The reactions were performed at 0 °C and 25 °C, respectively.[168] This is a simple method to functionalize terpenes at mild conditions. Since these reactions are usually carried out in dichloromethane it would be interesting to study them in o/IL microemulsions concerning the aspect of green and sustainable chemistry. The reaction equation is presented in Scheme IV-2.

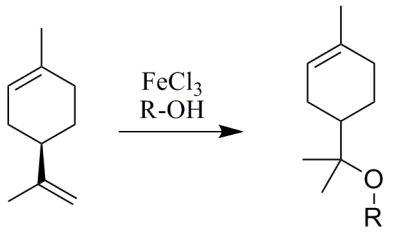

Scheme IV-2. Schematic illustration of the catalytically activated reaction of limonene and R-OH.

Further, some other applications of non-aqueous microemulsions that exhibit low-temperature-stability will be presented:

The utilization of ILs as media for enzymatic reactions has been also reported. It turned out that according to the special characteristics of IL based systems enzyme reactions exhibit excellent selectivity, including substrate-, regio- and enantioselectivity. Consequently, ILs and thereon based microemulsions can be considered as promising reaction media for biocatalytic reactions. Further, the application of the presented microemulsions can be of interest herein as they can be stable over a wide temperature range. Some reports on enzymatic activity in ILs are available, for example for lipase[169-170] and alcohol dehydrogenase.[171]

Another potential application of low-temperature-stable microemulsions could be as carriers for topical and transdermal drug delivery. *Monirruzaman et al.*[92, 172] demonstrated that IL based microemulsions can be suitable drug carriers for molecules that are sparingly soluble in water and oil. ILs turned out to be qualified candidates because they can be capable of dissolving various poorly soluble compounds including drug molecules. In future, the combination of low toxic and pharmaceutical acceptable compounds with the formulation of low-temperature-stable microemulsions could lead to new, required systems for drug delivery.

Lubricants could build another application field for IL based microemulsions. However, not only low-temperature-stability is of importance but also high temperature-stability is required. Under friction high temperatures occur while low temperatures could be adorable for the application of the lubricant.[173-174] Some of the main reasons for the interest in ILs as lubricants are their negligible volatility, non-flammability and their ability to withstand severe environments, such as high temperature or high vacuum.[175-176] Therefore, not only low temperatures should be studied but also the stability at elevated temperatures of the present systems. Further, the microemulsions have to feature a low corrosiveness to special materials depending of course on the material which should be lubricated. In winter these system could possibly also act as a combination of lubricant and lock de-icer. However, this application also requires low corrosiveness.

The potential of the present systems for applications in several fields could be clearly demonstrated in this short outlook. Surely, more experiments are needed to realize one of those suggestions. Nevertheless, the capability as reaction media has been already successfully proved.

Summary

The present work is divided in four main sections. The aim of the thesis was to formulate low-temperature-stable microemulsions. This comprises structured liquid systems that do not exclusively exist at temperatures around 25 °C but also at temperatures that are stable well below 0 °C. For this purpose water, the conventional polar phase in microemulsions was replaced by the ionic liquid 1-ethyl-3-methylimidazolium ethylsulfate ([emim][$etSO_4$]) comprising a glass transition temperature of -80 °C. In addition, a natural oil namely limonene that exhibits a very low melting point of -96 °C was incorporated in the microemulsions. The polar and apolar phase were kept constant and the effect of surfactant nature was studied. Three non-ionic amphiphiles have been used, Triton X-100 (HLB = 13.5), Triton X-114 (HLB = 12.4) and $C_{10}E_4$ (HLB = 10.6). The first two surfactants are commercial available surfactants with a special EO distribution and the last one is a pure surfactant, synthesized in the lab.

The first part of this work deals with the determination of critical aggregation concentrations (cac) of the used surfactants in water and the utilized ionic liquid, [emim][$etSO_4$]. The obtained values in water and ionic liquid are compared to each other and to values that were found in literature. As the cacs in ionic liquids are in general significantly higher than in water, this effect is discussed and explained.

The following part of the work comprises the establishment of a microemulsion system including the amphiphile Triton X-100. The system was characterized at ambient temperatures and temperatures down to -10 °C by means of small angle X-ray scattering, conductivity, viscosity and phase diagrams. The system shows a remarkable wide temperature range where microemulsions exist, for high IL-contents between (-10 and 40) °C. The hydrophilic lipophilic balance (HLB) is a measure of the degree of hydrophilicity and lipophilicity of a surfactant and results for Triton X-100 in a value of 13.5. The question arises which effect the hydrophobicity of the surfactant has on the formulation of low-temperature-stable microemulsions including an ionic liquid as polar phase.

Consequently, the third part of this work deals with the effect of surfactant hydrophobicity of non-aqueous microemulsions that should be stable well below 0 °C. Therefore, the system composed of [emim][$etSO_4$], limonene, and Triton X-114 (HLB = 12.4) was studied. The main difference between both surfactants is the number of ethyleneoxide groups. Triton

X-100 comprises in average 9.5 EO groups and Triton X-114 in average 7.5 EO groups. Thus, this exchange is an increase in surfactant hydrophobicity (lower HLB value). The two microemulsion systems have been compared. The main difference is the increased temperature range in which Triton X-114 microemulsions can be applied. Microemulsions with high IL-content do not undergo a phase separation or freezing down to -35 °C. This value indeed is limited by the enormous viscosity at those temperatures. Finally, the next goal was to formulate systems that exhibit lower viscosities and can be applied therefore as reaction media at low temperatures. Further, the assumption is obvious that a lower HLB value of the surfactant would lead to even better temperature stabilities.

The last part of this work describes the formulation and characterization of microemulsions containing the amphiphile $C_{10}E_4$. This surfactant was synthesized in the lab and is therefore of high purity in contrast to the previous used amphiphiles. This and the resulting low viscosities enable these microemulsions for their application as reaction media. Finally, this has been exemplarily shown for some selected reactions. The formation of catalytically active Ru-particles including a subsequent hydrogenation of the oil phase was reported as well as an epoxidation reaction of limonene in o/IL microemulsions.

Altogether, this work comprises a detailed study of low-temperature-stable microemulsions with the aim to formulate systems that are suitable for future application, *e.g.* as reaction media. The studied systems represent some model systems that can be enlarged to other surfactants, ionic liquids or oils, respectively. An important step has been done towards future works on low-temperature-stable microemulsions.

VI. Appendix

1. List of Publications

1. Zech, O.; Thomaier, S.; Kolodziejski, A.; Touraud, D.; Grillo, I.; Kunz, W., Ionic liquids in microemulsions-a concept to extend the conventional thermal stability range of microemulsions. *Chem. Eur. J.* **2010,** *16* (3), 783-6.
2. Zech, O.; Thomaier, S.; Kolodziejski, A.; Touraud, D.; Grillo, I.; Kunz, W., Ethylammonium nitrate in high temperature stable microemulsions. *J. Colloid Interface Sci.* **2010,** *347* (2), 227-32.
3. Zech, O.; Harrar, A.; Kunz, W., Non-aqueous Microemulsions Containing Ionic Liquids- Properties an Applications, Intech book chapter in "Ionic Liquids, Theory and Applications", *accepted*.
4. Harrar, A.; Zech, O.; Hartl, R.; Bauduin, P.; Zemb, T. N.; Kunz, W., [emim][$etSO_4$] as Polar Phase in Low-temperature-stable Microemulsions. *accepted Langmuir*.
5. Kunz, W.; Maurer, E.; Klein, R.; Touraud, D.; Rengstl, D.; Harrar, A.; Dengler, S.; Zech, O. *Low Toxic Ionic Liquids, Liquid Catanionics, and Ionic Liquid Microemulsions, accepted J. Disp. Sci. Techn.*
6. Harrar, A.; Zech, O.; Klaus, A.; Kunz, W., The Effect of Solvent Hydrophobicity on the Phase Behavior of Non-aqueous Microemulsions. *in preparation.*
7. Klaus, A.; Tiddy, G.J.T.; Grillo, I.; Tomšič, M.; Garcia, H.; Maurer, E.; Harrar, A.; Touraud, D.; Kunz, W. *Solubility of high amounts of triglycerides in water using extended surfactants, in preparation.*

2. List of Figures

Figure I-11. Definition of scattering vector *q*. k_i: incident wave vector, k_f: scattered wave vector, θ: scattering angle.

Figure I-12. Schematic illustration of a dilution plot including the cubic random cell model (black), the model of o/w and w/o microstructure, respectively (green), and the model of repulsive spheres (red).

Figure II-1. Illustration of the used SAXS equipment at the institute ICSM, CEA, Marcoule, France.

Figure II-2. Chemical structure of (*R*)-(+)-limonene, Triton X-100 and Triton X-114 surfactants.

Figure II-3. Chemical structure of [emim][$etSO_4$].

Figure II-4. Chemical structure of tetraethyleneglycol monodecyl ether ($C_{10}E_4$).

Figure III-1. Surface tension measurements for Triton X-100 (A), Triton X-114 (B), $C_{10}E_4$ (C) in water (left, 1) and in [emim][$etSO_4$] (right, 2).

Figure III-2. Ternary phase diagram of [emim][$etSO_4$], limonene, Triton X-100 at 25 °C. The arrow marks the experimental path. A cross highlights the sample investigated by SAXS.

Figure III-3. "Fish"-diagram at constant IL/oil mass ratio of 1:1. 1: single phase microemulsion, "fish-tail"; 3: three phase system, "fish–head"; $\overline{2}$: two phase system, oil/IL microemulsion and excess oil phase, $\underline{2}$: IL/oil microemulsions and excess IL phase.

Figure III-4. Conductivity measured at 25 °C along the experimental path marked in Figure III-2. A, B, C, D, and E mark the detectable subareas.

Figure III-5. Shear stress vs. shear rate at 25 °C obtained by measurements on a *Bohlin Instruments* rheometer for microemulsions with concentrations along the experimental path.

Figure III-6. Dynamic viscosities at 25 °C in dependence on volume fraction [emim][$etSO_4$]. The points A, B, C, D, and E mark the same points as in Figure III-3.

Figure III-7. Lower "Phase Segregation Temperatures" for microemulsions having a composition along the experimental path shown in Figure III-2. Samples between $\phi = 0.43$ and $\phi = 0.58$ do not show a segregation down to at least -20 °C.

Figure III-8. Shear stress vs. shear rate at (10, 15, 20, 25, 30, 35, 40, 45, 50, 55, 60) °C plotted for microemulsions including 50 wt%IL (a), 54 wt%IL (b), and 58 wt%IL.

Figure III-9. Dynamic viscosities for microemulsions with 50 wt% (●), 54 wt% (▲), 58 wt% (■) [emim][$etSO_4$] measured in a temperature range from 0 °C to 40 °C. The data points were connected by a solid line to guide the eye.

Figure III-10. Experimental SAXS data and Teubner-Strey Fit (solid lines) at 25 °C. 5 wt%IL (green), 10 wt%IL (red), 20 wt%IL (blue), 40 wt%IL (magenta), 50 wt%IL (yellow), 54 wt%IL (black), 58 wt%IL (orange).

Figure III-11. Experimental SAXS data (○) and Teubner-Strey-Fit (solid line) for 58 wt% [emim][$etSO_4$] (a), 54 wt% [emim][$etSO_4$] (b), and 50 wt% [emim][$etSO_4$] (c) at different temperatures varying from 40 °C down to -10 °C.

Figure III-12. Dilution plot: experimental data at 25 °C (●) including an assumed error of 15 %, CRC model (─·─), IL/o or o/IL (·····), repulsive spheres (─··─), DOC lamellae (----), DOC cylinder (─).

Figure III-13. Ternary phase diagram at 25 °C for the system: [emim][$etSO_4$], limonene, Triton X-114. The black arrow marks the experimental path that was chosen for further experiments. Crosses highlight the compositions that were further investigated by SAXS measurements.

Figure III-14. Conductivity along the dilution line at 25 °C; A, B, C, D mark the concentrations where a change in microstructure could be possible.

Figure III-15. Experimental SAXS data and TS-fit at ambient temperature for 7 sample compositions along the dilution line.

Figure III-16. Dilution plot: experimental data at 25 °C (●) including an assumed error of 15 %, CRC model (─), IL/o or o/IL (·····), repulsive spheres (─··─).

Figure III-17. Segregation temperatures recorded along the experimental path marked in the ternary phase diagram. The data points were connected to guide the eye.

Figure III-18. SAXS spectra: experimental data (●) and Teubner Strey fit (—) for samples 6 and 7 at -10 °C, 0 °C, 10 °C, 20 °C, 25 °C, 30 °C, and 40 °C.

Figure III-19. Viscosity measurements as a function of temperature. Sample 6 (56 wt%IL) (●). Sample 7 (60 wt%IL) (▼). The data points were connected to guide the eye.

Figure III-20. "Fish"-cut at $\alpha = 0.5$ and conductivity results at 35wt% Triton X-114 between 12 and 35 °C. The data points were connected to guide the eye.

Figure III-21. Ternary phase diagram for [emim][$etSO_4$], limonene and $C_{10}E_4$. The black arrow marks the investigated experimental path at ambient temperature. A cross highlights the microemulsion compositions that were investigated by SAXS measurements.

Figure III-22. Segregation temperatures for $C_{10}E_4$ based microemulsions with compositions along the experimental path.

Figure III-23. Conductivity measured along the experimental path at 25 °C. The line was drawn to guide the eye. ϕ_P denotes the determined percolation threshold.

Figure III-24. $\log(\kappa(\phi))$ plot for the determination of the percolation threshold for $C_{10}E_4$ microemulsions at 25 °C. Measured data is shown in points and the solid curve corresponds to the fourth order polynomial fit.

Figure III-25. Plot for the determination of the two characteristic parameters μ and *s*.

Figure III-26. Conductivity data for $C_{10}E_4$ microemulsions at 0 °C. The line was drawn to guide the eye.

Figure III-27. Conductivity data for $C_{10}E_4$ microemulsions at -15 °C. The line was drawn to guide the eye.

Figure III-28. Dynamic viscosities measured in a temperature range (30-5) °C for microemulsions along the experimental path containing 45 wt% $C_{10}E_4$. Black: 2 wt%, bright green: 6 wt%, blue: 10 wt%, magenta: 16 wt%, yellow: 22 wt%, orange: 28 wt%, green: 36 wt%, brown: 44 wt%, red: 52 wt% [emim][$etSO_4$]. The data points were connected to guide the eye.

Figure III-29. Dynamic viscosities along the experimental path for microemulsions containing $C_{10}E_4$ at 25 °C as a function of IL-content.

Figure III-30. SAXS spectra of $C_{10}E_4$ based microemulsions. Left: 63 wt% [emim][$etSO_4$], 2 wt% limonene, 35 wt% $C_{10}E_4$. Right: 61 wt% [emim][$etSO_4$], 4 wt% limonene, 35 wt% $C_{10}E_4$.

Figure III-31. Measured dynamic viscosities for the compositions: 61 wt% [emim][$etSO_4$], 35 wt% $C_{10}E_4$, 4 wt% limonene (●) and 63 wt% [emim][$etSO_4$], 35 wt% $C_{10}E_4$, 2 wt% limonene (■). The lines are to guide the eye.

3. List of Tables

Table III-5. Values of domain size d_{TS}, correlation length ξ, and amphiphilic factor f_a derived from Teubner-Strey Fits for 58 wt% [emim][etSO$_4$], 54 wt% [emim][etSO$_4$], and 50 wt% [emim][etSO$_4$] at various temperatures.

Table III-6. Results from SAXS data evaluation with Teubner-Strey-formula for measurements at 25 °C and sample 1 to sample 7.

Table III-7. Extracted experimental invariant Q_{exp}, calculated theoretical invariant Q_{theo}, *Porod* limit and specific surface Σ for the seven concentrations measured at 25 °C.

Table III-8. Results from Teubner-Strey evaluation of SAXS data for sample 6 and sample 7 and results for specific surface Σ at various temperatures.

Table III-9. Extracted parameter from *Teubner-Strey* evaluation of $C_{10}E_4$ based microemulsions.

Table III-10. Product/starting material ratio derived from NMR-analysis.

4. List of Schemes

Scheme III-1. Schematic illustration of the epoxidation of limonene with *m*-CPBA.

Scheme III-2. Limonene as starting material for the synthesis of (Z)-(1'S,3'R,4'S)(-)-2-(3',4'-Epoxy-4'-methylcyclohexyl)-6-methylhepta-2,5-diene.

Scheme III-3. Limonene as starting material for building blocks for the synthesis of vitamine D analogues.[166]

Scheme IV-1. Schematic illustration of the reaction of limonene and R-SH.

Scheme IV-2. Schematic illustration of the catalytically activated reaction of limonene and an alcohol.

References

1. Wasserscheid, P.; Keim, W., Ionic Liquids-New “Solutions” for Transition Metal Catalysis. *Angew. Chem., Int. Ed.* **2000,** *39*, 3772.

2. Earle, M. J.; Seddon, K. R., Ionic Liquids. Green solvents for the future. *Pure Appl. Chem.* **2000,** *72*, 8.

3. Welton, T., Room-Temperature Ionic Liquids. Solvents for Synthesis and Catalysis. *Chem. Rev.* **1999,** *99*, 2071.

4. Greaves, T. L.; Weerawardena, A.; Fong, C.; Krodkiewska, I.; Drummond, C. J., Protic Ionic Liquids: Solvents with Tunable Phase Behavior and Physicochemical Properties. *J. Phys. Chem. B* **2006,** *110*, 22479.

5. Greaves, T. L.; Drummond, C. J., Protic Ionic Liquids: Properties and Applications. *Chem. Rev.* **2007,** *108*, 206.

6. Tao, G.-h.; He, L.; Liu, W.-s.; Xu, L.; Xiong, W.; Wang, T.; Kou, Y., Preparation, characterization and application of amino acid-based green ionic liquids. *Green Chem.* **2006,** *8*, 639.

7. Fukaya, Y.; Iizuka, Y.; Sekikawa, K.; Ohno, H., Bio ionic liquids: room temperature ionic liquids composed wholly of biomaterials. *Green Chem.* **2007,** *9*, 1155.

8. Pernak, J.; Syguda, A.; Mirska, I.; Pernak, A.; Nawrot, J.; Pradzyńska, A.; Griffin, S. T.; Rogers, R. D., Choline-Derivative-Based Ionic Liquids. *Chem.--Eur. J.* **2007,** *13*, 6817.

9. Zech, O.; Kellermeier, M.; Thomaier, S.; Maurer, E.; Klein, R.; Schreiner, C.; Kunz, W., Alkali Metal Oligoether Carboxylates—A New Class of Ionic Liquids. *Chem.--Eur. J.* **2009,** *15*, 1341.

10. van Rantwijk, F.; Sheldon, R. A., Biocatalysis in Ionic Liquids. *Chem. Rev.* **2007,** *107*, 2757.

11. Pârvulescu, V. I.; Hardacre, C., Catalysis in Ionic Liquids. *Chem. Rev.* **2007,** *107*, 2615.

12. Haumann, M.; Riisager, A., Hydroformylation in Room Temperature Ionic Liquids (RTILs): Catalyst and Process Developments. *Chem. Rev.* **2008,** *108*, 1474.

13. Martins, M. A. P.; Frizzo, C. P.; Moreira, D. N.; Zanatta, N.; Bonacorso, H. G., Ionic Liquids in Heterocyclic Synthesis. *Chem. Rev.* **2008,** *108*, 2015.

14. Blanchard, L. A.; Hancu, D.; Beckman, E. J.; Brennecke, J. F., Green processing using ionic liquids and CO2. *Nature* **1999,** *399*, 28.

15. Hapiot, P.; Lagrost, C., Electrochemical Reactivity in Room-Temperature Ionic Liquids. *Chem. Rev.* **2008,** *108*, 2238.

16. Hao, J.; Zemb, T., Self-assembled structures and chemical reactions in room-temperature ionic liquids. *Current Opinion in Colloid & Interface Science* **2007,** *12*, 129.

17. Greaves, T. L.; Drummond, C. J., Ionic liquids as amphiphile self-assembly media. *Chem. Soc. Rev.* **2008,** *37*, 1709.

18. Qiu, Z.; Texter, J., Ionic liquids in microemulsions. *Curr. Opin. Colloid Interface Sci.* **2008,** *13*, 252.

19. Friberg, E.; Podzimek, M., A non-aqueous microemulsion. *Colloid & Polymer Science* **1984,** *262*, 252.

20. Rico, I.; Lattes, A., Waterless microemulsions. *New. J. Chem.* **1984,** *8*, 429.

21. Saidi, Z.; Mathew, C.; Peyrelasse, J.; Boned, C., Percolation and critical exponents for the viscosity of microemulsions. *Phys. Rev. A* **1990,** *42*, 872.

22. Ray, S.; Moulik, S. P., Dynamics and Thermodynamics of Aerosol OT-Aided Nonaqueous Microemulsions. *Langmuir* **1994,** *10*, 2511.

23. Chang, D. R., Conductivity of molten salts in the presence of oil and surfactant. *Langmuir* **1990,** *6*, 1132.

24. Gao, H.; Li, J.; Han, B.; Chen, W.; Zhang, J.; Zhang, R.; Yan, D., Microemulsions with ionic liquid polar domains. *Phys. Chem. Chem. Phys.* **2004,** *6*, 2914.

25. Atkin, R.; Warr, G. G., Phase behavior and microstructure of microemulsions with a room-temperature ionic liquid as the polar phase. *J. Phys. Chem. B* **2007,** *111*, 9309.

26. Thomaier, S.; Kunz, W., Aggregates in mixtures of ionic liquids. *J. Mol. Liq.* **2007,** *130*, 104.

27. Zech, O.; Thomaier, S.; Bauduin, P.; Rück, T.; Touraud, D.; Kunz, W., Microemulsions with an Ionic Liquid Surfactant and Room Temperature Ionic Liquids As Polar Pseudo-Phase. *J. Phys. Chem. B* **2008,** *113*, 465.

28. Zech, O.; Thomaier, S.; Kolodziejski, A.; Touraud, D.; Grillo, I.; Kunz, W., Ionic liquids in microemulsions-a concept to extend the conventional thermal stability range of microemulsions. *Chem.--Eur. J.* **2010,** *16*, 783.

29. Zech, O.; Thomaier, S.; Kolodziejski, A.; Touraud, D.; Grillo, I.; Kunz, W., Ethylammonium nitrate in high temperature stable microemulsions. *J. Colloid Interface Sci.* **2010,** *347*, 227.

30. Zech, O.; Bauduin, P.; Palatzky, P.; Touraud, D.; Kunz, W., Biodiesel, a sustainable oil, in high temperature stable microemulsions containing a room temperature ionic liquid as polar phase. *Energy Environ. Sci.* **2010,** *3*, 846.

31. Zech, O. Ionic Liquids in Microemulsions - A Concept to Extend the Conventional Thermal Stability Range of Microemulsions. University of Regensburg, Regensburg, 2010.

32. Gao, Y.; Li, N.; Hilfert, L.; Zhang, S.; Zheng, L.; Yu, L., Temperature-Induced Microstructural Changes in Ionic Liquid-Based Microemulsions. *Langmuir* **2009,** *25*, 1360.

33. Atkin, R.; Bobillier, S. M. C.; Warr, G. G., Propylammonium Nitrate as a Solvent for Amphiphile Self-Assembly into Micelles, Lyotropic Liquid Crystals, and Microemulsions. *J. Phys. Chem. B* **2010,** *114*, 1350.

34. Wasserscheid, P.; Welton, T., *Ionic Liquids in Synthesis*. Wiley-VCH: Weinheim, 2008; Vol. 1.

35. Gabriel, S., Ethylamine derivates. *Berichte der Deutschen Chemischen Gesellschaft* **1888,** *21*, 566.

36. Walden, P., Molecular weights and electrical conductivity of several fused salts. *Izv. Imp. Akad. Nauk (Bull. Acad. Imp. Sci. St.-Pétersbourg)* **1914,** *8*, 405.

37. Plechkova, N. V.; Seddon, K. R., Applications of ionic liquids in the chemical industry. *Chem. Soc. Rev.* **2008,** *37*, 123.

38. Evans, D. F.; Chen, S. H.; Schriver, G. W.; Arnett, E. M., Thermodynamics of Solution of Non-Polar Gases in a Fused Salt - Hydrophobic Bonding Behavior in a Non-Aqueous System. *Abstr. Pap. Am. Chem. Soc.* **1981,** *181*, 121.

39. Evans, D. F.; Yamauchi, A.; Wei, G. J.; Bloomfield, V. A., Micelle Size in Ethylammonium Nitrate as Determined by Classical and Quasi-Elastic Light-Scattering. *J. Phys. Chem.* **1983,** *87*, 3537.

40. MacFarlane, D. R.; Seddon, K. R., Ionic liquids- progress on the fundamental issues. *Aust. J. Chem.* **2007,** *60*, 3.

41. Weast, R. C., *Handbook of Chemistry and Physics*. 55 ed.; CRC Press: Cleveland, 1974.

42. Seddon, K. R., Ionic Liquids for Clean Technology. *J. Chem. Technol. Biotechnol.* **1997,** *68*, 351.

43. Born, M.; Landé, A., The absolute calculation of crystal properties with the aid of the Bohr atomic model. *Sitzb. kg. preuss. Akad.* **1918,** *45*, 1048.

44. Kapustinskii, A. F., Latice energy of ionic crystals. *Quart. Revs.* **1956,** *10*, 283.

45. Krossing, I.; Slattery, J. M.; Daguenet, C.; Dyson, P. J.; Oleinikova, A.; Weingärtner, H., Why Are Ionic Liquids Liquid? A Simple Explanation Based on Lattice and Solvation Energies. *J. Am. Chem. Soc.* **2006,** *128*, 13427.

46. Earle, M. J.; Esperanca, J. M. S. S.; Gilea, M. A.; Canongia Lopes, J. N.; Rebelo, L. P. N.; Magee, J. W.; Seddon, K. R.; Widegren, J. A., The distillation and volatility of ionic liquids. *Nature* **2006,** *439*, 831.

47. MacFarlane, D. R.; Pringle, J. M.; Johansson, K. M.; Forsyth, S. A.; Forsyth, M., Lewis base ionic liquids. *Chem. Commun.* **2006**, 1905.

48. Wasserscheid, P., Chemistry: Volatile times for ionic liquids. *Nature* **2006,** *439*, 797.

49. Angell, C. A., Formation of Glasses from Liquids and Biopolymers. *Science* **1995,** *267*, 1924.

50. Walden, P., Organic solvents and ionization media. III. Interior friction and its relation to conductivity. *Z. Phys. Chem.* **1906,** *55*, 207.

51. Xu, W.; Angell, C. A., Solvent-Free Electrolytes with Aqueous Solution-Like Conductivities. *Science* **2003,** *302*, 422.

52. Xu, W.; Cooper, E. I.; Angell, C. A., Ionic Liquids: Ion Mobilities, Glass Temperatures, and Fragilities. *J. Phys. Chem. B* **2003,** *107*, 6170.

53. Yoshizawa, M.; Xu, W.; Angell, C. A., Ionic Liquids by Proton Transfer: Vapor Pressure, Conductivity, and the Relevance of ΔpKa from Aqueous Solutions. *J. Am. Chem. Soc.* **2003,** *125*, 15411.

54. Fraser, K. J.; Izgorodina, E. I.; Forsyth, M.; Scott, J. L.; MacFarlane, D. R., Liquids intermediate between "molecular" and "ionic" liquids: Liquid Ion Pairs? *Chem. Commun.* **2007**, 3817.

55. Reichardt, C., Empirische Parameter der Lösungsmittelpolarität. *Angew. Chem.* **1965,** *77*, 30.

56. Reichardt, C., Polarity of ionic liquids determined empirically by means of solvatochromic pyridinium N-phenolate betaine dyes. *Green Chem.* **2005,** *7*, 339.

57. Byrne, N.; Howlett, P. C.; MacFarlane, D. R.; Forsyth, M., The Zwitterion Effect in Ionic Liquids: Towards Practical Rechargeable Lithium-Metal Batteries. *Adv. Mater.* **2005,** *17*, 2497.

58. Wang, P.; Zakeeruddin, S. M.; Moser, J.-E.; Grätzel, M., A New Ionic Liquid Electrolyte Enhances the Conversion Efficiency of Dye-Sensitized Solar Cells. *J. Phys. Chem. B* **2003,** *107*, 13280.

59. Yamanaka, N.; Kawano, R.; Kubo, W.; Kitamura, T.; Wada, Y.; Watanabe, M.; Yanagida, S., Ionic liquid crystal as a hole transport layer of dye-sensitized solar cells. *Chem. Commun.* **2005,** *41*, 740.

60. Hoar, T. P.; Schulman, J. H., Transparent water-in-oil dispersions: the oleopathic hydro-micelle. *Nature* **1943,** *152*, 102.

61. Schulman, J. H.; Stoeckenius, W.; Price, L. M., Mechanism of formation and structure of micro emulsions by electron microscopy. *Journal of Physical Chemistry* **1959,** *63*, 1677.

62. Danielsson, I.; Lindman, B., The definition of microemulsion. *Colloids and Surfaces* **1981,** *3*, 391.

63. Winsor, P. A., *Solvent properties of amphiphilc compounds*. Butterworth: London, 1954.

64. Salager, J.-L.; Antón, R. E., Ionic microemulsions. In *Handbook of Microemulsions Science and Technology*, Kumar, P.; Mittal, K. L., Eds. Dekker: New York, 1999; Vol. chap. 8, pp 247.

65. Paul, B. K.; Moulik, S. P., Microemulsions: an Overview. *J. Dispersion Sci. Technol.* **1997,** *18*, 301

66. Angel, L. R.; Evans, D. F.; Ninham, B. W., Three-component ionic microemulsions. *Journal of Physical Chemistry* **1983,** *87*, 538.

67. Bellocq, A. M.; Biais, J.; Bothorel, P.; Clin, B.; Fourche, G.; Lalanne, P.; Lemaire, B.; Lemanceau, B.; Roux, D., Microemulsions. *Adv. Colloid Interface Sci.* **1984,** *20*, 167.

68. Rakshit, A. K.; Moulik, S. P., Physicochemistry of W/O microemulsions. Formation, stability, and droplet clustering. . In *Surfactant Science Series*, 2009; Vol. 144 (Microemulsions), pp 17.

69. Pieruschka, P.; Marcelja, S., Monte Carlo Simulation of Curvature-Elastic Interfaces. *Langmuir* **1994,** *10*, 345.

70. Winsor, P. A., Hydrotropy, solubilization, and related emulsification processes. I. *Transactions of the Faraday Society* **1948,** *44*, 376.

71. Sottmann, T.; Stubenrauch, C., Phase Behaviour, Interfacial Tension and Microstructure of Microemulsions. In *Microemulsions,* Stubenrauch, C., Ed. Wiley: Chichester, 2009; pp 1.

72. Kahlweit, M.; Strey, R.; Firman, P., Search for tricritical points in ternary systems: water-oil-nonionic amphiphile. *J. Phys. Chem.* **1986,** *90*, 671.

73. Kahlweit, M.; Strey, R.; Firman, P.; Haase, D., Phase behavior of ternary systems: water-oil-nonionic surfactant as a near-tricritical phenomenon. *Langmuir* **1985,** *1*, 281.

74. Kahlweit, M.; Strey, R.; Firman, P.; Haase, D.; Jen, J.; Schomaecker, R., General patterns of the phase behavior of mixtures of water, nonpolar solvents, amphiphiles, and electrolytes. 1. *Langmuir* **1989,** *4*, 499.

75. Kahlweit, M.; Strey, R.; Haase, D.; Firman, P., Properties of the three-phase bodies in water-oil-nonionic amphiphile mixtures. *Langmuir* **1988,** *4*, 785.

76. Kahlweit, M.; Strey, R.; Busse, G., Microemulsions: a qualitative thermodynamic approach. *J. Phys. Chem.* **1990,** *94*, 3881.

77. Kahlweit, M.; Strey, R.; Busse, G., Weakly to strongly structured mixtures. *Phys. Rev. E: Stat., Nonlinear, Soft Matter Phys.* **1993,** *47*, 4197.

78. Kahlweit, M.; Strey, R.; Firman, P.; Haase, D.; Jen, J.; Schomaecker, R., General patterns of the phase behavior of mixtures of water, nonpolar solvents, amphiphiles, and electrolytes. 1. *Langmuir* **1988,** *4*, 499.

79. Evans, D. F.; Wennerström, H., *The Colloidal Domain- where Physics, Chemistry, Biology, and Tehcnology meet--2nd ed.* Wiley: New York, 1999.

80. Wormuth, K.; Lade, O.; Lade, M.; Schomäcker, R., Microemulsions. In *Handbook of Applied Surface and Colloid Chemistry*, Holmberg, K., Ed. Wiley: U.K, 2002; Vol. 2, pp 55.

81. Klier, J.; Tucker, C. J.; Kalantar, T. H.; Green, D. P., Properties and Applications of Microemulsions. *Adv. Mater.* **2000,** *12*, 1751.

82. Haegel, F.-H.-.; Lopez, J. C.; Salager, J.-L.; Engelskirchen, S., Microemulsions in Large Scale Applications. In *Microemulsions*, Stubenrauch, C., Ed. Wiley: Chichester, 2009; pp 302.

83. Lattes, A.; Rico, I., Aggregation in formamide solution: Reactivity and structure of non-aqueous microemulsions. *Colloids Surf.* **1989,** *35*, 221.

84. Evans, D. F.; Yamauchi, A.; Roman, R.; Casassa, E. Z., Micelle Formation in Ethylammonium Nitrate, a Low-Melting Fused Salt. *J. Colloid Interface Sci.* **1982,** *88*, 89.

85. Evans, D. F.; Kaler, E. W.; Benton, W. J., Liquid crystals in a fused salt: .beta.,.gamma.-distearoylphosphatidylcholine in N-ethylammonium nitrate. *J. Phys. Chem.* **1983,** *87*, 533.

86. Anderson, J. L.; Pino, V.; Hagberg, E. C.; Sheares, V. V.; Armstrong, D. W., Surfactant solvation effects and micelle formation in ionic liquids. *Chem. Commun.* **2003,** *39*, 2444.

87. Hao, J.; Song, A.; Wang, J.; Chen, X.; Zhuang, W.; Shi, F.; Zhou, F.; Liu, W., Self-Assembled Structure in Room-Temperature Ionic Liquids. *Chem.--Eur. J.* **2005,** *11*, 3936.

88. Patrascu, C.; Gauffre, F.; Nallet, F.; Bordes, R.; Oberdisse, J.; de Lauth-Viguerie, N.; Mingotaud, C., Micelles in ionic liquids: aggregation behavior of alkyl poly(ethyleneglycol)-ethers in 1-butyl-3-methyl-imidazolium type ionic liquids. *ChemPhysChem* **2006,** *7*, 99.

89. Schubert, K. V.; Busse, G.; Strey, R.; Kahlweit, M., Microemulsions with formamide as polar solvent. *J. Phys. Chem.* **1993,** *97*, 248.

90. Cheng, S.; Zhang, J.; Zhang, Z.; Han, B., Novel Microemulsions: Ionic Liquid-in-Ionic Liquid. *Chem. Commun.* **2007,** *43*, 2497.

91. Zhao, M.; Zheng, L.; Bai, X.; Li, N.; Yu, L., Fabrication of silica nanoparticles and hollow spheres using ionic liquid microemulsion droplets as templates. *Colloids Surf., A* **2009,** *346*, 229.

92. Moniruzzaman, M.; Tahara, Y.; Tamura, M.; Kamiya, N.; Goto, M., Ionic liquid-assisted transdermal delivery of sparingly soluble drugs. *Chem. Commun.* **2010,** *46*, 1452.

93. Gayet, F.; El Kalamouni, C.; Lavedan, P.; Marty, J.-D.; Brûlet, A.; Lauth-de Viguerie, N., Ionic liquid/oil microemulsions as chemical nanoreactors. *Langmuir* **2009,** *25*, 9741.

94. Yan, F.; Yu, S.; Zhang, X.; Qiu, L.; Chu, F.; You, J.; Lu, J., Enhanced Proton Conduction in Polymer Electrolyte Membranes as Synthesized by Polymerization of Protic Ionic Liquid-Based Microemulsions. *Chem. Mater.* **2009,** *21*, 1480.

95. Gao, Y.; Zhang, J.; Xu, H.; Zhao, X.; Zheng, L.; Li, X.; Yu, L., Structural Studies of 1-Butyl-3-methylimidazolium Tetrafluoroborate/TX-100/ p-Xylene Ionic Liquid Microemulsions. *ChemPhysChem* **2006,** *7*, 1554.

96. Gao, Y.; Wang, S.; Zheng, L.; Han, S.; Zhang, X.; Lu, D.; Yu, L.; Ji, Y.; Zhang, G., Microregion detection of ionic liquid microemulsions. *J. Colloid Interface Sci.* **2006,** *301*, 612.

97. Eicke, H. F.; Borkovec, M.; Das-Gupta, B., Conductivity of water-in-oil microemulsions: a quantitative charge fluctuation model. *J. Phys. Chem.* **1989,** *93*, 314.

98. Kallay, N.; Tomic, M.; Chittofrati, A., Conductivity of water-in-oil microemulsions: Comparison of the Boltzmann statistics and the charge fluctuation model. *Colloid & Polymer Science* **1992,** *270*, 194.

99. Kallay, N.; Chittofrati, A., Conductivity of microemulsions: refinement of charge fluctuation model. *J. Phys. Chem.* **1990,** *94*, 4755.

100. Hall, D. G., Conductivity of microemulsions: an improved charge fluctuation model. *J. Phys. Chem.* **1990,** *94*, 429.

101. Halle, B.; Bjorling, M., Microemulsions as macroelectrolytes. *J. Chem. Phys.* **1995,** *103*, 1655.

102. Lagües, M.; Ober, R.; Taupin, C., Study of structure and electrical conductivity in microemulsions : Evidence for percolation mechanism and phase inversion. *J. Physique Lett.* **1978,** *39*, 487.

103. Laguës, M., Electrical conductivity of microemulsions : a case of stirred percolation. *J. Physique Lett.* **1979,** *40*, 331.

104. Kirkpatrick, S., Classical Transport in Disordered Media: Scaling and Effective-Madium Theories. *Phys. Rev. Lett.* **1971,** *27*, 4.

105. Mehta, S. K.; Kaur, K.; Kaur, G.; Basin, K. K., Percolation Phenomenon in Microemulsions: Effect of External Entity. In *Microemulsions-Properties and Applications*, Fanun, M., Ed. CRC Press: 2009.

106. Blattner, C.; Bittner, J.; Schmeer, G.; Kunz, W., Electrical conductivity of reverse micelles in supercritical carbon dioxide. *Phys. Chem. Chem. Phys.* **2002,** *4*, 1921.

107. Grest, G. S.; Webman, I.; Safran, S. A.; Bug, A. L. R., Dynamic percolation in microemulsions. *Phys. Rev. A* **1986,** *33*, 2842.

108. Derrida, B.; Stauffer, D.; Herrmann, H. J.; Vannimenus, J., Transfer matrix calculation of conductivity in three-dimensional random resistor networks at percolation threshold. *J. Physique Lett.* **1983,** *44*, 701.

109. Ajith, S.; John, A. C.; Rakshit, A. K., Physicochemical studies of microemulsions. *J. Appl. Chem.* **1994,** *66*, 6.

110. Cates, M. E.; Candau, S. J., Statics and dynamics of worm-like surfactant micelles. *J. Phys.: Condens. Matter* **1990,** *2*, 6869.

111. Peyrelasse, J.; Moha-Ouchane, M.; Boned, C., Viscosity and the phenomenon of percolation in microemulsions. *Phys. Rev. A* **1988,** *38*, 4155.

112. Lindner, P.; Zemb, T., *Neutrons, X-rays and Light: Scattering Methods Applied to Soft Condensed Matter*. Elsevier: Amsterdam, 2002.

113. Dianouy, A.-J.; Lander, G., *Neutron Data Booklet*. 2 ed.; Institute Laue-Langevin: 2003.

114. Engelskirchen, S.; Elsner, N.; Sottmann, T.; Strey, R., Triacylglycerol microemulsions stabilized by alkyl ethoxylate surfactants--A basic study: Phase behavior, interfacial tension and microstructure. *J. Colloid Interface Sci.* **2007,** *312*, 114.

115. Teubner, M.; Strey, R., Origin of the scattering peak in microemulsions. *J. Chem. Phys.* **1987,** *87*, 3195.

116. Strey, R.; Glatter, O.; Schubert, K.-V.; Kaler, E. W., Small-angle neutron scattering of D[sub 2]O--C[sub 12]E[sub 5] mixtures and microemulsions with n-octane: Direct analysis by Fourier transformation. *J. Chem. Phys.* **1996,** *105*, 1175.

117. Eastoe, J.; Gold, S.; Rogers, S. E.; Paul, A.; Welton, T.; Heenan, R. K.; Grillo, I., Ionic Liquid-in-Oil Microemulsions. *J. Am. Chem. Soc.* **2005,** *127*, 7302.

118. Porod, G., The X-ray small angle scattering of close-packed colloid systems. I. *Kolloid Z.* **1951,** *124*, 32.

119. Glatter, O.; Kratky, O., *Small Angle X-Ray Scattering*. Academic Press: London, 1982.

120. Leitao, H.; da Gama, M. M. T.; Strey, R., Scaling of the interfacial tension of microemulsions: A Landau theory approach. *J. Chem. Phys.* **1998,** *108*, 4189.

121. Zemb, T.; Barnes, I.; Derian, P.; Ninham, B., Scattering as a critical test of microemulsion structural models. In *Trends in Colloid and Interface Science IV*, Zulauf, M.; Lindner, P.; Terech, P., Eds. Springer Berlin / Heidelberg: 1990; Vol. 81, pp 20.

122. Milner, S. T.; Safran, S. A.; Andelman, D.; Cates, M. E.; Roux, D., Correlations and structure factor of bicontinuous microemulsions. *J. Phys. France* **1988,** *49*, 1065.

123. Jouffroy, J.; Levinson, P.; de Gennes, P. G., Phase equilibria involving microemulsions (Remarks on the Talmon-Prager model). *J. Phys. France* **1982,** *43*, 1241.

124. Zemb, T., Flexibility, persistence length and bicontinuous microstructures in microemulsions. *C. R. Chim.* **2009,** *12*, 218.

125. Zemb, T. N., The DOC model of microemulsions: microstructure, scattering, conductivity and phase limits imposed by sterical constraints. *Colloids Surf., A* **1997,** *129-130*, 435.

126. Barnes, I. S.; Hyde, S. T.; Ninham, B. W.; Derian, P. J.; Drifford, M.; Zemb, T. N., Small-angle x-ray scattering from ternary microemulsions determines microstructure. *J. Phys. Chem.* **1988,** *92*, 2286.

127. Clausse, M.; Nicolas-Morgantini, L.; Zradba, A.; Touraud, D., *Surfactant Science Series, Microemulsions Systems*. Dekker: New York, 1987.

128. Wachter, R.; Barthel, J., *Ber. Bunsen-Ges. Phys. Chem.* **1979,** *83*, 9.

129. Barthel, J.; Feuerlein, F.; Neueder, R.; Wachter, R., Calibration of conductance cells at various temperatures. *J. Solution Chem.* **1980,** *9*, 209.

130. Robinson, R. A.; Stokes, R. H., *Electrolyte Solutions*. 2 ed.; Butterworth: London, 1970.

131. Kindler, M. Experimentelle Untersuchungen zur Bestimmung der Struktur nichtwässriger Elektrolytlösungen aus der Temperaturabhängigkeit ihrer elektrischen Leitfähigkeit. University of Regensburg, Regensburg, 1985.

132. Wachter, R. Experimentelle Untersuchungen zur Bestimmung der Struktur nichtwässriger Elektrolytlösungen aus der Temperaturabhängigkeit ihrer elektrischen Leitfähigkeit. University of Regensburg, Regensburg, 1973.

133. Gómez, E.; González, B.; Calvar, N.; Tojo, E.; Domínguez, Á., Physical Properties of Pure 1-Ethyl-3-methylimidazolium Ethylsulfate and Its Binary Mixtures with Ethanol and Water at Several Temperatures. *J. Chem. Eng. Data* **2006,** *51*, 2096.

134. Baker, G. A.; Pandey, S., Amphiphilic self organization in ionic liquids. In *ACS Symposium Series*, Rogers, R. D.; Seddon, K. R., Eds. 2005; Vol. 901, pp 234.

135. Evans, D. F.; Wennerström, H., *The colloidal domain: where physics, chemistry, biology, and technology meet, 2nd edition*. Wiley-VCH, pp. 37-42: 1998; p pp. 37.

136. Greaves, T. L.; Weerawardena, A.; Fong, C.; Drummond, C. J., Many protic ionic liquids mediate hydrocarbon-solvent interactions and promote amphiphile self-assembly. *Langmuir* **2007,** *23*, 402.

137. Gao, Y.; Li, N.; Li, X.; Zhang, S.; Zheng, L.; Bai, X.; Yu, L., Microstructures of Micellar Aggregations Formed within 1-Butyl-3-methylimidazolium Type Ionic Liquids. *J. Phys. Chem. B* **2008,** *113*, 123.

138. Tran, C. D.; Yu, S., Near-infrared spectroscopic method for the sensitive and direct determination of aggregations of surfactants in various media. *J. Colloid Interface Sci.* **2005,** *283*, 613.

139. Friberg, S. E.; Sun, W. M., A non-aqueous microemulsion system of ethylene glycol, sodium dodecyl sulfate, toluene, and decanol. *Colloid Polym. Sci.* **1990,** *268*, 755.

140. Armand, M.; Endres, F.; MacFarlane, D. R.; Ohno, H.; Scrosati, B., Ionic-liquid materials for the electrochemical challenges of the future. *Nat. Mater.* **2009,** *8*, 621.

141. Liu, J.-f.; Jiang, G.-b.; Jönsson, J. Å., Application of ionic liquids in analytical chemistry. *Trends Anal. Chem.* **2005,** *24*, 20.

142. Zhu, D. M.; Wu, X.; Schelly, Z. A., Investigation of the micropolarities in reverse micelles of Triton X-100 in mixed solvents of benzene and n-hexane. *J. Phys. Chem.* **1992,** *96*, 7121.

143. Almgren, M.; Van Stam, J.; Swarup, S.; Loefroth, J. E., Structure and transport in the microemulsion phase of the system Triton X-100-toluene-water. *Langmuir* **1986,** *2*, 432.

144. Anjum, N.; Guedeau-Boudeville, M.-A.; Stubenrauch, C.; Mourchid, A., Phase Behavior and Microstructure of Microemulsions Containing the Hydrophobic Ionic Liquid 1-Butyl-3-methylimidazolium Hexafluorophosphate. *J. Phys. Chem. B* **2009,** *113*, 239.

145. Seth, D.; Chakraborty, A.; Setua, P.; Sarkar, N., Interaction of Ionic Liquid with Water in Ternary Microemulsions (Triton X-100/Water/1-Butyl-3-methylimidazolium Hexafluorophosphate) Probed by Solvent and Rotational Relaxation of Coumarin 153 and Coumarin 151. *Langmuir* **2006,** *22*, 7768.

146. Seth, D.; Chakraborty, A.; Setua, P.; Sarkar, N., Interaction of ionic liquid with water with variation of water content in 1-butyl-3-methyl-imidazolium hexafluorophosphate ([bmim][PF[sub 6]])/TX-100/water ternary microemulsions monitored by solvent and rotational relaxation of coumarin 153 and coumarin 490. *J. Chem. Phys.* **2007,** *126*, 224512.

147. Gao, Y.; Han, S.; Han, B.; Li, G.; Shen, D.; Li, Z.; Du, J.; Hou, W.; Zhang, G., TX-100/Water/1-Butyl-3-methylimidazolium Hexafluorophosphate Microemulsions. *Langmuir* **2005,** *21*, 5681.

148. Safavi, A.; Maleki, N.; Farjami, F., Phase behavior and characterization of ionic liquids based microemulsions. *Colloids Surf., A* **2010,** *355*, 61.

149. Li, J.; Zhang, J.; Gao, H.; Han, B.; Gao, L., Nonaqueous microemulsion-containing ionic liquid [bmim][PF₆] as polar microenvironment. *Colloid Polym. Sci.* **2005,** *283*, 1371.

150. Li, N.; Gao, Y. a.; Zheng, L.; Zhang, J.; Yu, L.; Li, X., Studies on the Micropolarities of bmimBF4/TX-100/Toluene Ionic Liquid Microemulsions and Their Behaviors Characterized by UV−Visible Spectroscopy. *Langmuir* **2006,** *23*, 1091.

151. Lee, S. H.; Lee, S. B., The Hildebrand solubility parameters, cohesive energy densities and internal energies of 1-alkyl-3-methylimidazolium-based room temperature ionic liquids. *Chem. Commun.* **2005**, 3469.

152. Abécassis, B.; Testard, F.; Arleth, L.; Hansen, S.; Grillo, I.; Zemb, T., Electrostastic Control of Spontaneous Curvature in Catanionic Reverse Micelles. *Langmuir* **2007,** *23*, 9983.

153. Freiberger, N.; Moitzi, C.; de Campo, L.; Glatter, O., An attempt to detect bicontinuity from SANS data. *J. Colloid Interface Sci.* **2007,** *312*, 59.

154. Sottmann, T.; Strey, R.; Chen, S. H., A small-angle neutron scattering study of nonionic surfactant molecules at the water--oil interface: Area per molecule, microemulsion domain size, and rigidity. *J. Chem. Phys.* **1997,** *106*, 6483.

155. Rushforth, D. S.; Sanchez-Rubio, M.; Santos-Vidals, L. M.; Wormuth, K. R.; Kaler, E. W.; Cuevas, R.; Puig, J. E., Structural study of one-phase microemulsions. *J. Phys. Chem.* **1986,** *90*, 6668.

156. Barnes, I. S.; Derian, P.-J.; Hyde, S. T.; Ninham, B. W.; Zemb, T. N., A disordered lamellar structure in the isotropic phase of a ternary double-chain surfactant system. *J. Phys. France* **1990,** *51*, 2605.

157. Barnes, I.; Hyde, S.; Ninham, B.; Derian, P.; Drifford, M.; Warr, G.; Zemb, T., The disordered open connected model of microemulsions. In *Trends in Colloid and Interface Science II*, Degiorgio, V., Ed. Springer Berlin / Heidelberg: 1988; Vol. 76, pp 90.

158. Israelachvili, J. N.; Mitchell, D. J.; Ninham, B. W., Theory of self-assembly of hydrocarbon amphiphiles into micelles and bilayers. *J. Chem. Soc., Faraday Trans.* **1976,** *72*, 1525.

159. Testard, F.; Zemb, T., Solute Effect on Connectivity of Water-in-Oil Microemulsions. *Langmuir* **1999,** *16*, 332.

160. Roux, D.; Coulon, C.; Cates, M. E., Sponge phases in surfactant solutions. *J. Phys. Chem.* **1992,** *96*, 4174.

161. Wolf, L.; Hoffmann, H.; Talmon, Y.; Teshigawara, T.; Watanabe, K., Cryo-TEM imaging of a novel microemulsion system of silicone oil with an anionic/nonionic surfactant mixture. *Soft Matter* **2010,** *6*, 5367.

162. Fanun, M., Microemulsions with Mixed Nonionic Surfactants and Flavor Oil. *J. Surfactants Deterg.* **2010,** *13*, 321.

163. Gutel, T.; Garcia-Anton, J.; Pelzer, K.; Philippot, K.; Santini, C. C.; Chauvin, Y.; Chaudret, B.; Basset, J.-M., Influence of the self-organization of ionic liquids on the size of ruthenium nanoparticles: effect of the temperature and stirring. *J. Mater. Chem.* **2007,** *17*, 3290.

164. Paruch, E.; Ciunik, Z.; Wawrzeńczyk, C., Synthesis of Spirolactones from the Limonene System. *Eur. J. Org. Chem.* **1998,** *1998*, 2677.

165. Baker, R.; Borges, M.; Cooke, N. G.; Herbert, R. H., Identification and Synthesis of (Z)-(1'S,3'R,4'S)(-)-2-(3',4'-Epoxy-4'-methylcyclohexyl)-6-methylhepta-2,5-diene, the Sex Pheromone of the Southern Green Stinkbug, Nezara viridula (L.). *J. Chem. Soc., Chem. Commun.* **1987**, 3.

166. Rodriguez, R.; Ollivier, C.; Santelli, M., Vitamin D: a concise synthesis of the C19 hydroxylated enyne A-ring, an interesting precursor for the preparation of C19 substituted vitamin D analogues. *Tetrahedron Lett.* **2004,** *45*, 2289.

167. Mattos, M. C. S. d.; Bernini, R. B., The Reaction of (R)-Limonene with S-Thioacids. *J. Braz. Chem. Soc.* **2007,** *18*, 5.

168. Yadav, J. S.; Subba Reddy, B. V.; Narasimhulu, G.; Purnima, K. V., FeCl3-catalyzed functionalization of monoterpenes via hydroalkylation of unactivated alkenes. *Tetrahedron Lett.* **2009,** *50*, 5783.

169. Madeira Lau, R.; Van Rantwijk, F.; Seddon, K. R.; Sheldon, R. A., Lipase-Catalyzed Reactions in Ionic Liquids. *Org. Lett.* **2000,** *2*, 4189.

170. Schofer, S. H.; Kaftzik, N.; Wasserscheid, P.; Kragl, U., Enzyme catalysis in ionic liquids: lipase catalysed kinetic resolution of 1-phenylethanol with improved enantioselectivity. *Chem. Commun.* **2001**, 425.

171. Eckstein, M.; Villela Filho, M.; Liese, A.; Kragl, U., Use of an ionic liquid in a two-phase system to improve an alcohol dehydrogenase catalysed reduction. *Chem. Commun.* **2004**, 1084.

172. Moniruzzaman, M.; Kamiya, N.; Goto, M., Ionic liquid based microemulsion with pharmaceutically accepted components: Formulation and potential applications. *J. Colloid Interface Sci.* **2010,** *352,* 136.

173. Predel, T.; Pohrer, B.; Schlücker, E., Ionic Liquids as Alternative Lubricants for Special Applications. *Chem. Eng. Technol.* **2010,** *33,* 132.

174. Palacio, M.; Bhushan, B., A Review of Ionic Liquids for Green Molecular Lubrication in Nanotechnology. *Tribol. Lett.* **2010,** *40,* 247.

175. Jiménez, A.; Bermúdez, M., Ionic Liquids as Lubricants of Titanium–Steel Contact. Part 3. Ti6Al4V Lubricated with Imidazolium Ionic Liquids with Different Alkyl Chain Lengths. *Tribol. Lett.* **2010,** *40,* 237.

176. Lawes, S.; Hainsworth, S.; Blake, P.; Ryder, K.; Abbott, A., Lubrication of Steel/Steel Contacts by Choline Chloride Ionic Liquids. *Tribol. Lett.* **2010,** *37,* 103.

Herewith I declare that I have made this existing work single-handed. I have only used the stated utilities.

Regensburg, 13th January 2011

Agnes Harrar